



<https://theses.gla.ac.uk/>

Theses Digitisation:

<https://www.gla.ac.uk/myglasgow/research/enlighten/theses/digitisation/>

This is a digitised version of the original print thesis.

Copyright and moral rights for this work are retained by the author

A copy can be downloaded for personal non-commercial research or study,
without prior permission or charge

This work cannot be reproduced or quoted extensively from without first
obtaining permission in writing from the author

The content must not be changed in any way or sold commercially in any
format or medium without the formal permission of the author

When referring to this work, full bibliographic details including the author,
title, awarding institution and date of the thesis must be given

Enlighten: Theses

<https://theses.gla.ac.uk/>
research-enlighten@glasgow.ac.uk

**INVESTIGATION AND PREDICTION
OF
SPIRAL WOUND REVERSE OSMOSIS
MEMBRANE PERFORMANCE**

A thesis

Submitted to the faculty of Engineering
for the fulfilment of the requirements for the degree
of
Doctor of Philosophy, (Ph.D.)

by

Stamatios Avlonitis

Department of Mechanical Engineering

UNIVERSITY OF GLASGOW

May 1991

© Stamatios Avlonitis, 1991

ProQuest Number: 10984127

All rights reserved

INFORMATION TO ALL USERS

The quality of this reproduction is dependent upon the quality of the copy submitted.

In the unlikely event that the author did not send a complete manuscript and there are missing pages, these will be noted. Also, if material had to be removed, a note will indicate the deletion.



ProQuest 10984127

Published by ProQuest LLC (2018). Copyright of the Dissertation is held by the Author.

All rights reserved.

This work is protected against unauthorized copying under Title 17, United States Code
Microform Edition © ProQuest LLC.

ProQuest LLC.
789 East Eisenhower Parkway
P.O. Box 1346
Ann Arbor, MI 48106 – 1346

Για το κοριτσι και τη νυχτα

" Διαβαινοντας στενα σοκακια, σε εκεινες τις απομακρες πολιτειες που διαβαζεις στα παραμυθια. Ισορροπωντας μεταξυ θριαμβου και ατιμασης. Με το ονειρο να λικνιζεται απαλα τοσο κοντινο και απλησιαστο. Η μαγεια δεν ειναι στον αγωνα για το ονειρο, η μαγεια ειναι το ονειρο. Στο τελος τελός ισως ο χρονος δημιουργησει την εικονα του ονειρικου και ενδοξου ταυτοχρονα, που χαμενο καπου στη ληθη και στο καποτε μας χαμογελα για ολα τα μεγαλα και τα ενδοξα που τελειωσαν πια. Προχωρω και ολο μαθαινω."

SUMMARY

In this work an analytical solution for the performance of the spiral wound modules is presented for sea-water as feed. This analysis takes into account pressure losses in both permeate and brine channels, the effect of concentration polarization and the concentration gradient along the membrane. A five parameters model is introduced. These parameters are: k_{fb} (brine friction parameter), k_{fp} (permeate friction parameter), k_1 (water permeability coefficient), k (mass transfer coefficient), k_2 (solute permeability coefficient).

The explicit equations, which were developed, have been applied to experimental data collected with FilmTec FT30SW 2.5" modules. Two sets of experiments have been carried out. One set with distilled water as feed at different temperatures and another one with sea-water at various concentrations and temperatures. With the first set of data the water permeability coefficient and the friction parameters have been determined, and with the second set of data the mass transfer coefficient and the solute permeability coefficient have been found. Following the determination of the five parameters simple equations have been proposed to correlate all five parameters with the operating and flow conditions. All the equations proposed have been tested with new experimental data for FilmTec and ROGA spiral wound modules. A good agreement have been found with experimental and theoretical values for the water flux and the permeate concentration.

The analytical model can give the local values for concentration, pressure, flux, and velocity in the permeate and brine channel at every point on the membrane surface.

Finally suggestions have been made for optimum module geometry so that the maximum permeate flow could be achieved with better permeate quality.

ACKNOWLEDGEMENTS

I would like to express my sincere gratitude to my supervisor Dr. W.T. Hanbury, for his assistance throughout this work. His kindness and patient during my studies would be always appreciated.

I owe my special thanks to Mr. A Richie for his help in the experimental part of this work. I must also thank my friend and colleague, Mr. M.Ben Boudinar, for the valuable discussions we had throughout this work.

Finally I would also like to thank the GREEK Government (State Scholarship Foundation, I.K.Y.), and the International Desalination Association, I.D.A., for the financial support of my studies.

CONTENTS

SUMMARY	i
ACKNOWLEDGEMENTS	ii
CONTENTS	iii
LIST OF FIGURES	vi
LIST OF TABLES	x
LIST OF SYMBOLS	xi

CHAPTER I : INTRODUCTION

1.1 DESALINATION	1
1.2 REVERSE OSMOSIS	1
1.3 R.O. MODULES	3

CHAPTER II : LITERATURE REVIEW

2.1 INTRODUCTION	6
2.2 CHANGE OF CONDITIONS ALONG THE MEMBRANE	7
2.2.1 Pressure drop in the permeate and the brine channel	8
2.2.2 Concentration at the membrane surface	9
2.2.3 Concentration gradient along the membrane	9
2.3 PREVIOUS WORK	10

CHAPTER III : AN ANALYTICAL SOLUTION

3.1 INTRODUCTION	14
3.2 FLUID FLOW THROUGH POROUS MEDIA	14
3.3 CONCENTRATION POLARIZATION	16
3.4 WATER PERMEABILITY COEFFICIENT	18
3.5 FRICTION PARAMETERS FOR THE BRINE AND PERMEATE	

	CHANNEL	26
3.6	MASS TRANSFER COEFFICIENT	28
3.7	SOLUTE PERMEABILITY COEFFICIENT	37
3.8	OPTIMUM MODULE GEOMETRY	41

CHAPTER IV : EXPERIMENTAL WORK

4.1	INTRODUCTION	44
4.2	EXPERIMENTAL RIG	44
4.3	EXPERIMENTAL PROCEDURE	47
	4.3.1 Water permeability coefficient and brine friction parameter	47
	4.3.2 Mass transfer coefficient, solute permeability coefficient	50
	4.3.3 Permeate friction parameter	50

CHAPTER V : RESULTS AND DISCUSSION

5.1	INTRODUCTION	53
5.2	WATER PERMEABILITY COEFFICIENT AND FRICTION PARAMETERS	53
	5.2.1 Brine friction parameter	56
	5.2.2 Permeate friction parameter	58
	5.2.3 Water permeability coefficient	60
	5.2.4 Distilled water data analysis for membrane No1	63
5.3	MASS TRANSFER COEFFICIENT	66
5.4	SOLUTE PERMEABILITY COEFFICIENT	76
5.5	EFFECTIVE PRESSURE, WATER FLUX, WALL CONCENTRATION AND VELOCITY PROFILE	77
	5.5.1 Pressure and flux profile	77
	5.5.2 Concentration profile	79
	5.5.3 Velocity profile	80

LIST OF FIGURES

Fig.1.1	Water flow through a semipermeable membrane during Osmosis and Reverse Osmosis	2
Fig.1.2	Spiral wound membranes	4
Fig.1.3	Hollow fiber membrane	4
Fig.2.1	Semi-unwound Spiral wound module	8
Fig.3.1	Thin-film model for the mass transfer at membrane surface	16
Fig.3.2	Unwound spiral wound module	19
Fig.4.1	Experimental rig	45
Fig.4.2	High pressure tube with the membrane element	48
Fig.4.3	Hypodermic tubes in the inlet and the outlet of the membrane	49
Fig.4.4	Hypodermic tubes in the inlet and the outlet of the tube	49
Fig.5.1	Recovery performance of FilmTec modules	53
Fig.5.2	Salt Rejection performance of FilmTec modules	54
Fig.5.3	Permeate flow at different pressures for membrane No1	54
Fig.5.4	Variation of k_1 and k_{fp} for different brine friction parameters	56
Fig.5.5	$\ln(k_{fb})$ versus $\ln(Re)$ for different experimental data	57
Fig.5.6	k_{fp} values for different pressures and temperatures	58
Fig.5.7	$\ln(k_{fp})$ versus $\ln(Re)$ for different temperatures	59
Fig.5.8	$\ln k_1$ versus pressure for different temperatures (For membrane No 2)	61
Fig.5.9	$\ln k_1$ versus the relative increase in absolute temperature (For membrane No 2)	62
Fig.5.10	$\ln k_{1,0}$ versus the relative increase in absolute temperature (For membrane No 2)	63
Fig.5.11	$\ln k_1$ versus pressure for different temperatures (For membrane No 1)	64

Fig.5.12	$\ln k_{1,0}$ versus the relative increase in absolute temperature (For membrane No 1)	64
Fig.5.13	k_1 values for different pressures and temperatures	65
Fig.5.14	$\mu \times k_1$ values for different temperatures	66
Fig.5.15	Variation of the brine concentration with the membrane length for sea-water at 25° C, 60 bar and $u_f=7.3$ cm/sec	69
Fig.5.16	Variation of the brine concentration with the membrane length for sea-water at 25° C, 60 bar and $u_f=23$ cm/sec	70
Fig.5.17	$\ln(\text{Sh})$ versus $\ln(\text{Re}_f)$ for different operating conditions	73
Fig.5.18	$\ln(\text{Sh}) - n_2 \ln(\text{Re}_f)$ versus $\ln(C_f/\rho)$	74
Fig.5.19	$\ln(\text{Sh}) - n_2 \ln(\text{Re}_f)$ versus $\ln(P_b(0,w)/P^0)$	74
Fig.5.20	$\ln(\text{Sh}) - n_2 \ln(\text{Re}_f)$ versus $\ln(\text{Sc})$	75
Fig.5.21	Rejection properties for different operating conditions	76
Fig.5.22	$\ln k_2$ versus the relative increase in temperature	77
Fig.5.23	Effective pressure profile for distilled water solution at 20° C, 30 bar and $u_f=30.15$ cm/sec	78
Fig.5.24	Effective pressure profile for 35,000 ppm sea-water solution at 20° C, 55 bar and $u_f=12.25$ cm/sec	78
Fig.5.25	Salt wall concentration profile for 35,000 ppm sea-water solution at 20° C, 55 bar and $u_f=30.15$ cm/sec	79
Fig.5.26	Brine velocity profile for distilled water at 20° C and 30 bar	80
Fig.5.27	Permeate velocity profile for distilled water at 20° C and 30 bar	82
Fig.6.1	Average water flux and permeate concentration as a function of the applied pressure, for 25,000 ppm sea-water at 25° C and $Q_f=10.846$ lt/min	84
Fig.6.2.a	Average water flux for different conditions for sea-water solutions (membrane No1)	85

Fig.6.2.b	Permeate concentration flux for different conditions for sea-water solutions (membrane No1)	86
Fig.6.3.a	Average water flux at different low feed concentrations and flows for ROGA-4160 membranes	88
Fig.6.3.b	Permeate concentration at different low feed concentrations and flows for ROGA-4160 membranes	88
Fig.6.4	Permeate concentration and average water flux for different feed concentrations at 25° C 50 bar and $u_f=6.7$ cm/sec	89
Fig.6.5	Permeate concentration and average water flux for different feed velocities at 50 bar, 25,000 ppm and 25° C	90
Fig.6.6.a	Water flow per unit volume at 60 bar, 35,000 ppm sea-water, 25° C and $Q_f=10.421$ lt/min	92
Fig.6.6.b	Permeate concentration at 60 bar, 35,000 ppm sea-water, 25° C and $Q_f=10.421$ lt/min	93
Fig.6.7	Water flow per unit volume at 60 bar, 25° C and $Q_f=10.421$ lt/min..	93
Fig.6.8	Water flow per unit volume at 35,000 ppm, 25° C and $Q_f=10.421$ lt/min	94
Fig.6.9.a	Water flow per unit volume at 35,000 ppm, 60 bar and 25° C at constant feed velocity	94
Fig.6.9.b	Permeate concentration at 35,000 ppm, 60 bar and 25° C at constant feed velocity	95
Fig.6.10.a	Water flow per unit volume at 35,000 ppm, 60 bar and 25° C at constant feed flow	96
Fig.6.10.b	Permeate concentration at 35,000 ppm, 60 bar and 25° C at constant feed flow	96
Fig.6.11	Average water flux and permeate concentration at 35,000 ppm, 60 bar, $Q_f=7.692$ lt/min and 20° C for membrane No3 for different water permeability values.....	97

Fig.6.12	Average water flux and permeate concentration at 35,000 ppm, 60 bar, $Q_f=7.692$ lt/min and 20° C for membrane No3 for different brine friction parameter values	98
Fig.6.13	Average water flux and permeate concentration at 35,000 ppm, 60 bar, $Q_f=7.692$ lt/min and 20° C for membrane No3 for different permeate friction parameter values	98
Fig.6.14	Average water flux and permeate concentration at 35,000 ppm, 60 bar, $Q_f=7.692$ lt/min and 20° C for membrane No3 for different mass transfer coefficient values	99
Fig.6.15	Average water flux and permeate concentration at 35,000 ppm, 60 bar, $Q_f=7.692$ lt/min and 20° C for membrane No3 for different solute permeability values	100

LIST OF TABLES

Table 3.1	k ₁ values for ROGA-4160 module	26
Table 3.2	k ₂ values for ROGA-4160 module	41
Table 4.1	Experimental data with wet and dried membranes at 20 ^o C, 20 bar and C _f =5000 ppm NaCl	51
Table 5.1	Experimental data with distilled water for membrane No1 and No2	103
Table 5.2	Dimensions of the FT30SW 2.5" modules	55
Table 5.3	Water permeability coefficient and Friction parameters for membrane No1 and No2	107
Table 5.4	Mass transfer coefficient for ROGA-4160 module	68
Table 5.5	Mass transfer coefficient at 25 ^o C, 60 bar and 25,000 ppm sea-water	69
Table 5.6	Experimetal data for sea-water solutions and the values for the mass transfer and the solute permeability coefficients for membrane No1.	111
Table 6.1	Comparison between experimental and calculated data for membrane No 1	85
Table 6.2	Experimental data with distilled water for membrane No 3	86
Table 6.3	Comparison between experimental and calculated data for membrane No 3	87

LIST OF SYMBOLS

α_T	constant defined in eq.(5.9)
$\alpha_{fr.}$	constant defined in eq.(2.4)
B	constant defined by eq.(3.95), sec^{-1}
b	constant, defined by eq.(3.40), $\text{cm sec}^{-1} \text{bar}^{-1}$
c	concentration, g lt^{-1}
D	Diffusivity coefficient, $\text{cm}^2 \text{sec}^{-1}$
E	constant, defined in eq.(3.100)
ΔP_{ef}	driving Pressure, bar
ΔP	Pressure difference defined by eq.(3.84), bar
f	constant defined by eq.(3.68), gr cm^{-4}
h	height, cm
J	average volumetric water flux, cm sec^{-1}
$J(x,y)$	local volumetric flux, cm sec^{-1}
k	mass transfer coefficient, cm sec^{-1}
k^0	dimensionless constant defined in eq.(5.24), cm sec^{-1}
k^C	convective mass transfer coefficient, cm sec^{-1}
k_1	water permeability coefficient, $\text{cm sec}^{-1} \text{bar}^{-1}$
$k_{1,0}$	water permeability coefficient at zero pressure, $\text{cm sec}^{-1} \text{bar}^{-1}$
k_1^0	water permeability coefficient at 0°C , $\text{cm sec}^{-1} \text{bar}^{-1}$
k_1^{20}	water permeability coefficient at 20°C , $\text{cm sec}^{-1} \text{bar}^{-1}$
k_1^T	water permeability coefficient at K, $\text{cm sec}^{-1} \text{bar}^{-1}$
k_2	solute permeability coefficient, cm sec^{-1}
k_2^T	solute permeability coefficient at any temperature T, cm sec^{-1}
k_2^0	solute permeability coefficient at 0°C , cm sec^{-1}
k_f	friction parameter, cm^{-2}
k'_f	friction parameter defined in eq.(5.3), cm^{-2}

l	membrane length, cm
l_2	membrane length with glue, cm
n_1, n_2, n_3, n_4	dimensionless exponents defined in eq.(5.24)
\varnothing	constant at a given temperature, bar lt gr ⁻¹
P	pressure, bar
P^0	constant, (1 bar)
q	constant, defined by eq.(3.23), cm
Q	volumetric flow rate, cm ³ sec ⁻¹
Re	$(hu\rho/\mu)$ Reynolds Number
Sc	$(\mu/\rho D)$ Schmidt number
Sh	(kh_b/D) Sherwood number
T	absolute temperature
u	velocity, cm sec ⁻¹
w	membrane width, cm
w_2	membrane width with glue, cm
x	coordinate along the module axis, cm
y	coordinate along the membrane width, cm
(x,y)	any point in the two dimensions plane

Greek letters

α_P	constant defined in eq.(5.7), bar ⁻¹
α_T	constant defined in eq.(5.9)
β_T	dimensionless constant, defined by eq.(5.30)
$\gamma, \lambda, \xi, \theta, \phi$	dimensionless constants defined in eq.(3.85)
ε	constant defined by eq.(3.100), cm ^{1/2}
λ	dimensionless friction parameter in eq.(2.3)
λ'	dimensionless friction parameter in eq.(2.4)
μ	viscosity, g cm ⁻¹ sec ⁻¹

ν	dimensionless exponent in eq.(5.3)
π	Osmotic pressure, bar
ρ	density, g cm ⁻³
τ	dimensionless exponent in Darcy' s law

Subscripts

b	brine
ef	effective
f	feed
p	permeate
w	membrane wall
i	Membrane No1
j	Membrane No2

CHAPTER I

INTRODUCTION

1.1 DESALINATION

Desalination can be defined as a process by which pure water is produced from salt water. Although desalination technology was originally developed to produce tap water from brackish or sea water, today the production of ultrapure water or the treatment of waste water can be also achieved by desalination methods. The initial boost of research and development of new and more efficient desalination techniques was a result of the demand of more water for countries in the arid region and the increase in water consumption in other parts of the world. Since then many things have changed. We are now possibly witnessing a change in the world climate. Areas which used to have enough water resources seem to become dry. The pollution of rivers and lakes, not only with chemicals but also with the extensive use of fertilizers, is so high in other areas so that the ground and surface water need treatment in order to be used as tap water.

It can be said that every country in one way or the other is interested in the Desalination techniques. There are many desalination methods among which *Reverse Osmosis* (R.O.) plays a significant role. Today Reverse Osmosis technology has been improved in such a point so that it is competitive to the old desalination methods. The demand for more water is forcing Reverse Osmosis technology ahead and new more efficient R.O. desalination plants are available in the world market.

1.2 REVERSE OSMOSIS

Osmosis is a natural process involving the flow of a solvent driven by a difference in concentration across a *semipermeable membrane*. That is a membrane which will allow the water to pass through and will reject the salts. If a semipermeable membrane separates a solution (salt water) from a pure solvent (water), then the difference in chemical potentials of water either side of the membrane will result in a flow of solvent from the pure solvent side to the solution side, Fig.1.1.a.

The flow continues until the chemical potentials become equal. As this will never happen, in the case of a solution separated by the membrane from the solvent, the solvent

will constantly flow across the membrane. The flow can be stopped if a specific pressure is applied to the solution, see Fig.1.1.b. This pressure is called *Osmotic Pressure* and is given by eq.(1.1).

$$\pi = \varnothing C \tag{1.1}$$

where, π = osmotic pressure.

\varnothing = constant depending on the concentration, temperature and the kind of the salt.

C = solution concentration.

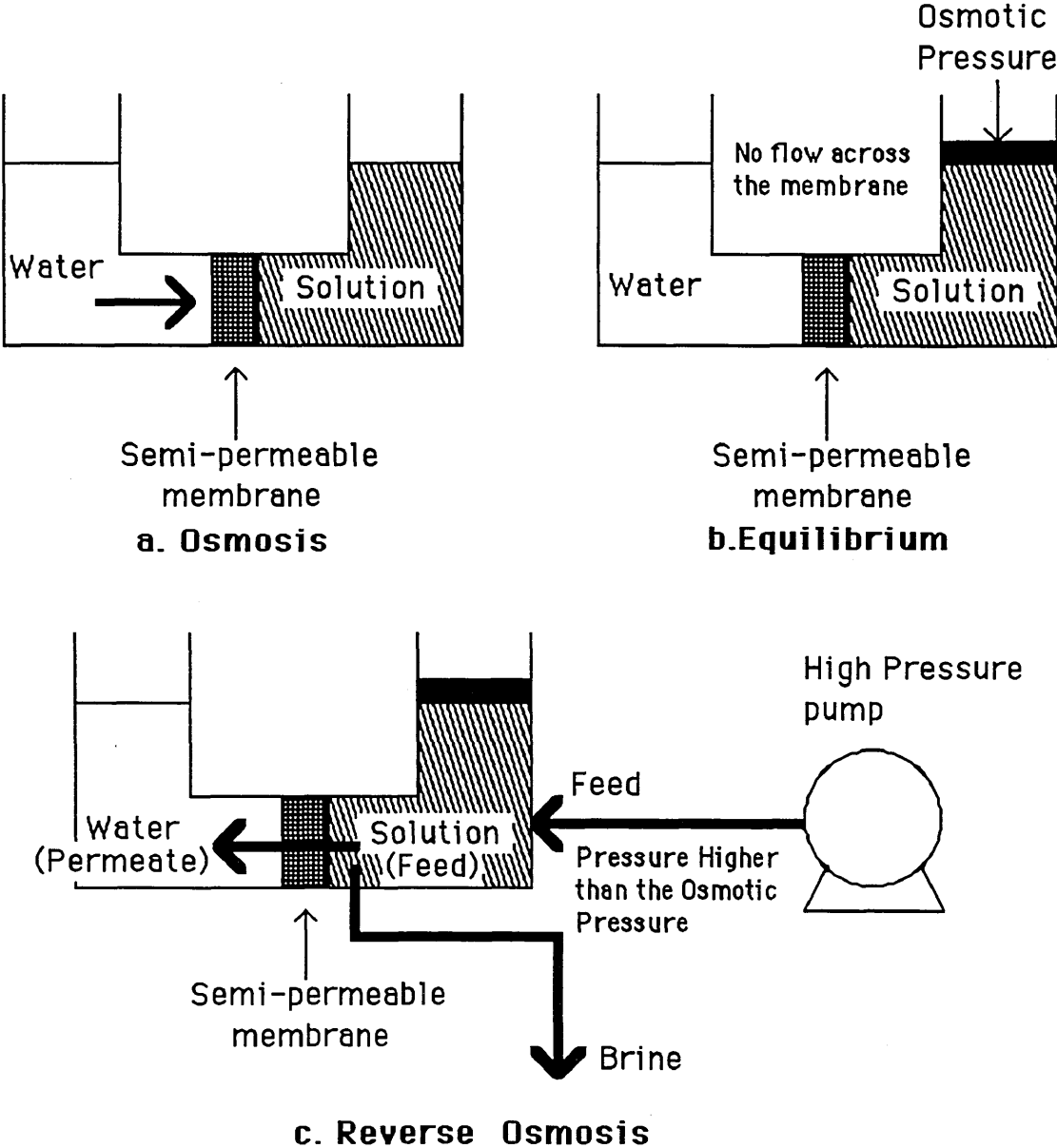


Fig.1.1 Water flow through a semipermeable membrane during Osmosis (a) and Reverse Osmosis (c).

Desalination can be accomplished by reversing the above mentioned process. If a pressure which is greater than the osmotic pressure is applied to the solution (Feed), then the solvent will flow from the solution to the solvent side (Permeate) and a solution with higher concentration will be rejected (Brine). This is the principle of the process called *Reverse Osmosis*, Fig.1.1.c.

The heart of every desalination process is the semipermeable membrane. A suitable Reverse Osmosis desalination membrane must combine good salt rejection and high water flux as well as long service life and resistant to chemical and biological attack. After the work of Loeb and Sourirajan asymmetric cellulose acetate membranes were commercially available in the early 1960' s. Since then a lot of polymeric materials have been synthesized and tried as R.O membranes, in the asymmetric or composite form, each having its own advantages and disadvantages. Both types of membranes consist of a very thin active layer on the top of the membrane responsible for the rejection properties and a highly porous substrate to support the first one. It is a long way to go until the ideal R.O. membrane is synthesized, though new membranes appear on the market more efficient than the old ones.

1.3 R.O. MODULES

In order to increase the water flow through the membrane, one can either increase the applied pressure and the consumption of energy or increase the surface area of the membrane. Various configurations have been tried in achieving high surface-to-volume ratio, but for commercial purposes two basic configurations have been used. These are:

- a) Spiral wound membrane, Fig.1.2.
- b) Hollow fibers membrane, Fig.1.3.

The spiral wound system is used for flat membranes and for materials with reasonably high water permeability. Two sheets of membranes are placed back to back and sealed along three of the sides to form an envelope into which a porous material is inserted. This material keeps the two membranes apart when the high pressure is applied and allows the permeate to flow towards the open end of the envelope. The open end of the envelope is sealed around a product collection pipe, through which the permeate can flow. The envelope together with a spacer, which allows the feed solution to flow along the membranes, is rolled around the collecting pipe to form a spiral wound unit and it is placed in a cylindrical pressure vessel, with one inlet for the feed and two outlets, one for the permeate and one for the brine.

Hollow fibers can be thought of as a heavy walled plastic pipe of a very small size which requires no support. The fibers are arranged as 'U' tubes in a bundle, open at one end. The feed water flows out radially and the fresh water is collected and carried away in the inner capillary. The collection of headers and fibers are placed in a cylindrical pressure vessel and the whole assembly is known as a permeator.

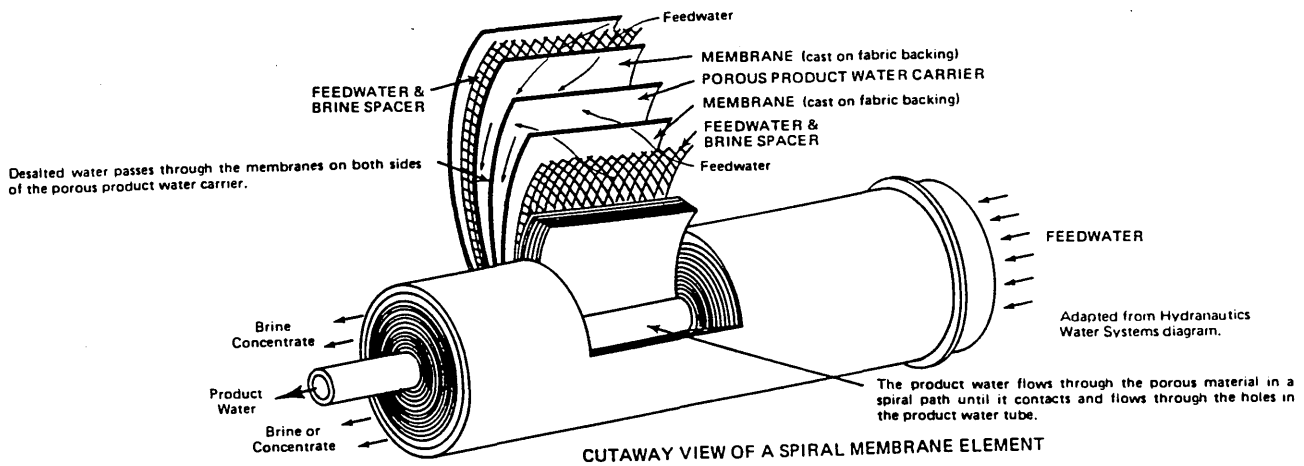


Fig.1.2 Spiral wound membrane.

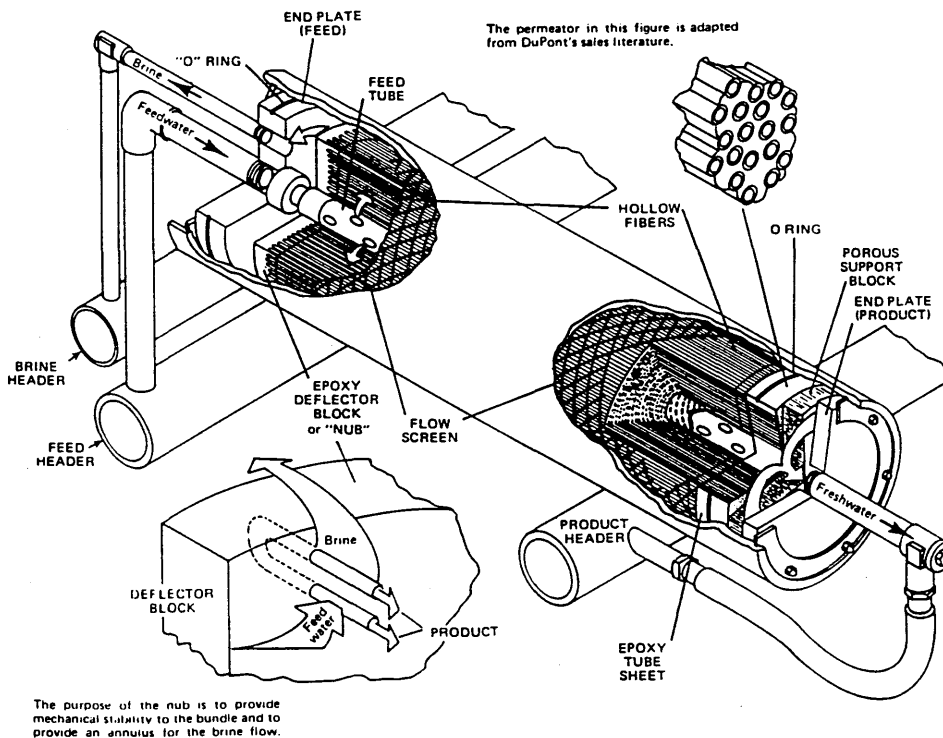


Fig.1.3 Hollow fiber membrane.

In a permeators millions fibers are used. These fibres have outside diameters of approximately 90 μm and inside diameters approximately 40 μm . With the hollow fiber configuration a very high surface area can be achieved for a given volume. This means that hollow fiber R.O. devices can utilize polymers with low water permeability. The flux (flow per unit membrane area) in hollow fibers membranes is up to 100 times less than the flux in the spiral wound ones.

The behaviour of reverse osmosis systems are usually described in terms of two major parameters. The solute removal efficiency, the *Rejection %*, and, the fraction of the feed water treated, the *Recovery %*. These are defined by eqs (1.2) and (1.3) respectively.

$$\text{Rejection} = \frac{C_f - C_p}{C_f} 100 \quad (1.2)$$

where, C_f = the concentration of solute in the feed
 C_p = the concentration in the permeate.

$$\text{Recovery} = \frac{Q_p}{Q_f} 100 \quad (1.3)$$

where, Q_p = The volumetric flow rate of the permeate.
 Q_f = The volumetric flow rate of the feed.

CHAPTER II

LITERATURE REVIEW

2.1 INTRODUCTION

One is tempted to think that the salt rejection by the membrane in a reverse osmosis process is similar to the filtration process. Unfortunately this is not the case. Salt rejection in R.O. is a much more complicated phenomenon.

In discussing the process two different approaches have been used. In one approach, which is called "*structural*", attempts have been made to correlate salt rejection with the chemical properties of the membrane. Such an approach can be useful qualitatively and can suggest a special membrane for a particular separation or indicate the use of particular polymer materials from which membranes could be made. However, the chemical system of water-salt-membrane is too complicated for a satisfactory treatment with the current theories. Different theories that have been proposed involving this structural approach include:

- a) Distillation mechanisms[1,2].
- b) Sieve mechanisms[3,4].
- c) Surface tension mechanisms[5,6,7].
- d) Hydrogen bonding mechanisms[8,9].

In the other approach, which is called "*phenomenological*", one attempts to correlate the rejection properties of a given membrane with macroscopic properties which can be measured. Although studies of this type give no information about microscopic properties or mechanisms, they are very useful in formulating the R.O. process, and making prediction about the effects of the factors which can affect the performance of an R.O. membrane. Also when a macroscopic description has been established, speculation about microscopic and structural mechanisms are easier. Many combinations of variables have been selected for use in equations describing transport through membranes in R.O. There are a number of different models using this approach. These include:

- a) The solution-diffusion model[10,11].
- b) The finely porous capillary model[12,13,14].
- c) The pores model[15].

Since the work that is presented in this thesis is based on the solution diffusion model a more detailed presentation of this model is given below.

This model is based on two essential steps: absorption and diffusion. Since electron microscope pictures of the surface of the R.O. membranes do not reveal the presence of easily identifiable pores, it has been suggested that there is no bulk flow of solvent or solute through the membrane skin layer. Instead, the direct transport of both components through the membrane may involve firstly their solution within the dense skin layer and secondly their diffusion across this skin layer. By the application of non-equilibrium thermodynamics to the diffusion part of the process, relationships for the flux of the solvent and of the solute can be obtained. For a particular membrane/solvent/solute system the mass flux of solvent, J_1 , is given by eq.(2.1).

$$J_1 = k_1 (\Delta P - \Delta \pi) \quad (2.1)$$

where, J_1 = The mass flow rate of solvent per unit area of membrane, $\text{gr cm}^{-2}\text{sec}^{-1}$.

k_1 = Water permeability coefficient, which is constant depending on the membrane, temperature and the solution properties, sec cm^{-1} .

ΔP = Difference in applied pressure between the feed and the permeate, $\text{gr cm}^{-1}\text{sec}^{-2}$.

$\Delta \pi$ = Difference in Osmotic pressure between the feed and the permeate, $\text{gr cm}^{-1}\text{sec}^{-2}$.

At the same time the salt flux is given by eq. (2.2).

$$J_2 = k_2 \Delta C \quad (2.2)$$

where, J_2 = The mass flow rate of solute per unit area of membrane, in $\text{gr cm}^{-2}\text{sec}^{-1}$.

k_2 = Solute permeability coefficient, which is a function of the same parameters as k_1 , in cm sec^{-1} .

ΔC = Difference in concentration between the feed and the permeate, in gr cm^{-3} .

2.2 CHANGE OF CONDITIONS ALONG THE MEMBRANE

The equations for the water flux and the salt flux, which have been derived by the solution diffusion model can not be applied for the membrane modules in this form.

Pressure velocity and concentration are continuously changing in the direction of flow in a membrane module on both the feed and the permeate sides as a direct result of the local production of permeate. Depending on the module design, this must be taken into account. Consequently eqs (2.1) and (2.2) are valid for a local element of the membrane only. If one wants to describe the performance of a whole spiral wound module the following factors should be taken into account.

2.2.1 Pressure drop in the permeate and the brine channel.

Fig.2.1 shows a semi-unwound spiral wound module with its construction details and

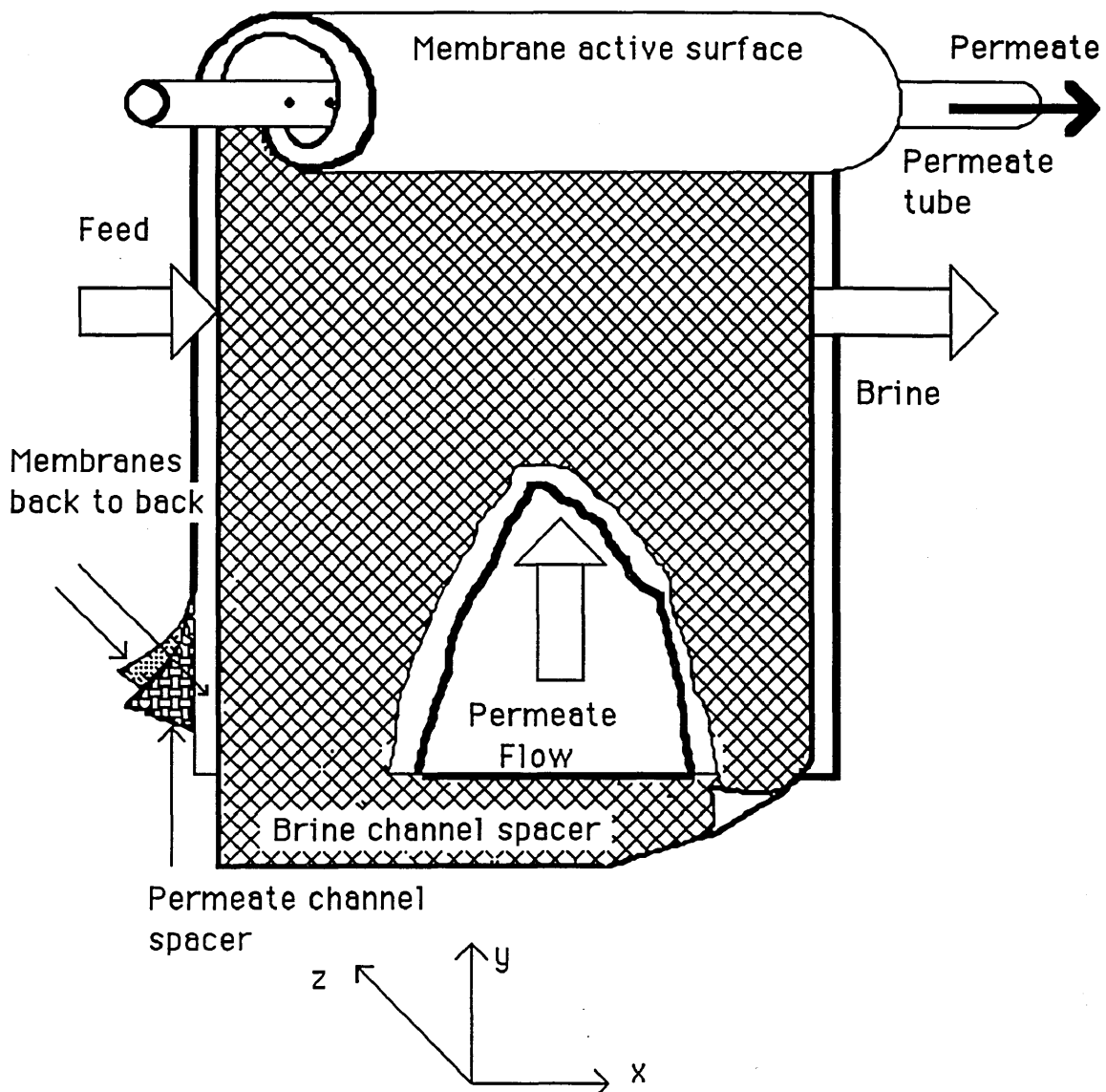


Fig.2.1 Semi-unwound Spiral wound module.

the directions of the brine and the permeate flows. If one considers the x direction (axial),

then the pressure in the brine channel starts from the maximum value in the inlet of the module to the minimum value in the outlet because of pressure losses in the brine channel. These losses are increased by the presence of the spacer in this channel. These losses could be almost eliminated if the brine channel height was increased. However this solution is restricted by the need to limit size of the spiral wound module. If the permeate channel now is considered in the y direction (tangential), the pressure in this channel starts from the maximum value at the closed end of the envelope to the minimum value (roughly atmospheric) at the open end of the envelope.

It is obvious that in two dimensions the pressure in the brine and the permeate channel changes from point to point. Consequently the pressure ΔP in formula (2.1) which at each point is the difference between the pressure in the brine and the permeate side is not constant, and eq.(2.1) can be applied only locally at each point of the membrane.

2.2.2 Concentration at the membrane surface.

The efficiency of a membrane process depends not only on the membrane properties but also on the flow conditions on the membrane surface.

In R.O. dissolved salt is transported by convection to membrane surface together with the solvent. As a result of the selectivity of the membrane most of the salt is rejected and has to be retransported to the bulk of the fluid under steady-state conditions. As the flow is almost laminar near the membrane, this back transfer can only be of a diffusive nature. For the diffusive transport a negative concentration gradient i.e. an increase in concentration at the membrane (*concentration polarization*) is necessary. This increase in the dissolved salt concentration on the membrane surface affects the separation process in two ways: The osmotic pressure increases and the salt flux increases because of the increased salt concentration difference, eq.(2.2). If one wants to apply eqs (2.1) and (2.2) the concentration at the wall of the membrane should be used rather than the bulk salt concentration.

2.2.3 Concentration gradient along the module.

If one follows the brine flow in the x direction one will realize that as the salt is rejected by the membrane and the water flows through the membrane the solution is becoming richer in salt and consequently the salt concentration increases continuously up to a maximum value, which is the concentration of the reject brine at the outlet. Even in the y direction there is a small change in concentration. This happens because the water

flux is higher near the open end of the envelope than near the closed end, since the pressure in the permeate channel is smaller at the open end than at the closed end. It can be expected that, downstream of the feed entry section, the brine salt concentration will increase from the closed end to the open end in the y direction. It is clear that the feed concentration is not constant but varies from point to point over the membrane surface and thus so does the osmotic pressure.

Due to the above phenomena, it has been found that eqs (2.1) and (2.2) from the solution diffusion model can not be applied to describe the performance of a spiral wound module as a whole. They can be applied only locally or for a very small surface area where all the variables which have been mentioned can be considered as being constant.

2.3 PREVIOUS WORK

An analytical solution to describe spiral wound module performance could be very useful not only to predict the performance of the module in new operating conditions but also to predict optimum geometry for the module for better permeate quality and higher water flux. Many researchers have tried to find an analytical solution for the spiral wound and hollow fibers modules and a review of some of this work for the spiral wound modules, is given below.

R. Rautenbach and W. Dahm^[16] have presented in a paper the design equations for spiral wound and hollow fibers modules. The spiral wound membrane was considered flat and a two dimensional model was applied. The analysis was based on several assumptions.

- 1) The influence of concentration polarization was neglected.
- 2) Constant fluid properties were assumed.
- 3) The calculation of the losses of the spacer-foil channels was based on experimentally determined values by Belford^[17].
- 4) The validity of solution-diffusion model.
- 5) Mean values for the velocity and concentration.
- 6) Negligible components of brine and permeate velocities along the y (axial) and x (tangential) axis respectively.

The set of equations based on the above assumptions was solved numerically and the recovery rate and the salt passage were determined. The accuracy of the mathematical

model was tested by a comparison with the experiments by Taniguchi[18]. An excellent agreement between calculation and experiment was found. It must be stated that the experimental data were for solutions with maximum concentration 2,000 ppm, so that the assumptions which have been made are reasonable. It is suspected that when the same model is applied for seawater (35,000 ppm) the calculated values could vary from the experimental ones.

Furthermore they tried to find the influence of the length/width ratio on the productivity, with the number of leaves as a parameter. They found that the volume specific productivity (permeate flow rate per unit volume), increases continuously with increasing packing density, (P_D), with a distinct maximum at $P_D = 3000 \text{ m}^2/\text{m}^3$. An increase of the volume specific productivity, however, is accompanied by a decrease of recovery rate, increasing pressure losses in both channels due to the decrease in channel height. Therefore an optimization concerning the packing density must be based on the product of the volume specific productivity and recovery ratio.

S.K. Guta[19] has suggested analytical design equations for tubular, spiral wound, flat and frames modules by using the solution diffusion model. In this analysis the pressure losses in both channels have been ignored as well as the concentration gradient along the membrane. His design equations are applicable for all values of J/k covering a complete range of laminar and turbulence flow. On the basis of this design equation, some simpler approximate design equations were also derived for solutions with negligible osmotic pressure or for small concentration polarization.

G. Schock and A. Miquel[20] have presented some experimental data for pressure drop and mass transfer characteristics in spiral wound elements and in spacer filled channels. Measurements on 2.5" elements from FilmTec, showed a pressure drop 0.2 bar/m for feed flow 600 lt/h and 0.8 bar/m for 1300 lt/h. For different brine spacers they suggested for the dimensionless friction parameter eq.(2.3).

$$\lambda = 6.23 \text{ Re}_f^{-0.3} \quad (2.3)$$

For the permeate spacer by using flat channel measurements they suggested eq.(2.4) for the permeate friction parameter.

$$\lambda' = a_{fr} \text{ Re}_p^{-0.8} \quad (2.4)$$

where, a_{fr} = constant depending on the type of spacer.

Although they managed to calculate mass transfer coefficients for flat membranes, they had severe problems to do the same with the spiral wound modules. As already has been mentioned the net driving pressure is different at every location of the leaf due to concentration and pressure gradients in both feed and permeate side. By using a computer programme, they found that the optimal number of leaves is almost independent of the driving pressure, concentration and water permeability coefficient.

R.L.C. Flemmer et al[21] have developed a mathematical model to describe the performance of spiral wound ultrafiltration modules with turbulence promoting nets. The validity of the final equation depends upon two principal assumptions; that the gel polarization model is valid and that eddy mass diffusivity is proportional to friction velocity. The model requires that certain constants must be evaluated from tests on filtration modules and thereafter a simple relation is available to predict performance at varying concentrations and flow rates, under conditions of gel polarization.

K.K. Sirkar et al[22] have developed simple analytical design equations to predict, for a given fractional water recovery, the average permeate solute concentration and the channel length of a spiral wound module for turbulent and laminar flow in the brine channel with spacer. For their calculations they have ignored the pressure losses and the concentration gradient along the membrane.

F. Evangelista and G. Jonsson[23] have derived simple explicit equations for the specific permeation rate of spiral wound modules with constant or tapered permeate channels. Taking into account the two dimensional character of the process the permeate flow rate was found analytically, ignoring the concentration gradient along the membrane. At the same time explicit relationships for optimum geometrical dimensions have been derived. This analytical method is in good agreement with experimental results at low feed concentrations given by Taniguchi[18].

Chiolle et al[31] have simulated a spiral wound module performance by using a computer programme and solving numerically the set of equations. They used hypothetical data for sea-water solution at 35,000 ppm, and for the mass transfer coefficient they have used an equation suggested by Winograd et al[25]. It is interesting to see that the predicted wall concentration at about 100 bar and recovery 5 %, is approximately 41,000 ppm at the inlet and increases linearly with the length of the membrane.

After this short literature review it is clear that as far as the analytical methods are

concerned, to take into account all the factors which can affect the performance of a spiral wound module is not an easy task. None of the analytical solutions available so far has taken into account all the factors, which has been mentioned in section 2.2.

CHAPTER III

AN ANALYTICAL SOLUTION

3.1 INTRODUCTION

In this work an analytical solution for the performance of a spiral wound module is presented. This analysis takes into account pressure losses in both permeate and brine channels, the effect of concentration polarization and the concentration gradient along the membrane in the axial direction.

A 'five parameter' model is introduced. These parameters are: k_{fb} (the brine friction parameter), k_{fp} (the permeate friction parameter), k (the mass transfer coefficient), k_1 (the water permeability coefficient), k_2 (the solute permeability coefficient). All five parameters will be found experimentally by using some explicit equations and when the values of these parameters have been determined, predictions can be made for the performance of the module in new operating conditions as well as suggestions for optimum module design for better performance. This analysis is based on the solution-diffusion model and some assumptions, which will be presented in the following sections.

3.2 FLUID FLOW THROUGH POROUS MEDIA

There are many important cases where a fluid flows through a porous material. For example, the movement of water through the ground or the filtration of a gas or a liquid. The exact analysis of this type of flow is not possible because the shape of the individual flow passages is so varied and so complex. However a number of approximate theories have been proposed, (Cozeny theory).

In 1856 Henry Darcy published experimental results from which he deduced what is known as Darcy's Law.

$$u_x = -\lambda_f \frac{\partial P}{\partial x} \quad (3.1)$$

where, u_x and P are the mean velocity and the pressure respectively in the x direction and λ_f is a constant at a given temperature for a particular fluid and porous medium.

The direct proportionality of u_x and $\partial P/\partial x$ is a characteristic of steady laminar flow. Further experiments have shown that the mean velocity is inversely proportional to the viscosity, μ , of a Newtonian fluid, and this result too is a characteristic of steady laminar flow. Equation (3.1) can be written as,

$$u_x = - \frac{\lambda'_f}{\mu} \frac{\partial P}{\partial x} \quad (3.2)$$

or,

$$\frac{\partial P}{\partial x} = - k_f \mu u_x \quad (3.3)$$

where, $k_f = 1/\lambda'_f$.

In the case of the spiral wound modules there is a porous spacer in the permeate channel so that the Darcy's Law can be applied. For the brine channel the spacer is not really a porous material but a "turbulence promoting" net, in order to increase the mass transfer and decrease the concentration polarization phenomena. Depending on the feed velocity the existence of the net can cause either turbulent or "chopped" laminar flow[24].

Solan et al[25] proposed that the concentration in the boundary layer starts developing at the beginning of each mesh step of length equal to the screen mesh size. After traversing the length equal to the screen mesh size, the concentration profile undergoes a sudden partial mixing at the location of the next screen wire beyond which the concentration profile starts developing again to repeat the process.

This saw-tooth development of laminar concentration boundary layer can be considered as a constant boundary layer thickness model, if one integrates the saw-tooth boundary layer over the screen mesh size. This is similar to assuming a constant non developing laminar mass transfer coefficient along the channel. This assumption is useful in developing analytical design equations for the spiral wound modules. If, due to a much higher feed velocity, turbulent flow mass transfer conditions exist in the brine feed channel, one can similarly assume a constant mass transfer coefficient with a significantly reduced degree of polarization. In this analysis Darcy's law was applied for both channels as a first approximation, though there are doubts whether the exponent of the velocity in the equation is unity or not[26].

3.3 CONCENTRATION POLARIZATION

The phenomenon of concentration polarization has been studied in detail and the effect of polarization on the membrane performance has been well understood. For most applications in R.O., relatively simple thin-film models have been found to predict the membrane performance quite well. The basic assumption of such models is that the resistance to the transfer of solute away from the membrane surface resides in a thin stagnant film next to the membrane surface, Fig.3.1.

In general the assumption of the thin boundary layer has been found to be reasonable provided that the Schmidt number ($Sc = \mu/\rho D$) is very small. In that case when a dynamic equilibrium has been established the rate of convective transfer of solute towards the surface of the membrane, $J (c_{bz} - c_p)$, must be at any point within the boundary layer equal to the rate of diffusion of solute back from the membrane, $-Ddc_{bz}/dz$. This means the establishment of a concentration gradient in the z direction, normal to the membrane surface, Fig.3.1.

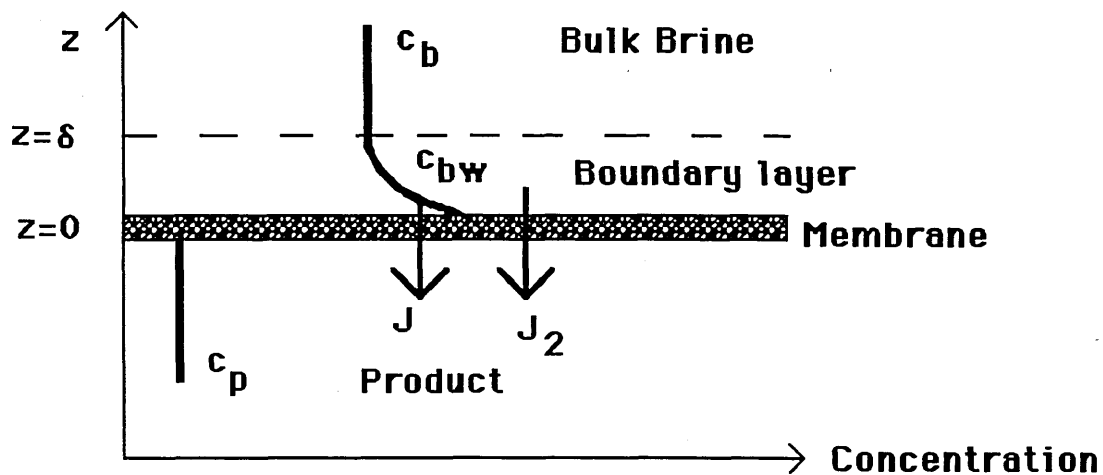


Fig.3.1 Thin-film model for mass transfer at membrane surface.

That is:

$$J (c_{bz} - c_p) = -D \frac{dc_{bz}}{dz} \quad (3.4)$$

where, J = Average volumetric flux, assumed to be constant at any point

c_{bz} = Solute concentration at height z

c_p = Permeate concentration

D = Diffusion coefficient of the solute.

By integration over the thin film thickness of δ , eq.(3.4) gives,

$$J \int_0^{\delta} dz = -D \int_{c_{bw}}^{c_b} \frac{dc_{bz}}{c_{bz} - c_p} \quad (3.5)$$

or,

$$J \delta = -D \ln \frac{c_b - c_p}{c_{bw} - c_p} \quad (3.6)$$

where,

c_b = Bulk feed concentration at each local point along the membrane.

c_{bw} = Concentration of the solute at the surface of the membrane.

Rearrangement of eq.(3.6) gives,

$$\frac{c_{bw} - c_p}{c_b - c_p} = e^{\frac{J \delta}{D}} \quad (3.7)$$

If it is further assumed that the thickness δ , is unaffected by the presence of the flux through the membrane and would be the same in the case of a solid wall, then δ can be related with the *convective mass transfer coefficient*, k , for the same solute under the same operating conditions, but at a solid wall. This assumption is questionable in this work and it will be discussed in section 5.3 in detail.

Since, $k = D/\delta$, equation (3.7) can be rewritten as,

$$\frac{c_{bw} - c_p}{c_b - c_p} = e^{\frac{J}{k}} \quad (3.8)$$

For a membrane with high rejection properties, as the membranes for sea-water, it can be assumed that $c_b \gg c_p$ and since $c_{bw} > c_b$, eq.(3.8) yields,

$$\frac{c_{bw}}{c_b} = e^{\frac{J}{k}} \quad (3.9)$$

The exponential term in eq.(3.9) can be expanded in a series form to give,

$$\frac{c_{bw}}{c_b} = 1 + \frac{J}{k} + \frac{1}{2!} \left(\frac{J}{k} \right)^2 + \frac{1}{3!} \left(\frac{J}{k} \right)^3 + \dots \quad (3.10)$$

Sirkar et al[22] showed that if $J/k \leq 0.2$ then the second-order and higher quantities can be neglected and eq.(3.10) gives,

$$\frac{c_{bw}}{c_b} = 1 + \frac{J}{k} \quad (3.11)$$

Although the ratio J/k is not known in advance for each membrane it is believed that for low feed concentration the concentration polarization is very small so that the k value is quite high and the ratio J/k quite small. On the other hand, for sea-water as feed solution the concentration polarization is relatively high, especially for high recovery. At the same time, because of the concentration polarization the flux decreases and the ratio J/k would be larger, but possibly near the critical value 0.2. However, as long as the ratio is smaller than one (1.0), the approximation that has been made is not unrealistic. The validity of this approximation could be checked by the ability of the final model to describe the membrane performance.

3.4 WATER PERMEABILITY COEFFICIENT, k_1

The following analysis is based on the idea that, when distilled water is used as feed solution, the effects of concentration polarization, concentration gradient and osmotic pressure have no meaning and they can be ignored. The basic assumptions for this analysis are summarized below:

- 1) Distilled water as feed solution.
- 2) Validity of Darcy' s law for permeate and brine channel.
- 3) Validity of the solution-diffusion model.
- 4) Unhindered flow of the locally produced permeate in the porous substructure of the assymetric or composite membrane.
- 5) Immediate and complete mixing of the locally produced permeate with the bulk flow in the permeate channel.
- 6) Module is made up of flat channels, with constant geometrical shape, Fig.3.2.

- 7) Constant fluid properties.
- 8) Negligible components of brine and permeate velocities along the y (tangential) and x (axial) axis respectively.
- 9) Negligible diffusive mass transport along the x (axial) and y (tangential) direction in both channels.

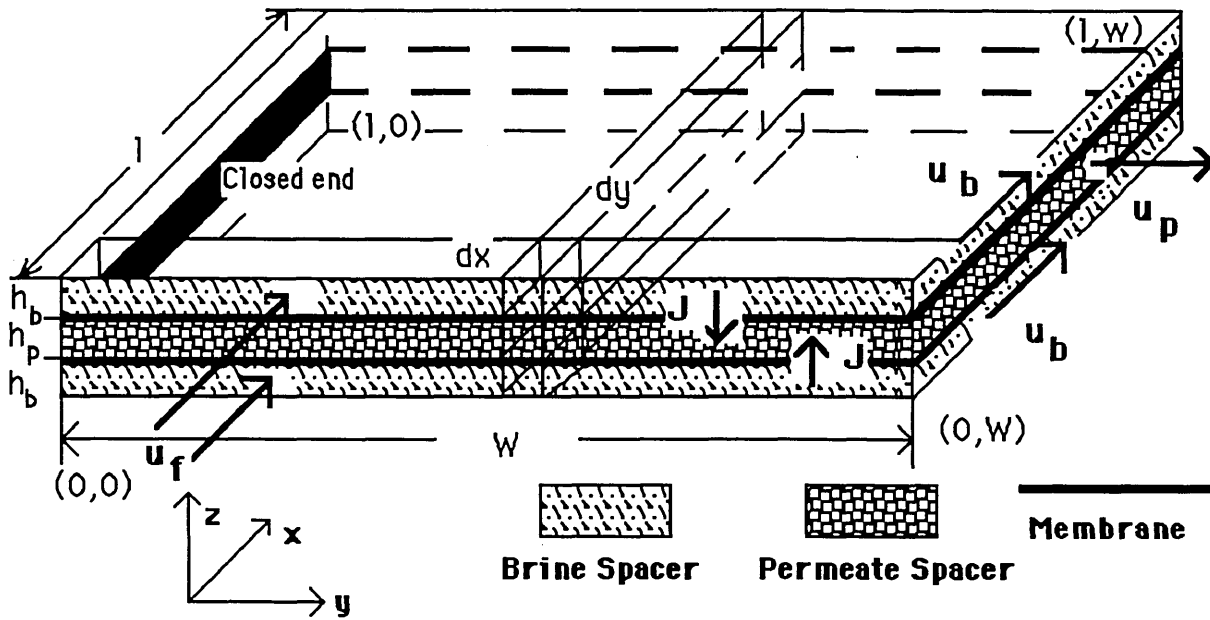


Fig.3.2 Unwound spiral-wound module. (Two brine channels and one permeate channel).

Fig.3.2 shows the volume elements in the feed and permeate channels for which the balances have to be formulated. The driving pressure in each point (x,y) is given by eq.(3.12), since there is no osmotic pressure effect.

$$\Delta P_{ef}(x,y) = P_b(x,y) - P_p(x,y) \quad (3.12)$$

where, $P_b(x,y)$ and $P_p(x,y)$ are the local pressures in the brine and the permeate channel respectively.

Accordingly the assumptions above, eq. (3.12) yields,

$$\frac{\partial \Delta P_{ef}(x,y)}{\partial y} = - \frac{dP_p(x,y)}{dy} \quad (3.13)$$

$$\frac{\partial \Delta P_{ef}(x,y)}{\partial x} = \frac{dP_b(x,y)}{dx} \quad (3.14)$$

If the volumetric flux, J , is used rather than the mass flux, J_1 , then eq.(1.4) gives,

$$J = \frac{k_1}{\rho} (\Delta P - \Delta \pi) \quad (3.15)$$

where, ρ = density

In two dimensions and ignoring $\Delta \pi$, eq.(3.15) can be rewritten as,

$$J(x,y) = k_1 \Delta P_{ef}(x,y) \quad (3.16)$$

$$\text{where, } k_1 = \frac{k_1}{\rho}$$

For the two different channels the following can be written.

Permeate channel

Mass balance

$$\frac{\partial u_p(x,y)}{\partial y} = \frac{2 J(x,y)}{h_p} \quad (3.17)$$

Momentum balance

$$\frac{dP_p(x,y)}{dy} = -k_{fp} \mu u_p(x,y) \quad (3.18)$$

Eqs (3.13) and (3.18) can give,

$$\frac{\partial \Delta P_{ef}(x,y)}{\partial y} = k_{fp} \mu u_p(x,y) \quad (3.19)$$

Division of eq.(3.19) by eq.(3.17) and using eq.(3.16) gives,

$$\frac{d\Delta P_{ef}(x,y)}{du_p(x,y)} = \frac{k_{fp} \mu u_p(x,y) h_p}{2k_1 \Delta P_{ef}(x,y)} \quad (3.20)$$

Rearrangement and integration yields,

$$u_p(x,y) = \left[\Delta P_{ef}^2(x,y) - \Delta P_{ef}^2(x,0) \right]^{1/2} \left[\frac{2 k_1}{k_{fp} \mu h_p} \right]^{1/2} \quad (3.21)$$

Eqs (3.19) and (3.21) yield,

$$\frac{d\Delta P_{ef}(x,y)}{dy} = \sqrt{\frac{2 k_1 k_{fp} \mu}{h_p}} \left[\Delta P_{ef}^2(x,y) - \Delta P_{ef}^2(x,0) \right]^{1/2} \quad (3.22)$$

By setting,

$$q = \sqrt{\frac{h_p}{2 k_1 k_{fp} \mu}} \quad (3.23)$$

eq.(3.22) can be integrated to give,

$$\frac{\Delta P_{ef}(x,y)}{\Delta P_{ef}(x,0)} = \cosh \frac{y}{q} \quad (3.24)$$

If the integration is carried out between the limits 0,w then eq.(3.25) is derived.

$$\frac{\Delta P_{ef}(x,w)}{\Delta P_{ef}(x,0)} = \cosh \frac{w}{q} \quad (3.25)$$

Division of eq.(3.24) by eq.(3.25) gives,

$$\Delta P_{ef}(x,y) = \Delta P_{ef}(x,w) \frac{\cosh \frac{y}{q}}{\cosh \frac{w}{q}} \quad (3.26)$$

If eq.(3.20) was integrated between the limits 0,w , then eq.(3.27) can be obtained.

$$u_p(x,w) = \sqrt{\frac{2 k_1}{k_{fp} \mu h_p}} \left[\Delta P_{ef}^2(x,w) - \Delta P_{ef}^2(x,0) \right]^{1/2} \quad (3.27)$$

or by using eq.(3.25),

$$u_p(x,w) = \sqrt{\frac{2 k_1}{k_{fp} \mu h_p}} \Delta P_{ef}(x,w) \tanh \frac{w}{q} \quad (3.28)$$

Equation (3.28) can be correlated with good approximation with the water volumetric flow rate, Q_p , eq.(3.29), to give eq.(3.30)

$$u_p(x,w) = u_p(x,y) = \frac{Q_p}{h_p l} \quad (3.29)$$

$$k_1 = \frac{Q_p^2 k_{fp} \mu}{2 h_p l^2 \Delta P_{ef}^2(x,w) \tanh^2 \frac{w}{q}} \quad (3.30)$$

Equation (3.30) can be used to calculate the k_1 values as long as the pressure drops in the brine channel can be ignored and the effective pressure is constant along the x axis. The k_1 values which are calculated by eq.(3.30) are always greater than those which are calculated by eq.(3.16), because by using eq.(3.16) we consider constant driving pressure along the membrane, $\Delta P_{ef}(x,w)$, which is the maximum driving pressure. Equation (3.30) considers the pressure drop in the permeate channel so that the driving pressure varies from a minimum value in the closed end to a maximum value, $\Delta P_{ef}(x,w)$. Consequently k_1 values calculated by eq.(3.30) will be closer to the true one.

Brine channel

Mass balance

$$\frac{\partial u_b(x,y)}{\partial x} = - \frac{2 J(x,y)}{h_b} \quad (3.31)$$

Momentum balance

$$\frac{dP_b(x,y)}{dx} = - k_{fb} \mu u_b(x,y) \quad (3.32)$$

A combination of eqs (3.32) and (3.14) gives,

$$\frac{\partial \Delta P_{ef}(x,y)}{\partial x} = - k_{fb} \mu u_b(x,y) \quad (3.33)$$

Eqs (3.33), (3.31) and (3.16) yield,

$$\frac{d\Delta P_{ef}(x,y)}{du_b(x,y)} = \frac{k_{fb} \mu u_b(x,y) h_b}{2k_1 \Delta P_{ef}(x,y)} \quad (3.34)$$

An integration of eq.(3.34) yields,

$$u_b(x,y) = \left\{ u_f^2 + \frac{2 k_1}{k_{fb} \mu h_b} [\Delta P_{ef}^2(x,y) - \Delta P_{ef}^2(0,y)] \right\}^{1/2} \quad (3.35)$$

Equation (3.35) is valid for every y, where $0 \leq y \leq w$, so it can be written as,

$$u_b(x,w) = \left\{ u_f^2 + \frac{2 k_1}{k_{fb} \mu h_b} [\Delta P_{ef}^2(x,w) - \Delta P_{ef}^2(0,w)] \right\}^{1/2} \quad (3.36)$$

Eq.(3.33) and eq.(3.36) yield,

$$\frac{d\Delta P_{ef}(x,w)}{dx} = -k_{fb}\mu \left\{ u_f^2 + \frac{2k_1}{k_{fb}\mu h_b} [\Delta P_{ef}^2(x,w) - \Delta P_{ef}^2(0,w)] \right\}^{1/2} \quad (3.37)$$

or,

$$\frac{d\Delta P_{ef}(x,w)}{dx} = - \left\{ k_{fb}^2 \mu^2 u_f^2 + \Delta P_{ef}^2(x,w) \frac{2k_1 k_{fb}\mu}{h_b} - \frac{2k_1 k_{fb}\mu}{h_b} \Delta P_{ef}^2(0,w) \right\}^{1/2} \quad (3.38)$$

or,

$$\frac{d\Delta P_{ef}(x,w)}{dx} = - \sqrt{\frac{2k_1 k_{fb}\mu}{h_b}} \left\{ \frac{k_{fb} h_b \mu}{2k_1} u_f^2 - \Delta P_{ef}^2(0,w) + \Delta P_{ef}^2(x,w) \right\}^{1/2} \quad (3.39)$$

By setting,

$$\frac{2k_1 k_{fb}\mu}{h_b} = a^2 \quad \text{and} \quad \frac{2k_1}{k_{fb}\mu h_b} = b^2 \quad (3.40)$$

eq.(3.39) can give,

$$\frac{d\Delta P_{ef}(x,w)}{dx} = -a \left[u_f^2 / b^2 - \Delta P_{ef}^2(0,w) + \Delta P_{ef}^2(x,w) \right]^{1/2} \quad (3.41)$$

Equation (3.41) can be integrated to give eq.(3.42),

$$\Delta P_{ef}(x,w) = \frac{b \Delta P_{ef}^2(0,w) \cosh(ax) - \frac{u_f^2 \sinh(ax)}{b} + \Delta P_{ef}(0,w) u_f e^{-ax}}{b \Delta P_{ef}(0,w) + u_f} \quad (3.42)$$

Equations (3.26) and (3.42) can give the analytical form for the effective pressure in every point (x,y).

$$\Delta P_{ef}(x,y) = \frac{b \Delta P_{ef}^2(0,w) \cosh(ax) \frac{u_f^2 \sinh(ax)}{b} + \Delta P_{ef}(0,w) u_f e^{-ax}}{b \Delta P_{ef}(0,w) + u_f} \frac{\cosh \frac{y}{q}}{\cosh \frac{w}{q}} \quad (3.43)$$

Equation (3.43) can be integrated to give the average volumetric flux, J,

$$J = \frac{\int_0^w \int_0^l k_1 \Delta P_{ef}(0,w) dy dx}{w l} \quad (3.44)$$

After integration we can have,

$$J = \frac{k_1 q \tanh \frac{w}{q} \left\{ b \Delta P_{ef}^2(0,w) \sinh(al) + \frac{u_f^2}{b} [1 - \cosh(al)] + \Delta P_{ef}(0,w) u_f [1 - e^{-al}] \right\}}{a w l [b \Delta P_{ef}(0,w) + u_f]} \quad (3.45)$$

Equation (3.45) can be solved numerically to find k_1 values for a spiral wound module taking into account the pressure losses in both channels. It is obvious that the membrane has been considered with uniform properties so that k_1 is the same at any point on the membrane surface. As it can be seen in eqs (3.45) or (3.30), for calculating the k_1 value the friction parameters in permeate and the brine channel or the permeate channel respectively are needed. It can be concluded from the presented equation and for those that will follow that it is impossible to separate the k_1 from the friction parameters as long as the experiments are carried out with a complete spiral wound module. A high k_1 value can be compensated by high friction parameters. Two solutions can be applied to this problem:

1) A first approximation can be made for the k_1 value and from which value the friction parameters can be calculated, as it will be shown below. These friction parameters can be used to calculate k_1 with better accuracy. With successive iterations the k_1 value will approach closer to the true k_1 value as more the iterations are.

2) If the true k_1 value is found independently with different experiments then the friction parameters can be calculated.

Eq. (3.45) can be verified by using the experimental data for ROGA spiral wound module^[18], see Table 3.1.

Table 3.1
k₁ values for ROGA-4160 module.

P (Atm)	k ₁ (cm/sec Atm) by Taniguchi	k ₁ (cm/sec Atm) by eq.3.45	k ₁ (cm/sec Atm) By Evagelista ^[27]
34.8	2.088x10 ⁻⁵	2.067x10 ⁻⁵	2.085x10 ⁻⁵
28.0	2.142x10 ⁻⁵	2.136x10 ⁻⁵	2.085x10 ⁻⁵

At the same time, using these data and the pressures in the permeate channel suggested by Evagelista^[27], the friction parameters were found: **k_{fb}=168,240 cm⁻²**, **k_{fp}=616,740 cm⁻²** , at 34.8 Atm and **k_{fb}=176,040 cm⁻²**, **k_{fp}=518,440 cm⁻²**, at 28 Atm. Evagelista^[27] have found them to be **k_{fb}=183,673 cm⁻²**, **k_{fp}=744,444 cm⁻²**.

3.5 FRICTION PARAMETERS FOR THE BRINE AND PERMEATE CHANNEL

The following procedure assumes that the k₁ value is known, either as the true value or as a first approximation to the true value.

Brine friction parameter, k_{fb}

Equation (3.34) can be integrated between the limits 0,l to give eq.(3.46)

$$\Delta P_{ef}^2(l,y) - \Delta P_{ef}^2(0,y) = \frac{k_{fb} \mu h_b}{2 k_1} [u_b^2(l,y) - u_f^2] \quad (3.46)$$

Equation (3.46) is valid for every y, where 0 ≤ y ≤ w, so it can be written as,

$$\Delta P_{ef}^2(l,w) - \Delta P_{ef}^2(0,w) = \frac{k_{fb} \mu h_b}{2 k_1} [u_b^2(l,w) - u_f^2] \quad (3.47)$$

and since approximately,

$$u_b(l,w) = u_b(l,y) = \frac{Q_b}{h_b w} \quad (3.48)$$

eq.(3.47) gives,

$$\Delta P_{ef}^2(0,w) - \Delta P_{ef}^2(l,w) = \frac{k_{fb} \mu}{2 k_1 w^2 h_b} [Q_f^2 - Q_b^2] \quad (3.49)$$

Eq.(3.49) correlates experimental data with the friction parameter and the k_1 , and it can be solved to give the k_{fb} values.

$$k_{fb} = \frac{2 k_1 w^2 h_b}{\mu} \frac{\Delta P_{ef}^2(0,w) - \Delta P_{ef}^2(l,w)}{Q_f^2 - Q_b^2} \quad (3.50)$$

Permeate Friction parameter, k_{fp}

If the same procedure is applied for the permeate channel, one can get by using eq.(3.20).

$$u_p^2(x,w) = \frac{2 k_1}{k_{fp} \mu h_p} [\Delta P_{ef}^2(x,w) - \Delta P_{ef}^2(x,0)] \quad (3.51)$$

or,

$$u_p^2(0,w) = \frac{2 k_1}{k_{fp} \mu h_p} [\Delta P_{ef}^2(0,w) - \Delta P_{ef}^2(0,0)] \quad (3.52)$$

or by using eq.(3.29),

$$\Delta P_{ef}^2(0,w) - \Delta P_{ef}^2(0,0) = \frac{k_{fp} \mu}{2 k_1 l^2 h_p} Q_p^2 \quad (3.53)$$

or,

$$k_{fp} = \frac{2 k_1 l^2 h_p}{\mu} \frac{\Delta P_{ef}^2(0,w) - \Delta P_{ef}^2(0,0)}{Q_p^2} \quad (3.54)$$

3.6 MASS TRANSFER COEFFICIENT, k

In this section an analytical solution for the water flux through the membrane for sea water as feed solution will be found. This analysis is based on the following assumptions:

- 1) Validity of Darcy' s law for permeate and brine channel.
- 2) Validity of the solution-diffusion model.
- 3) Validity of the thin film theory, with a mass transfer coefficient depending on the water flux.
- 4) Unhindered flow of the locally produced permeate in the porous substructure of the assymmetric or composite membrane.
- 5) Immediate and complete mixing of the locally produced permeate with the bulk flow in the permeate channel, so that a uniform permeate concentration can be assumed.
- 6) Module is made up of flat channels, with constant geometrical shape, Fig.3.2.
- 7) Constant fluid properties.
- 8) Negligible components of brine and permeate velocities along the y (tangential) and x (axial) axis respectively.
- 9) Negligible diffusive mass transport along the x and y direction in both channels.
- 10) For membranes for sea-water with high rejection properties, the permeate concentration can be ignored compared with the feed concentration. However, it must be stated that the same procedure can be applied even when the permeate concentration is high. In that case the difference in concentration and osmotic pressure between the feed and the permeate side must be considered, in other words eq.(3.55) can be used.

$$c_b'(x,y) = c_b(x,y) - c_p(x,y) \quad (3.55)$$

When salt solution is fed to the membrane the effective pressure at each point of the membrane will be given by eq.(3.56).

$$\Delta P_{ef}(x,y) = P_b(x,y) - P_p(x,y) - \pi_{bw}(x,y) + \pi_p(x,y) \quad (3.56)$$

If a membrane with high rejection is considered, then $\pi_{bw}(x,y) \gg \pi_p(x,y)$, because $c_{bw}(x,y) \gg c_p(x,y)$ and eq.(3.56) is transformed to eq.(3.57).

$$\Delta P_{ef}(x,y) = P_b(x,y) - P_p(x,y) - \pi_{bw}(x,y) \quad (3.57)$$

These assumptions lead to the following equations,

$$\frac{\partial \Delta P_{ef}(x,y)}{\partial y} = - \frac{dP_p(x,y)}{dy} \quad (3.58)$$

$$\frac{\partial (\Delta P_{ef}(x,y) + \pi_{bw}(x,y))}{\partial x} = \frac{dP_b(x,y)}{dx} \quad (3.59)$$

Permeate channel

As it can be seen from eq.(3.58), the analysis, which has been made for the pure water for the permeate channel, is applicable for salt water since osmotic pressure is assumed not to change in the y direction. So eq.(3.26) can be derived.

$$\Delta P_{ef}(x,y) = \Delta P_{ef}(x,w) \frac{\cosh \frac{y}{q}}{\cosh \frac{w}{q}} \quad (3.26)$$

where,

$$q = \sqrt{\frac{h_p}{2 k_1 k_{fp} \mu}} \quad (3.23)$$

The ability to find an analytical solution relies entirely on finding the analytical form for $\Delta P_{ef}(x,w)$. An attempt to do this is made below.

Brine channel

Solvent material balance

$$\frac{\partial u_b(x,y)}{\partial x} = - \frac{2 J(x,y)}{h_b} \quad (3.31)$$

Momentum balance

$$\frac{dP_b(x,y)}{dx} = -k_{fb} \mu u_b(x,y) \quad (3.32)$$

Solute material balance

$$\frac{\partial c_b(x,y)}{\partial x} = \frac{2 J(x,y)}{u_b(x,y) h_b} [c_b(x,y) - c_p(x,y)] \quad (3.60)$$

According to what has been mentioned above eq.(3.60) is simplified to eq.(3.61).

$$\frac{\partial c_b(x,y)}{\partial x} = \frac{2 J(x,y)}{u_b(x,y) h_b} c_b(x,y) \quad (3.61)$$

Division of eq.(3.31) by eq.(3.61) will give,

$$\frac{du_b(x,y)}{dc_b(x,y)} = - \frac{u_b(x,y)}{c_b(x,y)} \quad (3.62)$$

or

$$\frac{du_b(x,w)}{dc_b(x,w)} = - \frac{u_b(x,w)}{c_b(x,w)} \quad (3.63)$$

Integration of eq.(3.63) results in

$$u_b(x,w) = \frac{c_f}{c_b(x)} u_f \quad (3.64)$$

where $c_f = c_b(0)$

A combination of eqs (1.1), (3.11) and (3.56) can give,

$$\frac{\partial P_b(x,y)}{\partial x} = \left[1 + \frac{\sigma k_1}{k} c_b(x) \right] \frac{\partial \Delta P_{ef}(x,y)}{\partial x} + \left[1 + \frac{\sigma k_1}{k} \Delta P_{ef}(x,y) \right] \frac{\partial c_b(x)}{\partial x} \quad (3.65)$$

or by using eq.(3.32)

$$-k_{fb} \mu u_b(x,y) = \left[1 + \frac{\sigma k_1}{k} c_b(x) \right] \frac{\partial \Delta P_{ef}(x,y)}{\partial x} + \left[1 + \frac{\sigma k_1}{k} \Delta P_{ef}(x,y) \right] \frac{\partial c_b(x)}{\partial x} \quad (3.66)$$

Eqs (3.66), (3.64) and (3.61) give,

$$\left[1 + \frac{\sigma k_1}{k} c_b(x) \right] \frac{\partial \Delta P_{ef}(x,y)}{\partial c_b(x)} + 1 + \frac{\sigma k_1}{k} \Delta P_{ef}(x,y) = - \frac{k_{fb} c_b^2(0,y) u_b^2(0,y) h_b}{2k_1 \Delta P_{ef}(x,y) c_b^2(x)} \quad (3.67)$$

If eq.(3.67) could be solved analytically, then, by using that solution and eqs (3.26), (3.64) and (3.66), an analytical form for the driving pressure could be found. Unfortunately life is not so simple and the differential equation (3.67) cannot be solved, at least analytically.

In order to overcome this difficulty one more assumption has to be made. It can be assumed that the brine concentration varies linearly with the distance in the axial direction. See eq.(3.68) below. There is also a small variation of the brine concentration in the y direction. This variation though has been ignored.

$$c_b(x) = c_f + f x \quad (3.68)$$

$$\text{where, } f = \frac{c_b(l) - c_f}{l}$$

This is realistic taking into account that, in normal operating conditions, the difference in concentration between the inlet and the outlet is not great.

Eqs (3.64) and (3.68) give the brine velocity as a function of the distance,

$$u_b(x,w) = \frac{c_f u_f}{c_f + f x} \quad (3.69)$$

Eqs (3.56) and (3.59) yield,

$$\frac{\partial(\Delta P_{ef}(x,y) + \pi_{bw}(x,y))}{\partial x} = -k_{fb} \mu u_b(x,y) \quad (3.70)$$

A combination of eqs (1.1), (3.11), (3.16), (3.68), (3.69) and (3.70) results in,

$$\begin{aligned} \frac{d\Delta P_{ef}(x,y)}{dx} + \varnothing \left[1 + \frac{k_1 \Delta P_{ef}(x,y)}{k} \right] \frac{d(c_f + fx)}{dx} + \varnothing \frac{k_1}{k} (c_f + fx) \frac{d\Delta P_{ef}(x,y)}{dx} = \\ = - \frac{c_f u_f k_{fb} \mu}{c_f + fx} \end{aligned} \quad (3.71)$$

or,

$$\frac{d\Delta P_{ef}(x,y)}{dx} + \frac{\frac{f\varnothing k_1}{k}}{1 + \frac{k_1}{k} \varnothing (c_f + fx)} \Delta P_{ef}(x,y) = - \frac{\frac{c_f u_f k_{fb} \mu}{c_f + fx} + \varnothing f}{1 + \frac{k_1}{k} \varnothing (c_f + fx)} \quad (3.72)$$

Equation (3.72) is a linear, $(dy/dx + A(x)y = B(x))$, differential equation, and the general solution is given by the formula,

$$y = e^{-\int A(x)dx} \left[c + \int B(x) e^{\int A(x)dx} dx \right] \quad (3.73)$$

The integrals can be calculated as,

$$\int A(x)dx = \ln \left[1 + \frac{k_1}{k} \varnothing (c_f + fx) \right]$$

$$e^{\int A(x) dx} = \left[1 + \frac{k_1}{k} \varnothing (c_f + fx) \right]$$

$$e^{-\int A(x) dx} = \frac{1}{1 + \frac{k_1}{k} \varnothing (c_f + fx)}$$

$$\int B(x) e^{\int A(x) dx} dx = \frac{c_f u_f k_{fb} \mu}{f} \ln \frac{1}{c_f + fx} - \varnothing fx$$

By using the above integrals eq.(3.73) becomes,

$$\Delta P_{ef}(x,y) = \frac{1}{1 + \frac{k_1}{k} \varnothing (c_f + fx)} \left\{ C + \frac{c_f u_f k_{fb} \mu}{f} \ln \frac{1}{c_f + fx} - \varnothing fx \right\} \quad (3.74)$$

The constant C can be calculated by the boundary conditions, for $x=0$, $\Delta P_{ef}(x,y) = \Delta P_{ef}(0,y)$ and the final formula giving the effective pressure in the x direction is given by eq.(3.75).

$$\Delta P_{ef}(x,y) = \frac{1}{1 + \frac{k_1}{k} \varnothing (c_f + fx)} \left\{ \Delta P_{ef}(0,y) \left[1 + \frac{k_1 \varnothing c_f}{k} \right] + \frac{c_f u_f k_{fb} \mu}{f} \ln \frac{c_f}{c_f + fx} - \varnothing fx \right\} \quad (3.75)$$

Eq.(3.75) is valid for every $0 \leq y \leq w$ so it can be written as,

$$\Delta P_{ef}(x,w) = \frac{1}{1 + \frac{k_1}{k} \varnothing (c_f + fx)} \left\{ \Delta P_{ef}(0,w) \left[1 + \frac{k_1 \varnothing c_f}{k} \right] + \frac{c_f u_f k_{fb} \mu}{f} \ln \frac{c_f}{c_f + fx} - \varnothing fx \right\} \quad (3.76)$$

Eqs (3.26) and (3.76) can give the analytical form for the driving pressure,

$$\Delta P_{ef}(x,y) = \frac{1}{1 + \frac{k_1}{k} \phi (c_f + fx)} \left\{ \Delta P_{ef}(0,w) \left[1 + \frac{k_1 \phi c_f}{k} \right] + \frac{c_u k_{fb} \mu}{f} \ln \frac{c_f}{c_f + fx} - \phi fx \right\} \frac{\cosh \frac{y}{q}}{\cosh \frac{w}{q}} \quad (3.77)$$

Equation (3.77) can be integrated, to give the average volumetric flux, J,

$$J = \int_0^l \int_0^w \frac{k_1}{w l} \frac{1}{1 + \frac{k_1}{k} \phi (c_f + fx)} \left\{ \Delta P_{ef}(0,w) \left[1 + \frac{k_1 \phi c_f}{k} \right] + \frac{c_u k_{fb} \mu}{f} \ln \frac{c_f}{c_f + fx} - \phi fx \right\} \frac{\cosh \frac{y}{q}}{\cosh \frac{w}{q}} dx dy \quad (3.78)$$

If the integration of eq.(3.78) is carried out by parts we can have,

$$\int_0^w \frac{\cosh \frac{y}{q}}{\cosh \frac{w}{q}} dy = q \tanh \frac{w}{q}$$

$$\int_0^l \frac{\Delta P_{ef}(0,w) \left[1 + \frac{k_1 \phi c_f}{k} \right]}{1 + \frac{k_1}{k} \phi (c_f + fx)} dx = \frac{\Delta P_{ef}(0,w) [k + k_1 \phi c_f]}{k_1 \phi f} \ln \frac{k + k_1 \phi c_b(l)}{k + k_1 \phi c_f}$$

$$\int_0^l \frac{\phi f x}{1 + \frac{k_1}{k} \phi (c_f + fx)} dx = \frac{k^2}{k_1^2 \phi f} \left\{ \frac{k_1}{k} \phi [c_b(l) - c_f] + \left[1 + \frac{k_1}{k} \phi c_f \right] \left[\ln \frac{k + k_1 \phi c_f}{k + k_1 \phi c_b(l)} \right] \right\}$$

$$\int_0^l \frac{c_f u_f k_{fb} \mu}{f} \frac{\ln \frac{c_f}{c_f + fx}}{1 + \frac{k_1}{k} \theta (c_f + fx)} dx = \frac{c_f u_f k_{fb} \mu k}{f^2 k_1 \theta} \left[\frac{k_1 \theta}{k} (c_b(l) - c_f) - \ln \frac{c_b(l)}{c_f} \ln \left[1 + \frac{k_1 \theta c_b(l)}{k} \right] - \frac{k_1^2 \theta^2}{4 k^2} [c_b^2(l) - c_f^2] \right]$$

$$\text{if, } \left[\frac{k_1 \theta c_f}{k} \right]^2 < 1$$

or,

$$\int_0^l \frac{c_f u_f k_{fb} \mu}{f} \frac{\ln \frac{c_f}{c_f + fx}}{1 + \frac{k_1}{k} \theta (c_f + fx)} dx = \frac{c_f u_f k_{fb} \mu k}{f^2 k_1 \theta} \left\{ \frac{[\ln \frac{k_1 \theta c_b(l)}{k}]^2}{2} + \frac{k}{k_1 \theta c_f} - \frac{k}{k_1 \theta c_b(l)} - \ln \frac{c_b(l)}{c_f} \ln \left[1 + \frac{k_1 \theta c_b(l)}{k} \right] - \frac{[\ln \frac{k_1 \theta c_f}{k}]^2}{2} \right\}$$

$$\text{if, } \left[\frac{k_1 \theta c_f}{k} \right]^2 > 1$$

At this stage it must be stated that for the membranes available so far for sea-water and for reasonable operating pressures the ratio $k_1 \theta c_f / k$ is always less than one, so that only first solution of the last integral has practical use.

A substitution of the above integrals to eq.(3.78) gives eq.(3.79).

$$J = \frac{q \tanh \frac{W}{q}}{\theta f w l} \left\{ (k + k_1 \theta c_f) \ln \frac{k + k_1 \theta c_b(l)}{k + k_1 \theta c_f} \left[\Delta P_{ef}(0, w) + \frac{k}{k_1} \right] - k \theta [c_b(l) - c_f] + \frac{u_f c_f k_{fb} \mu}{f} \left[k_1 \theta (c_b(l) - c_f) - k \ln \frac{c_b(l)}{c_f} \ln \frac{k + k_1 \theta c_b(l)}{k} - \frac{k_1^2 \theta^2}{4 k} (c_b^2(l) - c_f^2) \right] \right\} \quad (3.79)$$

Equation (3.79) can give the flux for a spiral wound module for sea-water as a feed solution. In this analysis the change in the feed concentration and the concentration polarization effect as well as the pressure losses in the channels have been taken into account. Eq.(3.79) is an explicit relation to describe the performance of any spiral wound module for sea water with high rejection. If the permeate concentration has been taken into account then eq.(3.79) can be transformed to eq.(3.80).

$$J = \frac{q \tanh \frac{w}{l}}{\delta f w l} \left\{ [k+k_1 \delta (c_f - c_p)] \ln \frac{k+k_1 \delta (c_b(l) - c_p)}{k+k_1 \delta (c_f - c_p)} \left[\Delta P_{ef}(0, w) + \frac{k}{k_1} \right] - \right. \\ \left. -k \delta [c_b(l) - c_f] + \frac{u_f (c_f - c_p) k_{fb} \mu}{f} \left[k_1 \delta (c_b(l) - c_f) - k \ln \frac{c_b(l) - c_p}{c_f - c_p} \right. \right. \\ \left. \left. \ln \frac{k+k_1 \delta (c_b(l) - c_p)}{k} - \frac{k_1^2 \delta^2}{4k} (c_b^2(l) - c_f^2) \right] \right\} \quad (3.80)$$

The value of $\Delta P_{ef}(0, w)$ can be found by using eq.(3.55) as,

$$\Delta P_{ef}(0, w) = P_b(0, w) - P_p(0, w) - \pi_{bw}(0, w) + \pi_p(0, w) \quad (3.81)$$

or,

$$\Delta P_{ef}(0, w) = P_b(0, w) - P_p(0, w) - \delta c_f [1 + J(0, w)/k] + \delta c_p \quad (3.82)$$

and finally $\Delta P_{ef}(0, w)$ will be given by eq.(3.83).

$$\Delta P_{ef}(0, w) = \frac{[P_b(0, w) - P_p(0, w) - (c_f - c_p) \delta] k}{k + \delta c_f k_1} \quad (3.83)$$

A combination of eqs (3.80) and (3.83) yields,

$$J = \frac{q \tanh \frac{w}{l}}{\delta f w l} \left\{ [k+k_1 \delta (c_f - c_p)] \ln \frac{k+k_1 \delta (c_b(l) - c_p)}{k+k_1 \delta (c_f - c_p)} \left[\frac{[\Delta P - (c_f - c_p) \delta] k}{k + \delta c_f k_1} + \frac{k}{k_1} \right] - \right. \\ \left. -k \delta [c_b(l) - c_f] + \frac{u_f (c_f - c_p) k_{fb} \mu}{f} \left[k_1 \delta (c_b(l) - c_f) - k \ln \frac{c_b(l) - c_p}{c_f - c_p} \right. \right. \\ \left. \left. \ln \frac{k+k_1 \delta (c_b(l) - c_p)}{k} - \frac{k_1^2 \delta^2}{4k} (c_b^2(l) - c_f^2) \right] \right\}$$

$$\ln \left[\frac{k+k_1 \phi (c_b(l)-c_p)}{k} - \frac{k_1^2 \phi^2}{4k} (c_b^2(l)-c_f^2) \right] \} \quad (3.84)$$

where, $\Delta P = P_b(0,w) - P_p(0,w)$

Eq.(3.84) can be simplified by introducing the following dimensionless parameters to eq.(3.86).

$$\frac{k+k_1 \phi [c_b(l)-c_p]}{k+k_1 \phi (c_f-c_p)} = \gamma, \quad \frac{k+k_1 \phi [c_b(l)-c_p]}{k} = \lambda, \quad \frac{c_b(l)-c_p}{c_f-c_p} = \xi$$

$$\frac{k+k_1 \phi [c_f-c_p]}{k} = \frac{\lambda}{\gamma} = \theta, \quad \frac{k+k_1 \phi [c_b(l)-c_p]}{k} = \lambda \left[1 - \frac{1}{\gamma} \right] = \phi \quad (3.85)$$

$$J = \frac{q k \tanh \frac{w}{q}}{w l \phi f} \left\{ [\Delta P - (c_f - c_p) \phi] \ln \gamma - \frac{k}{k_1} [\phi - \theta \ln \gamma] + \frac{(c_f - c_p) u_f k_{fb} \mu}{f} [\phi - \ln \xi \ln \lambda - \frac{k_1^2 \phi^2}{k^2} (c_b^2(l) - c_p^2)] \right\} \quad (3.86)$$

This analytical solution could be used to predict optimum structure and dimensions for the module so that the maximum flux could be achieved. Eq.(3.86) can also be solved numerically to give the k values.

3.7 SOLUTE PERMEABILITY COEFFICIENT, k_2

The salt flux at every point (x,y) in the two dimensional plane will be given by eq.(3.87).

$$J_2(x,y) = k_2 [c_{bw}(x,y) - c_p(x,y)] \quad (3.87)$$

The permeate concentration can be considered as constant and the feed concentration at the wall can be expressed by using eq.(3.12).

$$J_2(x,y) = k_2 \left[c_b(x,y) \left[1 + \frac{J(x,y)}{k} \right] - c_p \right] \quad (3.88)$$

Eqs (3.68), and (3.88) can give,

$$J_2(x,y) = k_2 \left[c_f + fx - c_p + \frac{k_1}{k} [c_f + fx] \Delta P_{ef}(x,y) \right] \quad (3.89)$$

Eqs (3.77) and (3.89) can give the analytical form for the salt flux for every point (x,y).

$$J_2(x,y) = k_2 \left[c_f + fx - c_p + \frac{k_1 (c_f + fx)}{k + k_1 \phi (c_f + fx)} \left\{ \Delta P_{ef}(0,w) \left[1 + \frac{k_1 \phi c_f}{k} + \frac{c_u k_f \mu}{f} \ln \frac{c_f}{c_f + fx} - \phi fx \right] \frac{\cosh \frac{y}{q}}{\cosh \frac{w}{q}} \right\} \right] \quad (3.90)$$

Eq.(3.90) can be integrated to give the average salt flux,

$$J_2 = \frac{\int_0^l \int_0^w J_2(x,y) dx dy}{w l} \quad (3.91)$$

If the integration is carried out in parts one can get,

$$\int_0^w \frac{\cosh \frac{y}{q}}{\cosh \frac{w}{q}} dy = q \tanh \frac{w}{q}$$

$$\int_0^l (c_f - c_p + fx) dx = [c_f - c_p] l + \frac{fl^2}{2}$$

$$\int_0^l \frac{k_1 \Delta P_{ef}(0, w)}{k} [k+k_1 \varnothing c_f] \frac{c_f+fx}{k+k_1 \varnothing (c_f+fx)} dx = \frac{\Delta P_{ef}(0, w) [k+k_1 \varnothing c_f]}{k f k_1 \varnothing^2} \left\{ k_1 \varnothing \Delta c - k \ln \frac{k+k_1 \varnothing c_b(l)}{k+k_1 \varnothing c_f} \right\}$$

$$\int_0^l \frac{k_1 \varnothing f x (c_f+fx)}{k+k_1 \varnothing (c_f+fx)} dx = \frac{1}{2k_1^2 \varnothing^2 f} \left\{ 2k[k+k_1 \varnothing c_f] \ln \frac{k+k_1 \varnothing c_b(l)}{k+k_1 \varnothing c_f} - k_1 \varnothing \Delta c [2k-k_1 \varnothing \Delta c] \right\}$$

$$\int_0^l \frac{k_1 [c_f+fx]}{k+k_1 \varnothing [c_f+fx]} \frac{c_f u_f k_{fb} \mu}{f} \ln \frac{c_f}{c_f+fx} dx = \frac{c_f u_f k_{fb} \mu \ln \frac{c_b(l)}{c_f}}{f^2 \varnothing^2 k_1} \left[k \ln \frac{k+k_1 \varnothing c_b(l)}{k} k_1 \varnothing c_b(l) + \frac{k_1^2 \varnothing^2}{4k} [c_b^2(l) - c_f^2] \right]$$

$$\text{if, } \left[\frac{k_1 \varnothing c_b(l)}{k} \right]^2 < 1$$

or,

$$\int_0^l \frac{k_1 [c_f+fx]}{k+k_1 \varnothing [c_f+fx]} \frac{c_f u_f k_{fb} \mu}{f} \ln \frac{c_f}{c_f+fx} dx = \frac{c_f u_f k_{fb} \mu k}{f^2 \varnothing^2 k_1} \left\{ \ln \frac{c_b(l)}{c_f} \left[\ln \frac{k+k_1 \varnothing c_b(l)}{k} - \ln \frac{k_1 \varnothing \sqrt{c_f c_b(l)}}{k} \right] - \frac{k}{k_1 \varnothing} \left[\frac{1}{c_f} - \frac{1}{c_b(l)} \right] - \frac{k_1 \varnothing c_f}{k} \left[\frac{c_b(l)}{c_f} \left[\ln \frac{c_b(l)}{c_f} - 1 \right] + 1 \right] \right\}$$

$$\text{if, } \left[\frac{k_1 \varnothing c_f}{k} \right]^2 > 1$$

Again the second solution of the last integral can be ignored, so that the analytical solution for the average salt flux will be given by eq.(3.92).

$$J_2 = \frac{k_2}{w l} \left\{ (c_f - c_p) w l + \frac{f l^2 w}{2} + \frac{q \tanh \frac{w}{q}}{k_1 f \theta^2 k} \left[k_1 \theta (c_b(l) - c_f) [\Delta P_{ef}(0, w) (k + k_1 \theta c_f) + \frac{k^2}{k_1} - \frac{k \theta (c_b(l) - c_f)}{2}] - k (k + k_1 \theta c_f) \ln \frac{k + k_1 \theta c_b(l)}{k + k_1 \theta c_f} [\Delta P_{ef}(0, w) + \frac{k}{k_1}] + \frac{k c_f u_f k_{fb} \mu \ln \frac{c_b(l)}{c_f}}{f} [k \ln \frac{k + k_1 \theta c_b(l)}{k} - k_1 \theta c_b(l) + \frac{k_1^2 \theta^2}{4 k} (c_b^2(l) - c_f^2)] \right] \right\} \quad (3.92)$$

The salt flux can be related with the water flux, J, by eq.(3.93).

$$J_2 = J c_p \quad (3.93)$$

By combining eqs (3.92) and (3.93) an analytical solution to determine the k_2 values can be found. When the k_2 value has been determined then eq.(3.92) can be used to predict the quality of the produced water. If the permeate concentration has been taken into account, eq.(3.92) can be written by using the dimensionless parameters, see eq.(3.85), and eq.(3.83), as

$$J_2 = \frac{k_2}{w l} \left\{ [c_f - c_p] w l + \frac{f l^2 w}{2} + \frac{q k \tanh \frac{w}{q}}{f k_1 \theta^2} \left[(\Delta P - c_f \theta) (\varphi - \ln \gamma - 1) - \frac{k}{2 k_1} (2 \theta \ln \gamma + \varphi^2 - 4 \varphi + 3) + \frac{c_f u_f k_{fb} \mu \ln \xi}{f} [\ln \lambda - \lambda + 1 + \frac{k_1^2 \theta^2}{4 k^2} (c_b^2(l) - c_f^2)] \right] \right\} \quad (3.94)$$

In this chapter an analytical solution to describe the performance of the spiral wound modules was presented. A 'five parameter' model was used and after making some assumptions these parameters could be determined experimentally. When these parameters are known, by using the same equations, predictions can be made for the module performance in new operating conditions or for optimum geometry for the module.

If the experimental data for the ROGA module are applied in eq.(3.94), with the mass transfer coefficient at $k=9 \times 10^{-3}$ cm/sec, the following values for the k_2 are obtained, see Table 3.2 below. The higher values for k_2 , which have been found by using eq.(3.94), can be explained by eq.(2.2). Since in our calculations higher mass transfer coefficient has

been used than Taniguchi, the salt wall concentration will be less, so that a higher k_2 value is needed to give the experimental salt flux. It is believed that the important thing is the consistency of the k_2 values for different experimental data rather the absolute value of k_2 .

Table 3.2
 k_2 values for ROGA-4160 module.

P (Atm)	u_f (cm/min)	c_f (ppm)	k_2 (cm/sec) by Taniguchi	k_2 (cm/sec) by eq.3.94
34.5	514	1953	0.986×10^{-5}	1.790×10^{-5}
27.2	174	1879	1.352×10^{-5}	1.820×10^{-5}
27.2	237	1895	1.143×10^{-5}	1.778×10^{-5}

3.8 OPTIMUM MODULE GEOMETRY

In order to predict optimum module geometry eq.(3.86) can be used,

$$J = \frac{q k \tanh \frac{w}{q}}{w l \phi f} \left\{ [\Delta P - (c_f - c_p) \phi] \ln \gamma - \frac{k}{k_1} [\phi - \theta \ln \gamma] + \frac{(c_f - c_p) u_f k_{fb} \mu}{f} [\phi - \ln \xi \ln \lambda - \frac{k_1^2 \phi^2}{4 k^2} (c_b^2(l) - c_f^2)] \right\} \quad (3.86)$$

By setting,

$$B = \frac{1}{w l \phi f} \left\{ [\Delta P - (c_f - c_p) \phi] \ln \gamma - \frac{k}{k_1} [\phi - \theta \ln \gamma] + \frac{(c_f - c_p) u_f k_{fb} \mu}{f} [\phi - \ln \xi \ln \lambda - \frac{k_1^2 \phi^2}{4 k^2} (c_b^2(l) - c_f^2)] \right\} \quad (3.95)$$

eq.(3.86) will give,

$$J = q B \tanh \frac{w}{q} \quad (3.96)$$

In order to predict the optimum permeate channel height for the maximum permeate flux the quantity, volumetric flow per unit volume is introduced, Q_p/V , which will be called *specific productivity* and it will be given by equation (3.97).

$$\frac{Q_p}{V} = \frac{2 q B l w \tanh \frac{w}{q}}{l_2 w_2 (h_p + h_b + 2h_m)} \quad (3.97)$$

or,

$$\frac{Q_p}{V} = \frac{2 B w l h_p^{1/2} \tanh \frac{w \sqrt{2k_1 k_{fp} \mu}}{h_p^{1/2}}}{l_2 w_2 \sqrt{2k_1 k_{fp} \mu} (h_p + h_b + 2h_m)} \quad (3.98)$$

Eq.(3.98) has a maximum Q_p/V value when,

$$\frac{d\left(\frac{Q_p}{V}\right)}{dh_p} = 0 \quad (3.99)$$

By setting,

$$\frac{2 B l w}{l_2 w_2 \sqrt{2k_1 k_{fp} \mu}} = E \quad \text{and} \quad w \sqrt{2k_1 k_{fp} \mu} = \varepsilon \quad (3.100)$$

eqs (3.98), (3.99) and (3.100) will yield,

$$\frac{[h_p^2 + (h_b + 2h_m)h_p] \operatorname{sech}^2(\epsilon h_p) \epsilon h_p + \tanh(\epsilon h_p) [h_p - (h_b + 2h_m)h_p]}{2 [h_p^2 + (h_b + 2h_m)h_p]^2} = 0 \quad (3.101)$$

or,

$$[h_p^2 + (h_b + 2h_m)h_p] \operatorname{sech}^2(\epsilon h_p) \epsilon h_p + \tanh(\epsilon h_p) [h_p - (h_b + 2h_m)h_p] = 0 \quad (3.102)$$

Equation (3.102) can be solved numerically to give the optimum permeate channel height for the maximum permeate flux per unit volume. Another way is to plot the graph of $Q_p/V = f(h_p)$ and find out the value of h_p where Q_p/V is maximum.

Eq.(3.98) can be used to find the effect of the other factors like: the membrane length, l , the membrane width, w , the brine height, h_b etc. on the volumetric flow per unit volume of the module.

CHAPTER IV

EXPERIMENTAL WORK

4.1 INTRODUCTION

The aim of this experimental work is to validate the model which has been presented in the previous chapter. As a first step the five parameters, which can describe the spiral wound module performance, will be determined experimentally. This means that macroscopic parameters will be measured and by using these values and the equations developed in CHAPTER III, the five parameters will be determined. As a second step predictions for the module performance and comparison with experimental data will be made.

The effect of other factors, like temperature, pressure brine velocity, on the five parameters will be also examined. The operating conditions will cover a wide range as far as the pressure, flow, concentration, recoveries and temperature are concerned, in order to make a conclusive assessment about the performance of the spiral wound modules not only in normal operating conditions but also in extreme ones.

4.2 EXPERIMENTAL RIG

The experimental apparatus consists of a Reverse Osmosis Rig designed to accommodate any module, spiral wound or hollow fiber. The rig can be operated over a wide range of pressures (0-100 bar) and temperatures under carefully controlled conditions. As it can be seen in Fig.4.1 below, the rig is a closed loop and consists of different elements, which are presented below.

Reservoir and Solution

The reservoir containing the solution has a capacity of 1,000 litres. In order to maintain the temperature of the solution at any desired temperature, a cooler as well as a heater have been installed. Both of them were made of stainless steel in order to avoid any corrosion problems especially at high concentrations. The heater is controlled by a thermostat.

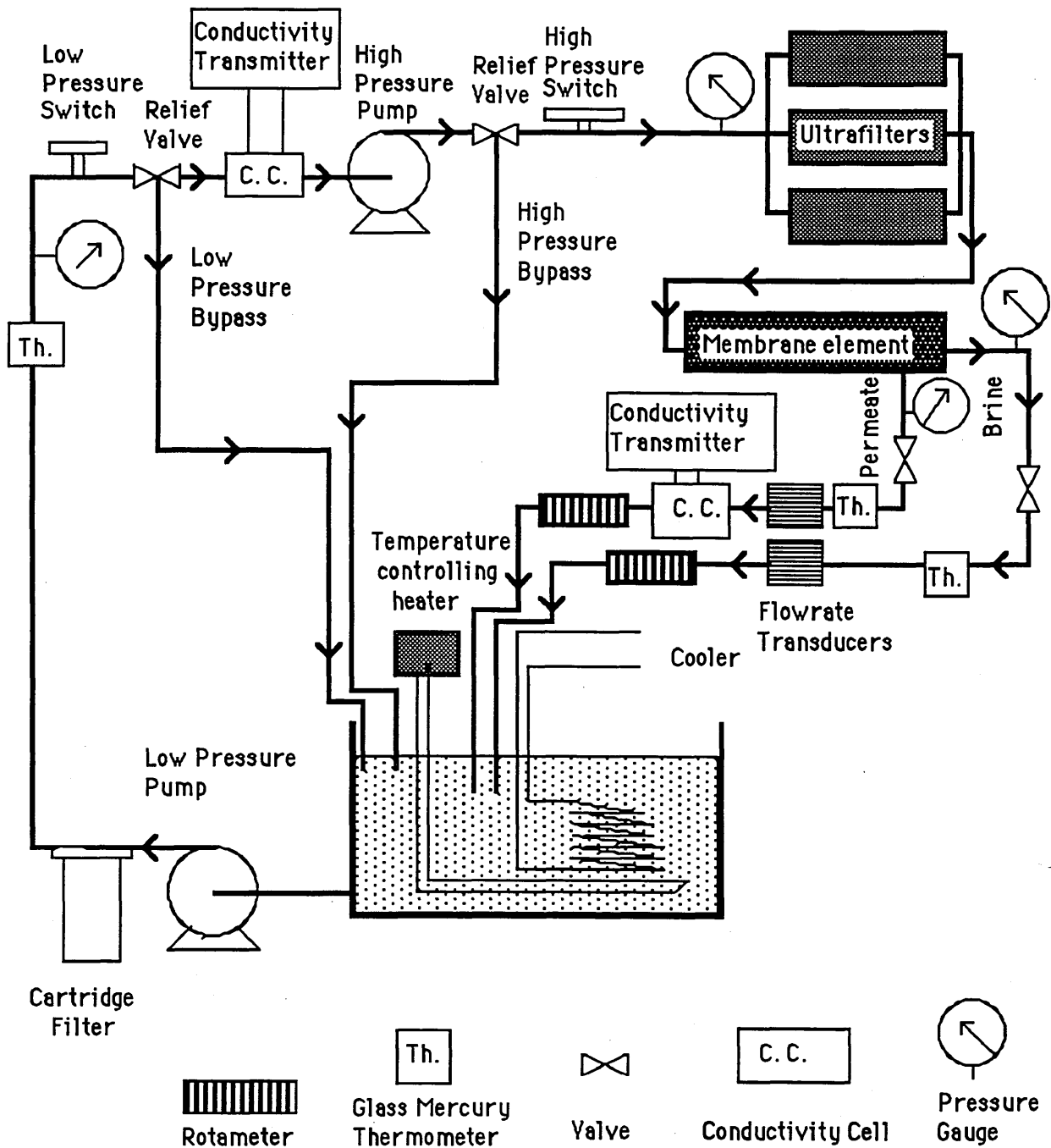


Fig.4.1 Experimental Rig

Low Pressure Pump

The solution is fed to the system by a low pressure pump (5 bar). The solution passes through a fine cartridge filter to retain any solid particles present in the solution. A number of visual measuring devices are used at this stage, which allow one to measure and control the condition of the feed solution in terms of temperature and pressure. The flow rate of the solution as well as the pressure entering the high pressure pump is

controlled by a low pressure relief valve and a by-pass line returns the excess solution to the tank.

High Pressure Pump

The high pressure in the feed solution is obtained by a high pressure reciprocating plunger pump, which is driven by a three phase electric motor of 7.5 KW capacity. This high pressure pump delivers up to 19 lt/min at a maximum pressure 175 bar at a speed up to 1100 rpm. In order to avoid pressure pulses usually caused by this type of pumps, an accumulator is used. It is has been precharged by nitrogen at a pressure of 90 % of the maximum operating pressure. A high pressure by-pass is sent back to the tank via a pressure controlling relief valve, which controls the operating pressure. Low and high pressure switches have been used as a safety system for the high pressure pump. They have been preset to give an appropriate operating range to the pump. The low pressure switch is set to 1 bar, below which the power supply to the high pressure pump is cut, in case of low feed flow from the low pressure pump, so that any damages to the high pressure pump because of cavitation can be avoided. The high pressure switch is set to 120 bar to avoid any excessive build up of pressure in the system. To avoid any corrosion problems a stainless steel pump has been selected.

Ultra-Filters

The high pressure feed from the high pressure pump is divided into three lines by using a manifold. These lines are connected with three ultra-filters (UF-20-4040) serving the pretreatment for the membrane and fulfil sterilization of the feed solution.

Membrane Unit

The solution leaving the ultra-filters enters the membrane unit. The membrane, which is a FT 30 SW 2.5" spiral wound module produced by FilmTec, is accommodated in a high pressure vessel, with an inlet for the feed and two outlets for the permeate and the brine. Both permeate and brine lines return to the feed tank.

Instrumentation

As it can be seen in Fig.4.1 some of the instruments are visual giving instant readings of the temperature pressure and flow rate at different locations of the rig. These include, pressure gauges, glass mercury thermometers and rotameter flow gauges. Another set of

instruments and transducers is used, which can be connected with a data logging system and data can be recorded continuously. These recording devices are described below.

Conductivity cells and transmitters, for the feed and product solution. Two Kent flow-line conductivity cells allow the measurement of the conductivity of the feed and product solutions. Each cell has a different range and is connected to its conductivity transmitter. The output of the transmitter is in mA, and the range of both of them is from 4 mA to 20 mA. The permeate side conductivity cell operates in a conductivity range of 0-10,000 $\mu\text{S/cm}$ and the feed side one in the range of 25,000-150,000 $\mu\text{S/cm}$.

Two digital **Pressure indicators and Transducers** were used, which can display the pressure measured and at the same time can send an external output signal in mVolts.

The **Flow-meters** for the brine and the permeate line are two paddle wheel sensors connected to signal transmitters. The output signal is set to operate in a range of 0 to 5 Volts.

Thermocouples are used to record the temperature at the feed, permeate and brine lines.

4.3 EXPERIMENTAL PROCEDURE

Before the main experimental work was started all the instruments were calibrated. In order to make assessments about the modules performance and the variation of the performance of different FT-30-SW-2.5" spiral wound modules, four different membrane were tested in normal operating conditions, while all the instruments were connected to a data-logger (3530 ORION DATA LOGGING-SYSTEM) and reading were recorded at a preset time interval.

The main experimental work is divided into four different experiments, depending on the parameters which are going to be determined.

4.3.1 Water Permeability Coefficient and brine friction parameter.

For this experiment distilled water was used as feed solution. It was decided to use six different brine flowrates for all the experiments so that conclusions can be made about the

effect of the brine velocity on the different parameters which are examined like, pressure drop, flux etc. The two pressure transducers were fitted as the Fig.4.2 shows. For five different brine flowrates (3.524, 6.769, 9.353, 12.03, and 14.773 lt/min) readings were taken for the pressure in the inlet and the outlet of the high pressure tube and for the brine feed and permeate flowrates. For each set of readings the pressure was adjusted to the desired value (10-60 bar) and the rig was left running at least for 15 min before the readings were taken. After scanning all the pressures the temperature was changed and the same procedure was followed. Four different temperature were used, (20° C , 25° C, 30° C and 35° C).

The pressure drop between the two points, where the transducers were fitted, had a maximum value of 1.3 bar. This value was considered too high and it was suspected that a high portion of this pressure drop was due to pressure losses in the fittings, as Fig.4.2 shows.

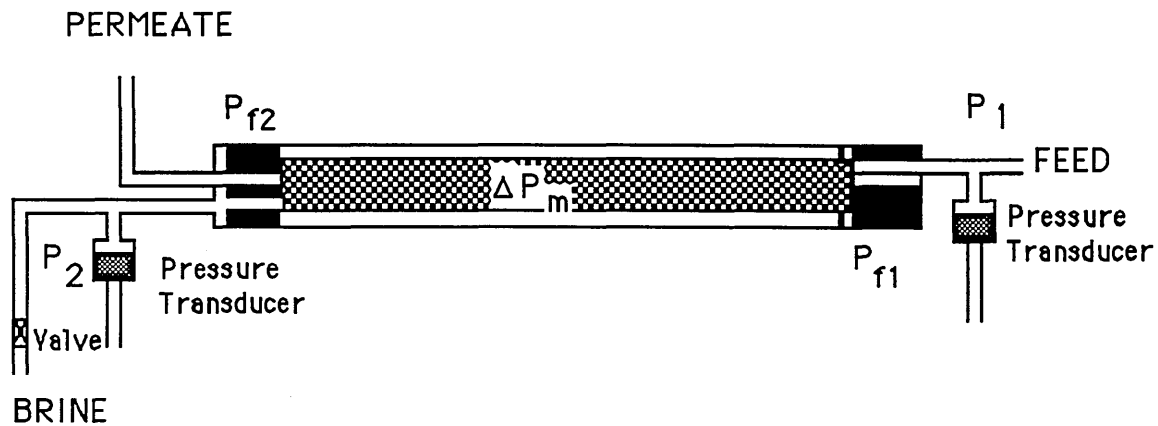


Fig.4.2 High Pressure tube with the membrane element.

In order to eliminate the pressure drop in the fittings, another experimental approach was tried. Very fine stainless steel hypodermic tubes (Outer Diameter 1 mm), were inserted in the inlet and the outlet of the tube, see Fig.4.3 below. The tubes were sealed with special fittings and the pressure transducer was fitted at the other end of the hypodermic tubes. Because there was not flow in the hypodermic tubes there were not pressure losses in the system except the pressure losses in the brine channel. The same experimental procedure as before was followed, recording the pressures and the flowrates for different applied pressures and temperatures.

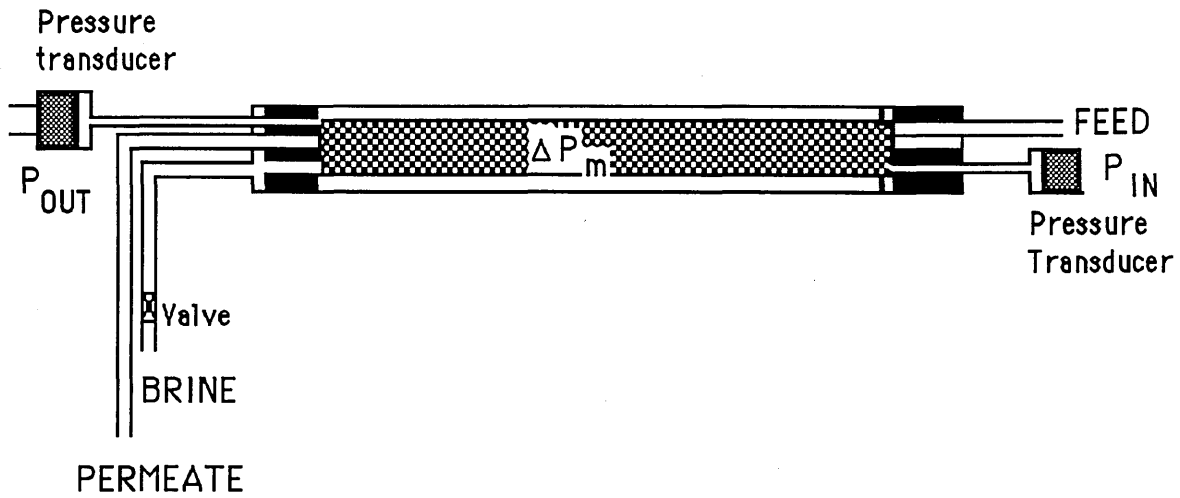


Fig.4.3 Hypodermic tubes in the inlet and outlet of the membrane.

In order to eliminate any pressure losses, (P_k), not due to the membrane, it was decided to carry out the same experiments and take the readings for the pressures and the flowrates but without the membrane being in the pressure vessel. The membrane's resistance to the water flow was simulated by the permeate valve so that as far as the flowrates are concerned they were exactly the same as when the membrane was into the pressure tube, see Fig.4.4.

By using Fig.4.3 and Fig.4.4 it can be written.

$$P_{OUT} = P_{IN} - P_k - \Delta P_m \tag{4.1}$$

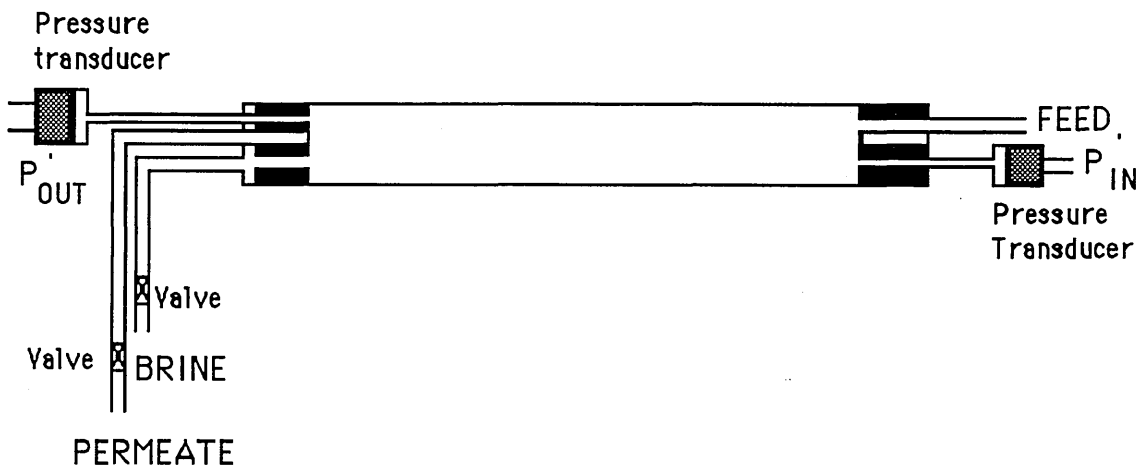


Fig.4.4 Hypodermic tubes in the inlet and outlet of tube.

$$P'_{OUT} = P'_{IN} - P_k \quad (4.2)$$

A combination of eqs (4.1) and (4.2) will give,

$$\Delta P_m = P'_{OUT} - P_{OUT} \quad (4.3)$$

The maximum pressure drop across the element found this way was 0.8 bar, which is similar with that found by Sock and Miquel[20].

4.3.2 Mass transfer coefficient, solute permeability coefficient.

In order to calculate the mass transfer coefficient and the solute permeability coefficient a series of experiments were carried out. Four different sea-water solutions (Instant Ocean) were used at concentrations of 25,000, 35,000, 40,000, and 25,200 ppm. For each solution and at the same temperatures as before, the brine permeate and feed flowrates were recorded as well as the permeate concentration and the pressures at the inlet and the outlet of the membrane. The pressures applied ranged from 10 bar to 90 bar and the same six brine flowrates were used so that the experimental results in this experiment could be associated with those from the pure water experiments. As far as the pressures in the inlet and the outlet of the membrane are concerned, no difference was found with the previous experiment with distilled water and one can conclude that the existence of salt has no significant effect on the fluid dynamics of the water as it was expected. Theoretically the maximum difference on the pressure drop between distilled water and salt solution at 40,000 ppm is less than 9 %.

4.3.3 Permeate friction parameter.

It can be seen from eq.(3.54) that the pressures in the open and the closed end of the envelope as well as the permeate flow are needed in order to calculate the permeate friction parameter. It can be assumed that the pressure at the open end of the envelope is equal to the atmospheric pressure (1 bar) and the permeate flowrate can be easily measured, so that the only problem is how the pressure at the closed end could be measured.

It was decided to insert a very fine stainless steel hypodermic tube into the envelope by which the pressure could be measured with a pressure transducer being fitted at the other end of the tube. This idea must overcome several problems which are presented below.

The height of the permeate channel is 0.43 mm so that the hypodermic tube must be very small in order not to change the flow conditions and to avoid damaging the membrane when the high operating pressure is applied. For this reason a very fine hypodermic stainless-steel tube was used, outside diameter 0.5 mm and inside diameter 0.33 mm.

For the sealing of the hypodermic tube as it comes out from the pressure vessel "O" rings and special fittings were used so that the system could be dismantled and reassembled easily.

Another problem was how to seal the area of the membrane where the tube was inserted. For this a 4" module was opened and pieces of the membrane were tried to be glued together in wet conditions by different adhesives. None of the adhesives proved successful.

The same adhesives were tried with dry membranes, and it was found that Araldite 2005 was very good. In order to test the resin under operating conditions, small envelopes were made with hypodermic tubes being inserted into the envelopes. The envelopes were placed inside a pressure vessel with the tubes coming out of the vessel and they were sealed. A pressure was applied with salt water as feed solution (20,000 ppm NaCl). The permeate from the hypodermic tubes was tested up to 60 bar and it was found to be in terms of concentration between 2,500 ppm to 500 ppm. It is believed that the adhesive affects in some way the membrane performance although there is no direct leak between the brine and the permeate side. At the same time the performance of the dry pieces of the membrane was tested with small cells against the performance of wet membranes and no significant change was noticed, see Table 4.1.

Table 4.1

Experimental data with wet and dried membranes at 20° C, 20 bar and $c_f = 5000$ ppm NaCl.

Membrane	c_p^a (ppm)	c_p^b (ppm)	J^a (cm/min)	J^b (cm/min)
No 1	164	120	0.0308	0.0317
No 2	180	160	0.0273	0.0273
No 3	219	188	0.0308	0.0335

a= wet membranes, b= dried membranes and tested again.

After all these the following procedure was applied. A portion of the fiberglass cover of the membrane was removed at the inlet side of the membrane, as well as the tape which covers the membrane below the fiberglass cover. A hole was opened near the closed end and a small area near the hole was dried with a hair drier, while the rest of the membrane was kept wet. The tube was inserted into the membrane and sealed with the Araldite 2005 and a piece of membrane was placed on top. The resin was left for 24 hours to dry. After that, the open part of the membrane was wrapped with tape and placed back into the pressure vessel, and the hypodermic tube was sealed at the outlet of the vessel.

Before fitting the pressure transducer at the open end of the hypodermic tube, the rig was run with the salt water (20,000 ppm) as feed in order to test the permeate quality which confirms that there is no brine-leak into the system. This process was not very successful with the first module giving permeate with very poor quality and after many attempts with no success, another module (Membrane No 2) was used. The permeate quality coming out of the tube for the second module, was found to be about 700 ppm, although the overall quality of the permeate was 70 ppm, which was the permeate quality before the module was opened. After that, the transducer was fitted, the salt water removed, and distilled water was used as feed solution. Readings were taken for the pressure in the inlet and the outlet of the membrane and the closed end of the permeate channel, and for the feed, permeate and brine flowrates at constant temperatures. After that the thermostat was set to another temperature and the experiment was repeated. The conditions were kept the same as for membrane No1.

In all the experimental work an effort was made to use always the same values for pressure and the brine flow rate so that the results could be correlated and conclusions could be made for the factors which affect the membrane performance.

CHAPTER V

RESULTS AND DISCUSSION

5.1 INTRODUCTION

In this chapter the analysis of the experimental data will be presented. The analysis will be based on the mathematical model presented in Chapter III. The analysis and the discussion of the results will be divided into two main parts. One part will involve the data concerning experiments with distilled water. The other one will involve those with sea-water solutions. In the first part the values of the water permeability coefficient, k_1 , the brine friction parameter, k_{fb} , and the permeate friction parameter, k_{fp} , will be calculated at various operating conditions. In the second part the values of the mass transfer coefficient, k , and the solute permeability coefficient, k_2 , will be found.

5.2 WATER PERMEABILITY COEFFICIENT AND FRICTION PARAMETERS

It has been mentioned in Chapter IV that in order to test, from a statistical point of view, the performance of the FilmTec membranes, four (No1, No2, No3, No4) 2.5" modules were used, under normal operating conditions, (56 Atm, 25° C, 35,000 ppm sea-water). The performance of each membrane was recorded continually with the datalogger and the results can be seen in Fig.5.1 and Fig.5.2.

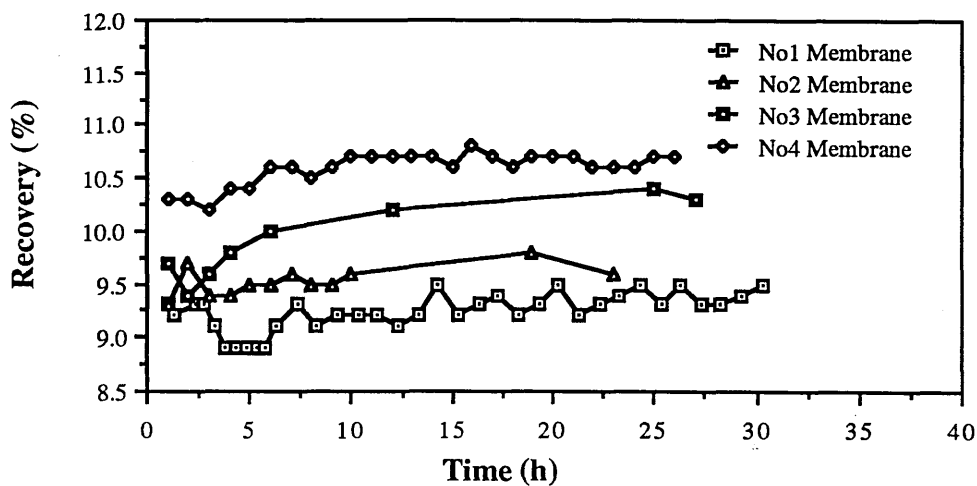


Fig.5.1 Recovery performance of FilmTec modules.

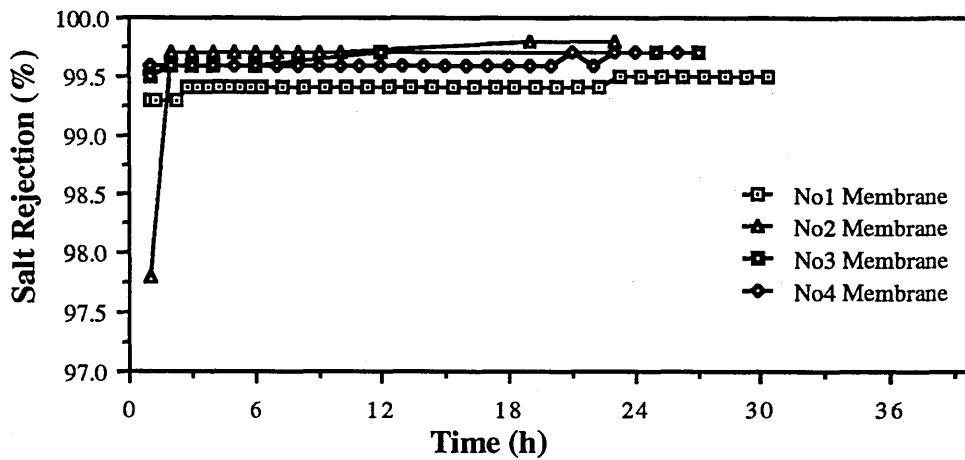


Fig.5.2 Salt Rejection performance of FilmTec modules.

There is about 10 % variation on the performance of the different modules. The main experimental work started with the membrane No1. Another point that should be mentioned is that when extreme operating conditions were used for the first time with distilled water (20° C & 68 bar, 35° C & 45 bar) the performance of the membrane No1, changed irreversibly, see Fig.5.3. This is probably due to the very high water flux at these conditions. After this the experiments were repeated until repeatable membrane performance for different conditions was achieved.

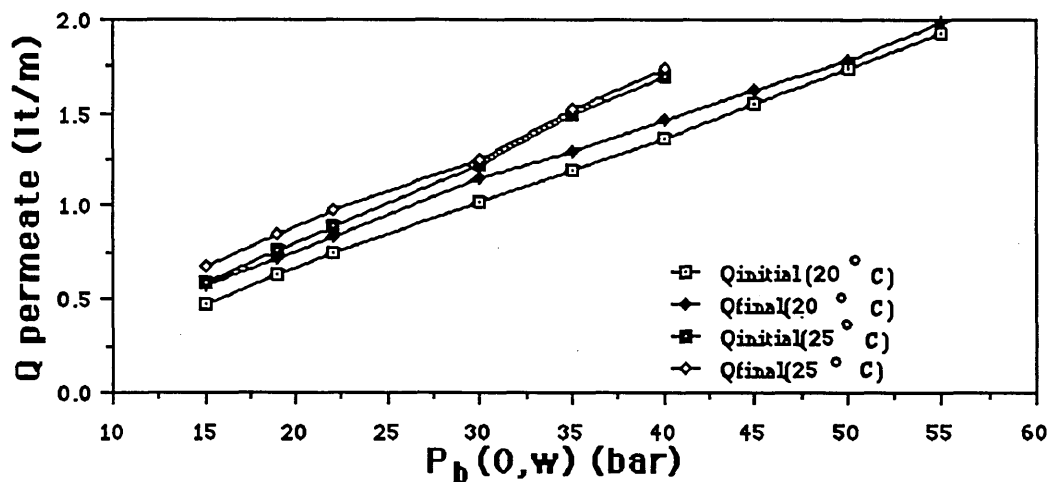


Fig.5.3 Permeate flow at different pressures for membrane No1.

For the membranes No2 and No3, after the initial test no further significant change on the performance was noticed. All these experimental data collected with distilled water, for membrane No 1 (with subscript i) and membrane No 2 (with subscript j), are presented in Table 5.1, see page 103. The dimensions of the spiral wound modules, which have been used are given in Table 5.2 below.

Table 5.2

Dimensions of the FT 30 SW 2.5" modules (in cm).

permeate channel height: $h_p = 0.043$,	total membrane length: $l_{\text{with glue}} = 94.65$
brine channel height: $h_b = 0.077$,	active membrane length: $l_{\text{without glue}} = 86.65$
membrane height: $h_m = 0.014$,	brine spacer width: $W_{\text{brine spacer}} = 134$
	active membrane width: $W_{\text{without glue}} = 117$

Since the pressures in the permeate channel were measured for membrane No2, the analysis that follows concern the data for this membrane.

In order to calculate the water permeability values and the friction parameters a computer programme was written, (see Appendix I, PROGRAM PAR1). The principle of the calculation has been described in Chapter III. A first guess for the k_1 was found by using the simple equation (5.1). With this value and using eqs (3.50) and (3.54) the values of k_{fb} and k_{fp} were found as a first approximation.

$$k_1 = \frac{J}{\Delta P_{ef}(0, w)} \quad (5.1)$$

By using eq.(3.45) and the k_{fb} , k_{fp} values found before, a new k_1 value can be found which is closer to the true one. With many iterations the k_1 value can be converged with the desired accuracy, and consequently the k_{fb} and k_{fp} will be found as well. The programme was run for each set of experimental data and the values of k_1 , k_{fb} and k_{fp} have been found for membrane No 2, see Table 5.3 in page 107.

From these results the following can be noticed:

- The brine friction parameter does not depend on the applied pressure. It depends on the brine flow and on the temperature as well.
- The permeate friction parameter increases slightly with increasing pressure and temperature. The brine flow has no significant effect on the permeate friction parameter.
- The water permeability, k_1 , depends on the applied pressure and operating temperature. Although k_1 varies slightly with the brine flow, this small variation is due to the variation of the k_{fb} values. It is rather an effect of the procedure of

calculations than an effect because of the changes on brine velocities and it can be ignored.

5.2.1 Brine friction parameter.

Darcy's law was discussed in section 3.2, and it was assumed that is valid for the flow in the brine channel, although the brine spacer is not really a porous material, but a turbulence promoting net. According eq.(3.32) k_{fb} should be constant if Darcy's law was applied. It can be seen from Table 5.3 that k_{fb} does vary with the brine velocity. The variation is the same for the different operating conditions as far as the pressure and temperature is concerned. It is believed that the exponent of the velocity in eq.(3.31) is other than unity, so that eq.(3.32) should be written as,

$$\frac{dP_b(x,y)}{dx} = - k_{fb} \mu u_b^\tau(x,y) \quad (5.2)$$

This type of formula is supported by others[20,26]. By introducing the exponent τ in eq.(3.32), the simplicity of this equation has been lost, and the system of the differential equations is becoming very complicated. Since the pressure drop in the brine channel is relatively small for normal operating conditions, (for $Q_b = 8.1 \text{ lt/m}$ $\Delta P_{brine} = 0.3 \text{ bar}$) and even at extreme conditions is less than 1.0 bar, it is suspected that the effect of the variation of the value of k_{fb} on the values of k_1 and k_{fp} would be very small. Indeed if the value of k_{fb} varies from $15,000 \text{ cm}^{-2}$ to $35,000 \text{ cm}^{-2}$ the variation of k_1 and k_{fp} is about 1%, see Fig.5.4.

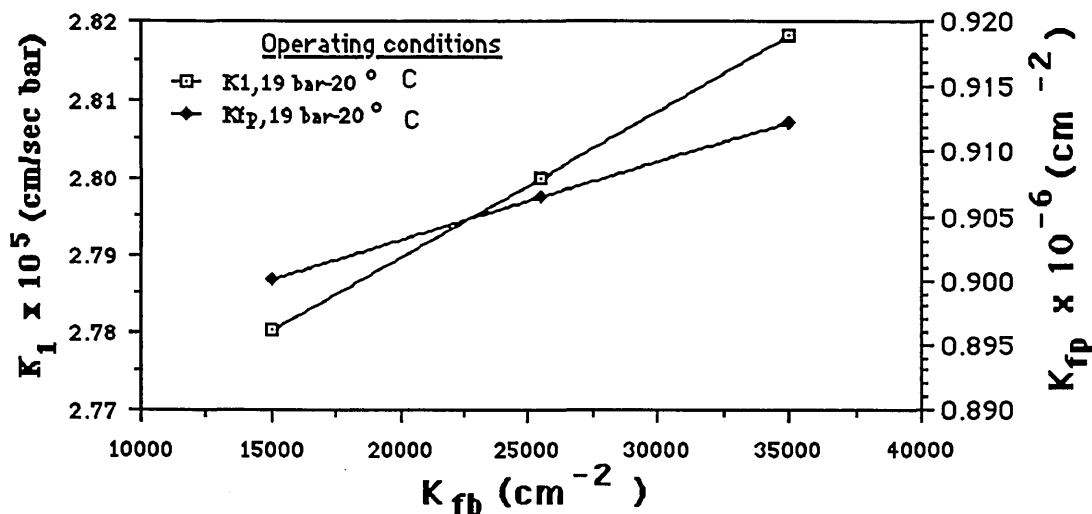


Fig.5.4 Variation of k_1 and k_{fp} for different k_{fb} values.

It can be concluded that as far as an analytical solution is concerned and under the operating conditions of the spiral wound modules eq.(3.32) is a good approximation to eq.(5.2). So for the Brine friction parameter, k_{fb} , the average of the values found for the different brine flows ($k_{fb} = 23,000 \text{ cm}^{-2}$), may be used without any loss of accuracy.

If one wants to predict the module performance by using the five parameter model and one is not satisfied with considering k_{fb} as being constant, it could be assumed and the experimental data confirm this, that the brine friction parameter is related to the *Reynolds Number* by the equation (5.3).

$$k_{fb} = k'_{fb} \text{Re}_f^v \quad (5.3)$$

where, k'_{fb} is constant in cm^{-2} , $v = \text{constant}$ and $\text{Re} = \frac{h_b u_f \rho}{\mu}$, $\rho = \text{density}$

or,

$$\ln k_{fb} = \ln k'_{fb} + v \ln \text{Re}_f \quad (5.4)$$

The values of k'_{fb} and v can be found by plotting the graph of equation (5.4), see Fig.5.5.

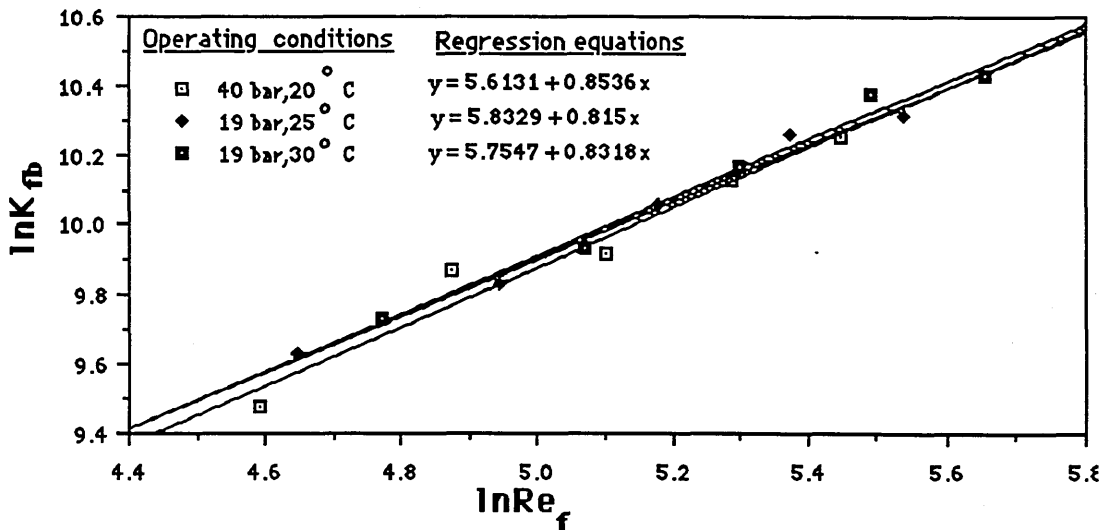


Fig.5.5 $\ln(k_{fb})$ versus $\ln(\text{Re}_f)$ for different experimental data.

If the same procedure is applied for all the data the values of k'_{fb} and v can be found for different conditions. It can be concluded that as far as analytical solution is concerned,

the value of k_{fb} can be considered as being either constant at $k_{fb} = 23,000 \text{ cm}^{-2}$, for the type of the module tested, or eq.(5.5) can be used to give the brine friction parameter for different Reynolds numbers.

$$k_{fb} = 309 \text{ Re}_f^{0.83} \quad (5.5)$$

5.2.2 Permeate Friction Parameter.

In these experiments with distilled water, the applied pressure is roughly the driving pressure, so that the permeate flow is higher, (typically 1.5 lt/min), than what it would be at normal operating conditions with sea-water as feed ($Q_p = 0.9 \text{ lt/min}$). It can be seen in Fig.5.6 that the permeate friction parameter varies with the temperature and pressure, increasing with both. The small variations for different brine flows, see Table 5.3, are due to the variation of the k_{fb} and the effect that this variation has on the k_1 . The way that k_{fp} changes is consistent for all the different temperatures.

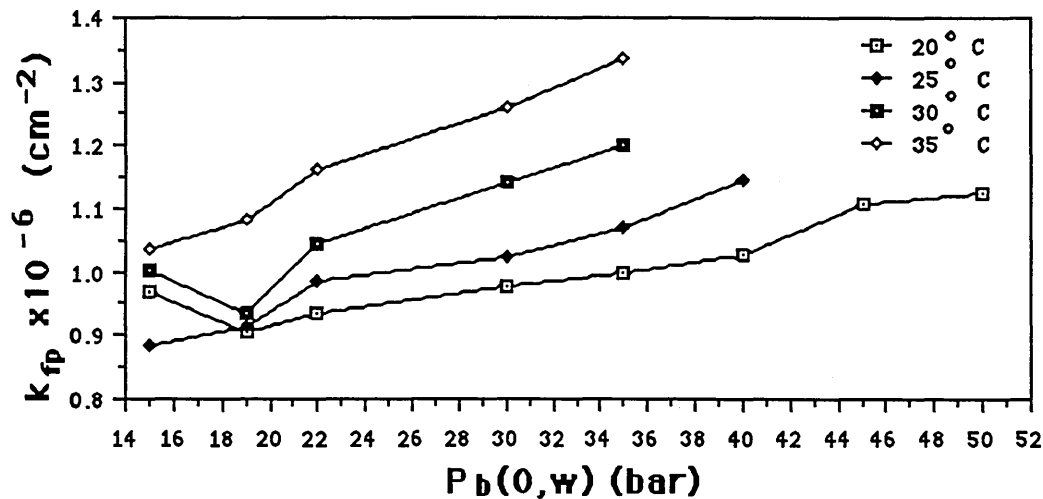


Fig.5.6 k_{fp} values for different pressures and temperatures.

These variations are not considered to be significant, since a maximum variation of 30 % on the k_{fp} causes a 1.3 % variation on the calculated values of k_1 and k_{fb} . This variation can be ignored as far as an analytical solution is concerned and a constant value for the permeate friction parameter at $k_{fp} = 1,100,000 \text{ cm}^{-2}$ can be used without any loss of accuracy. However, according the Darcy's law the coefficient k_{fp} should be independent of the pressure and the temperature. These variations can be explained with two ways:

a) An explanation, for this variation of k_{fp} , could be a decrease in permeate channel height because of the applied pressure. If the permeate height varies from 0.043 cm to 0.037 cm at 20° C & 50 bar, or to 0.0365 cm at 25° C & 40 bar, or to 0.0345 cm at 30° C & 35 bar, or to 0.031 cm at 35° C & 35 bar, gradually as the pressure is applied, then the k_{fp} would remain approximately constant at $k_{fp}=960,000 \text{ cm}^{-2}$. This assumption could also explain the variation of k_{fp} with the temperature, since even for the same pressure at higher temperature the porous material is softer and hence more susceptible to compaction.

b) Another explanation for these variations could be the existence of an exponent on the velocity in Darcy's law, as was the case for the brine friction parameter. In this case though, the exponent must be very close to unity. If the same procedure, as for the brine friction parameter, is applied for the permeate friction parameter, see Fig.5.7, a similar equation to eq.(5.5) can be obtained, see eq.(5.6). Eq.(5.6) is valid, as long as a constant permeate channel height is assumed.

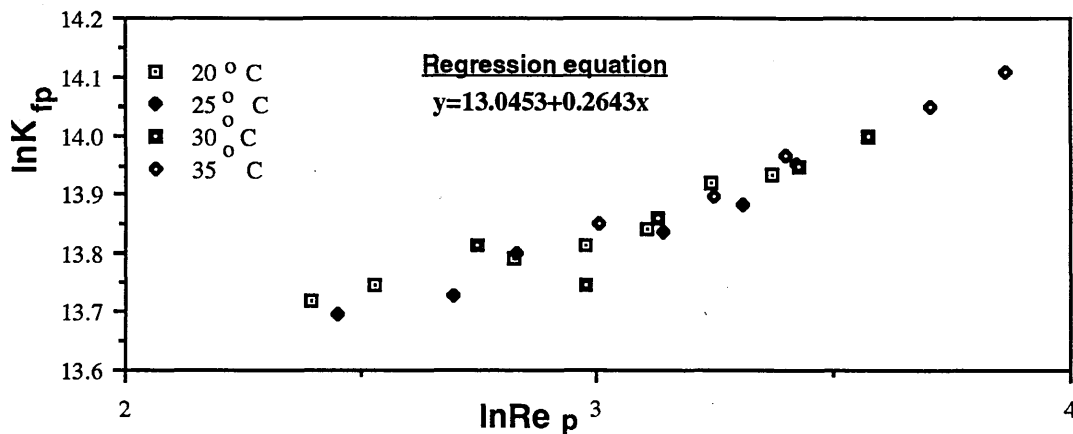


Fig.5.7 $\ln(k_{fp})$ versus $\ln(Re_p^3)$ for different temperatures.

$$k_{fp} = 462,915 \text{ Re}_p^{0.26} \quad (5.6)$$

It can be concluded that the application of Darcy's law for the permeate channel is very successful as far as an analytical solution is concerned and either a constant value for the permeate friction parameter can be assumed for this type of membranes at $k_{fp} = 1,100,000 \text{ cm}^{-2}$, or eq.(5.6) can be used to give the permeate friction parameter for different permeate flows.

5.2.3 Water permeability coefficient.

The effect of pressure on the water permeability coefficient has been well established. In early experiments with cellulose acetate membranes Loeb^[28] and Lonsdale et al. ^[29] noticed a decline on the permeate rate as well as on the permeate quality for long term experiments. This have been caused by the compaction of the membrane due to the applied pressure. Fortunately the larger part of this compaction is reversible and the membrane properties will readjust to its original characteristics when the pressure is removed. The reversible change of the water permeability coefficient can be described^[15,30] by eq.(5.7).

$$k_1 = k_{1,0} e^{-\alpha_p P_b(0,w)} \quad (5.7)$$

where, $k_{1,0}$ is the extrapolated value of k_1 when $P_b(0,w)=0$ and α_p is a constant in bar^{-1} .

It can be said that $k_{1,0}$ measures the initial porous structure of the membrane and α_p expresses the compaction effect on the pure water permeability characteristics of the membrane under pressure. The values of $k_{1,0}$ and α_p may be expected to be different if the membrane is subjected to different initial pressure treatment. Eq.(5.7) can be transformed to,

$$\ln k_1 = \ln k_{1,0} - \alpha_p P_b(0,w) \quad (5.8)$$

If an equation similar to eq.(5.8) is assumed for the polyamide composite membranes, then a plot of $\ln k_1$ versus $P_b(0,w)$ can give us the values of $k_{1,0}$ and α_p . Fig.5.8 below, shows these types of plots at different temperatures.

The values of α_p vary from **0.0025 at 30° C to 0.00082 at 20° C** and the values of $k_{1,0}$ from **$4.9467 \cdot 10^{-5}$ at 35° C to $2.7874 \cdot 10^{-5}$ at 20° C**. It must be stated that if the simple formula (5.1) was used to determine the k_1 values, then there is no correlation with the pressure. It is believed that these equations, developed for k_1 and the friction parameters, give a more accurate description of the characteristics of the membrane.

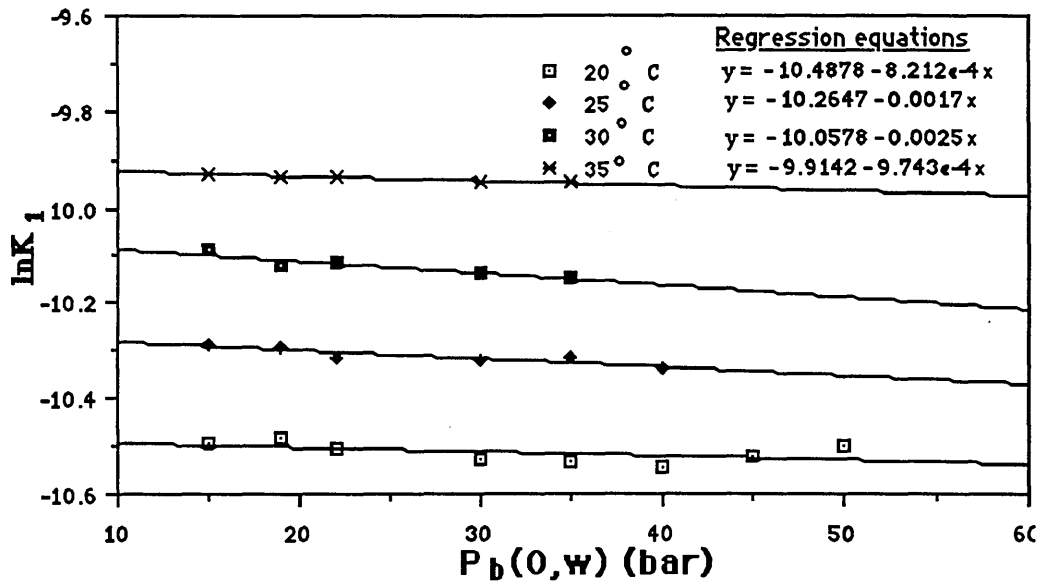


Fig.5.8 $\ln k_1$ versus Pressure for different temperatures (For membrane No2).

The k_1 values are also dependent on temperature. The temperature dependence can be described^[15] by an Arrhenius' type equation,

$$k_1^T = k_1^0 e^{\alpha_T \frac{T-T_0}{T_0}} \quad (5.9)$$

where, k_1^T is the water permeability coefficient at any temperature T

k_1^0 is the water permeability coefficient at temperature T_0

α_T is a constant.

Eq.(5.9) can be transformed to,

$$\ln k_1^T = \ln k_1^{20} + \alpha_T \frac{T-T_{20}}{T_{20}} \quad (5.10)$$

where, T and T_{20} are the absolute temperatures at any degrees and 20°C respectively.

The graph of eq.(5.10), at 25°C , 30°C and 35°C is given in Fig.5.9 below. It is interesting to see that the values of k_1 , which have been determined by the Fig.5.9, at 20°C , are very close to the experimental ones. k_1^{20} (by the graph at 22 bar) = $2.7597 \times 10^{-5} \text{ cm/sec bar}$, k_1^{20} (experimentally at 22 bar) = $2.7362 \times 10^{-5} \text{ cm/sec bar}$,

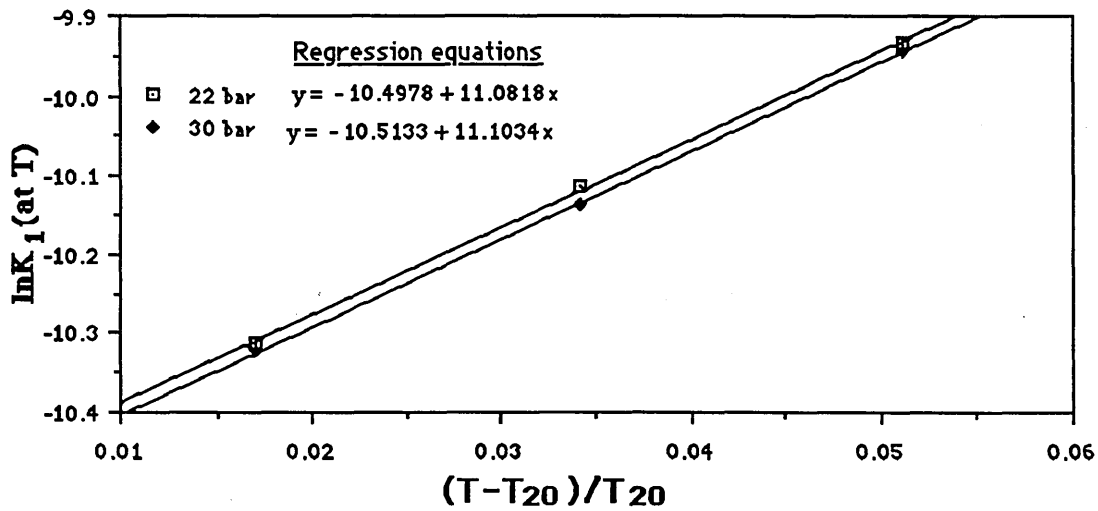


Fig.5.9 $\ln k_1$ versus the relative increase on absolute temperature (For membrane No2).

k_1^{20} (by the graph at 30 bar) = 2.7172×10^{-5} cm/sec bar, k_1^{20} (experimentally at 30 bar) = 2.6778×10^{-5} cm/sec bar.

It can be concluded that the k_1 values, which have been calculated, follow exactly the theoretical equation (5.9). Since $k_{1,0}$ depends on the temperature it can be assumed that it follows the general equation (5.9) and it can be written as,

$$k_{1,0}^T = k_{1,0}^{20} e^{\alpha_T \frac{T-T_{20}}{T_{20}}} \quad (5.11)$$

or,

$$\ln k_{1,0}^T = \ln k_{1,0}^{20} + \alpha_T \frac{T-T_{20}}{T_{20}} \quad (5.12)$$

The graph of eq.(5.12) can be seen in Fig.5.10 below. From the graph the value of $\ln k_{1,0}^{20}$ can be found as $\ln k_{1,0}^{20} = -10.1321$, which is almost the same with what it was found in Fig.5.8. After all these eq.(5.11) can be rewritten as,

$$k_{1,0}^T = 2.955 \times 10^{-5} e^{10.2697 \frac{T-T_{20}}{T_{20}}} \quad (5.13)$$

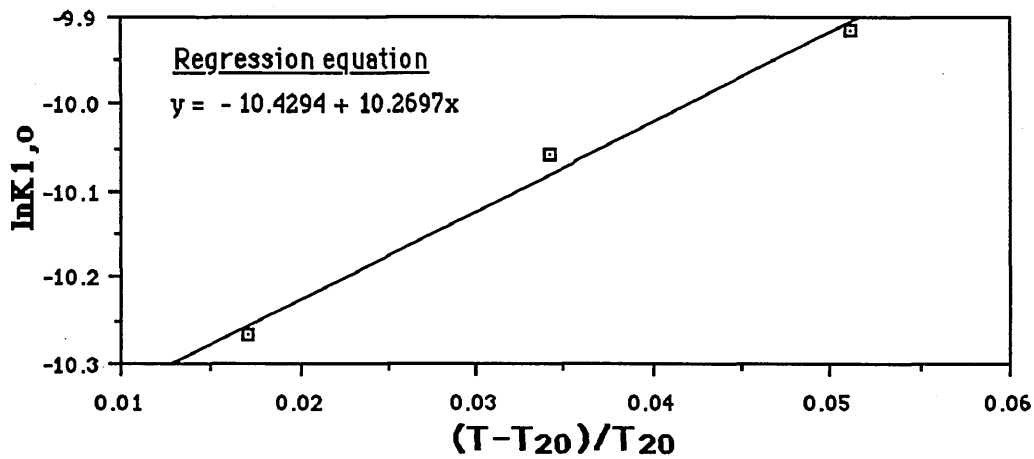


Fig.5.10 $\ln k_{1,0}$ versus the relative increase on absolute temperature (For membrane No2).

A combination of eq.(5.13) and eq.(5.7) yields,

$$k_1 = 2.955 \times 10^{-5} e^{10.2697 \frac{T-T_{20}}{T_{20}} - 0.0015 P_b(0,w)} \quad (5.14)$$

where, $\alpha_p = 0.0015 \text{ bar}^{-1}$.

Equation (5.14) can give the water permeability coefficient at any temperature and pressure for the membrane No2 and it can be used to predict the membrane performance at different operating conditions.

It can be concluded that the method which have been used to determine the friction parameters and the water permeability coefficient give reliable results and consistent with the general equations for the R.O. membranes performance.

5.2.4 Distilled water data analysis for membrane No1.

Both membranes No1 and No2 were found to have the same dimensions. It is reasonable to assume that the permeate porous material and the brine spacer are the same for the modules of this type, so that eqs (5.5) and (5.6) can be used to give the brine friction and the permeate friction parameters, for the membrane No1 as well. By using these equations and the experimental data from Table 5.1, the values of k_1 can be found, (see Appendix 1, PROGRAM PAR 2). It must be stated that all the experimental data with sea water were taken with membrane No1, so that the necessity of finding the k_1 values is obvious.

The intention in this section is to find a similar equation to eq.(5.14), so that the k_1 value will be given at any temperature and pressure for membrane No1. For this the same procedure as in section 5.2.3 was followed. By using Fig.5.11 the values of $k_{1,0}$ at different temperatures can be found as well as the values of α_p .

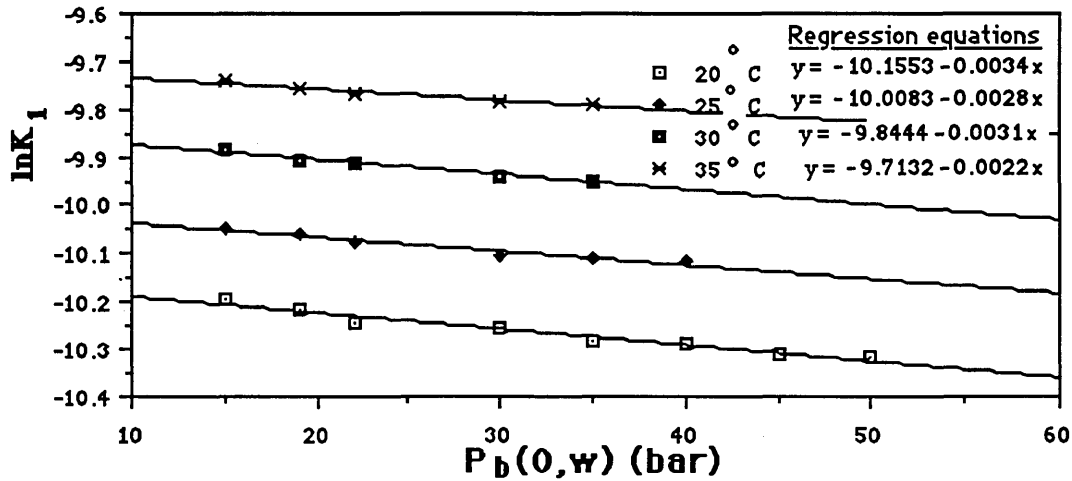


Fig.5.11 $\ln k_1$ versus Pressure for different temperatures (For membrane No1) .

If the values of $\ln k_{1,0}$ are plotted versus the relative increase in absolute temperature, then the values of $k_{1,0}^{20}$ and α_T could be determined, see Fig.5.12 . After all these eq.(5.15) will give the k_1 at any temperature and pressure for membrane No1.

$$k_1 = 3.9060 \times 10^{-5} e^{8.6464 \frac{T-T_{20}}{T_{20}} - 0.0028 P_b(0,w)} \quad (5.15)$$

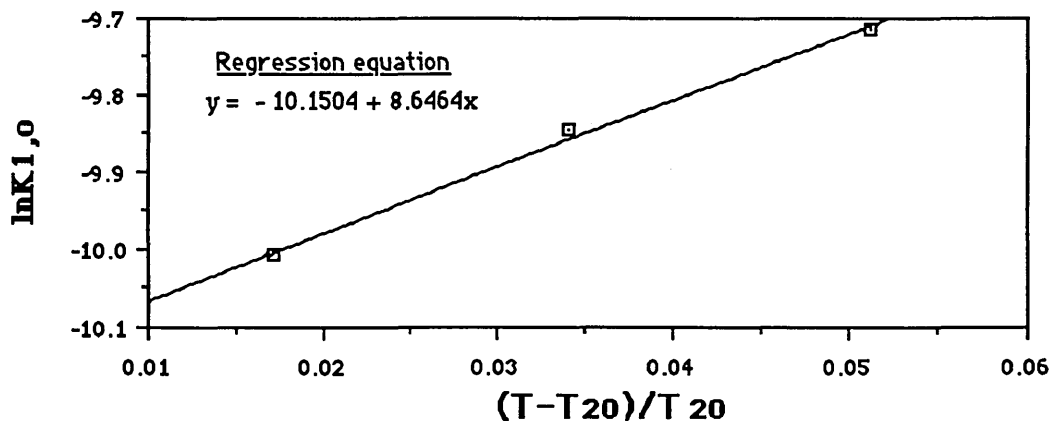


Fig.5.12 $\ln k_{1,0}$ versus the relative increase on absolute temperature (For membrane No1).

It is interesting to see the k_1 values calculated by the two different equations, (3.45) and (5.15), see Fig.5.13. It can be concluded that the values given by these two equations are in good agreement.

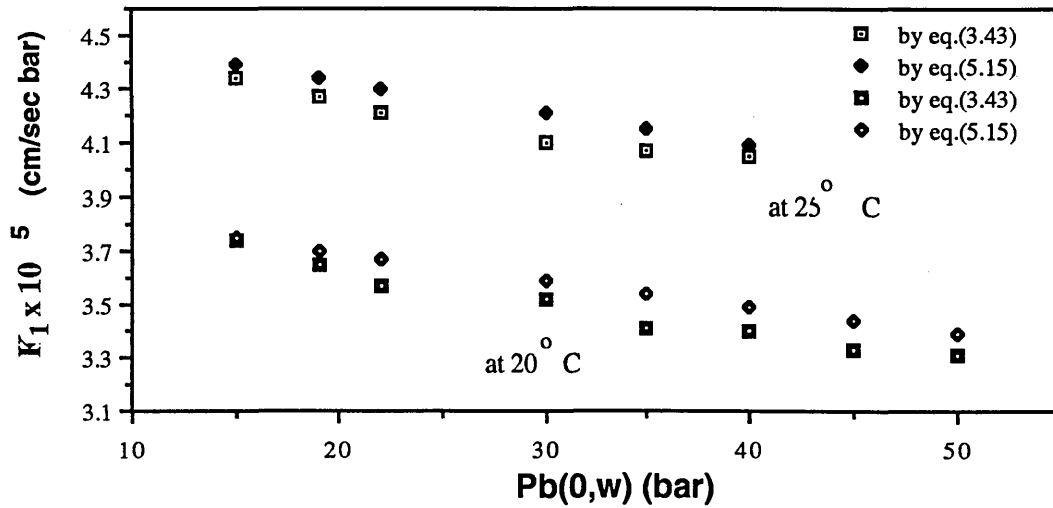


Fig.5.13 k_1 values for different Pressures and Temperatures.

It has been suggested^[13], after a limited amount of experimental data, that the viscosity and the water permeability coefficient could be related, at a given temperature and pressure, by eq.(5.16). It has been recognized, though, that eq.(5.16) may not always be a reasonable approximation for all the membranes under all conditions of pressure and temperature.

$$\mu k_1 \approx \text{constant} \quad (5.16)$$

However, if eq.(5.16) is applied for the calculated values for membrane No1, one can have:

$$\begin{aligned} \text{at } 20^\circ \text{ C and 19 bar : } & \quad \mu \times k_1 = 3.674 \times 10^{-7} \\ \text{at } 25^\circ \text{ C and 19 bar : } & \quad \mu \times k_1 = 3.807 \times 10^{-7} \\ \text{at } 30^\circ \text{ C and 19 bar : } & \quad \mu \times k_1 = 3.965 \times 10^{-7} \\ \text{at } 35^\circ \text{ C and 19 bar : } & \quad \mu \times k_1 = 4.160 \times 10^{-7} \end{aligned}$$

If the the μk_1 values are plot versus temperature there is actually a small variation with the temperature, see Fig.5.14 below.

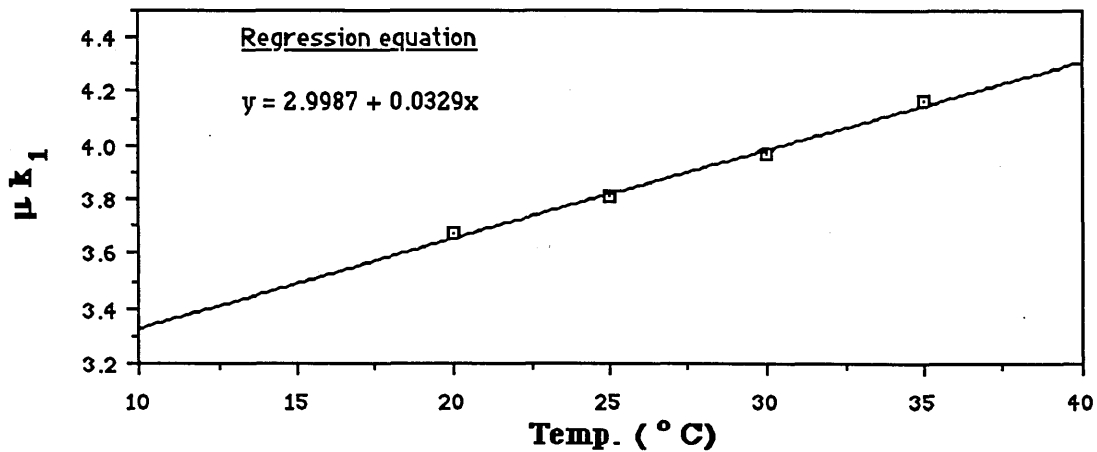


Fig.5.14 $\mu \times k_1$ values for different temperatures.

5.3 MASS TRANSFER COEFFICIENT

The mass transfer coefficient was defined by eq.(3.9) in section 3.3. It is worthwhile to state again that a mass transfer coefficient for vanishing flux, see eq.(5.17), has been suggested by many previous workers. This assumption is questionable in this work.

$$k = \lim_{J \rightarrow 0} k^c = \frac{D}{\delta} \quad (5.17)$$

where, k^c = convective mass transfer coefficient.

D = diffusivity coefficient.

δ = effective boundary layer thickness.

It has been proposed^[15] that the mass transfer coefficient is a function of the flow parallel to the membrane and the material properties of the fluid and is not affected by the flux itself. However experimental results ^[30] showed that operating pressure and boundary concentration also affects the values of k . It was suggested^[15] that in the case of forced convective flow the *Sherwood number* ($Sh=kd/D$), can be related to the *Reynolds number* ($Re=dup/\mu$) and the *Schmidt Number* ($Sc=\mu/\rho D$) with a relationship of the form,

$$Sh = f(Re, Sc, geometry) \quad (5.18)$$

The well-known relationships for calculating the heat-transfer coefficient have been

found to apply also, for the mass transfer at the membrane surface. Different equations have been proposed to give the mass transfer coefficient and a review of these equations has been presented by Gekas^[36]. In the same paper there is strong criticism about the validity of these equations. Some of the most commonly used equation are presented below.

Chiolle et al^[31] proposed eq.(5.19). This equation was used to describe the mass transfer in parallel channels for electro dialysis^[32].

$$k = 0.753 \left(\frac{M}{2-M} \right)^{\frac{1}{2}} Sc^{-\frac{1}{6}} \left(\frac{Pe h_b}{2 \Delta l} \right)^{\frac{1}{2}} \frac{2 D}{h_b} \quad (5.19)$$

where, M = the mixing efficient of the spacer .

$Pe = Peclet\ number = h_b u_b / D$.

Δl = characteristic length of the net.

Schock and Miquel^[20] have proposed eq.(5.20) after experiments with flat membranes separated with a spacer, with feed concentration at 300 ppm NaCl.

$$Sh = 1.85 \left[Re Sc \frac{d_h}{l} \right]^{0.33} \quad (5.20)$$

where, d_h = Hydraulic diameter.

In many turbulence cases the Dittus-Boelter heat transfer correlation can be used to estimate k with sufficient accuracy^[33], see eq.(5.21).

$$Sh = 0.023 Re^{0.8} Sc^{0.33} \quad (5.21)$$

For laminar flow eq.(5.22) has been proposed^[15].

$$Sh = \left[3.66^3 + 1.61^3 Re Sc \frac{d_h}{l} \right]^{\frac{1}{3}} \quad (5.22)$$

At this stage it must be stated that to the best of our knowledge all the experimental data available so far are for low feed concentrations and concern tubular and plate and frame

systems where an analogy in heat and mass transport could be used to derive the mass transport characteristics[20]. It is believed that for the spiral-wound modules this approach is not very successful. The only experimental data[18,34], concerning spiral wound modules, were for feed concentrations of not more than 2,000 ppm NaCl. Since there are different equations predicting the mass transfer coefficient, it is interesting for anyone to apply these equations and to compare the calculated values of k, for different experimental data.

Ohya and Taniguchi[34] and Taniguchi[18] have published experimental data for three spiral wound modules using NaCl solutions at concentrations not more than 2,000 ppm. The values they suggested, by using an numerical optimization method, for k were between 0.4×10^{-3} cm/sec to 1.4×10^{-3} cm/sec. For the same experimental data eqs (5.19), (5.20), (5.22) were applied and the calculated k values are presented in Table 5.4 . From these results it can be seen that there are great discrepancies between the k values by using different equations.

Table 5.4

Mass transfer coefficient for ROGA-4160 module.

<u>k(cm/sec)</u>					
<u>P(Atm)</u>	<u>Uf(cm/sec)</u>	by Taniguchi	by eq.(5.19)	by eq.(5.20)	by eq.(5.22)
29	2.99	0.4×10^{-3}	1.92×10^{-3}	1.15×10^{-3}	1.15×10^{-3}
27.2	18.7	1.4×10^{-3}	4.8×10^{-3}	2.1×10^{-3}	1.90×10^{-3}

If the relationship between the mass transfer coefficient and the effective boundary layer thickness is recalled then, $\delta=D/k$ and this means: according Taniguchi between 30%-105% of the brine channel is occupied by the effective boundary layer. According eq.(5.20) or (5.22) the boundary layer occupies between 20%-36%, and according eq(5.19) between 9%-22% of the brine channel height.

From these simple calculations it seems unrealistic for a boundary layer to be extended so much at these low concentration conditions. It is believed that the more realistic values for k are given by eq.(5.19).

The application of the previous equations for the mass transfer coefficient for data

presented in this work can be seen in Table 5.5.

Table 5.5

Mass transfer coefficient at 25° C, 60 bar and 25000 ppm Sea-water.

P(Atm)	u_f (cm/sec)	k(cm/sec)		
		by eq.(3.86) (Presented in this work)	by eq.(5.20)	by eq.(5.22)
60	7.8	4.311×10^{-3}	1.13×10^{-3}	1.09×10^{-3}
60	26	6.93×10^{-3}	1.72×10^{-3}	1.53×10^{-3}

From Table 5.5 it can be seen that the values which are calculated by these different equations show a great discrepancy. The boundary layer covers according eqs (5.20) or (5.22) from 18 % to 35 % of the brine channel height. It must be pointed out that the application of eq.(5.19) is not possible since the mixing efficiency of the brine spacer is not known. According eq.(3.86) the boundary layer height is from 5.5% to 8.8 % of the brine channel height.

Another important consideration is the wall concentration. If this wall concentration, C_{bw}' , is calculated with the k values from eqs (5.20) or (5.22), then it can be found to be at: $C_{bw}' = 65,000$ ppm for $u_f = 7.3$ cm/sec and $C_{bw}' = 52,000$ ppm for $u_f = 26$ cm/sec. According eq.(3.86) the wall concentrations, C_{bw} , are: $C_{bw} = 31,000$ ppm for $u_f = 7.8$ cm/sec and $C_{bw} = 30,150$ ppm for $u_f = 26$ cm/sec, see Fig.5.15 and Fig.5.16.

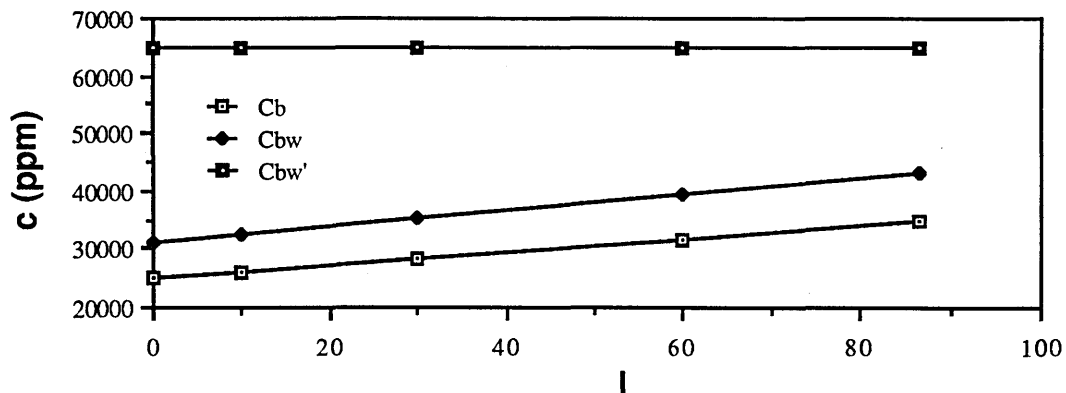


Fig.5.15 Variation of the brine concentration with the membrane length for 25,000 ppm at 25° C, 60 bar and $u_f = 7.3$ cm/sec.

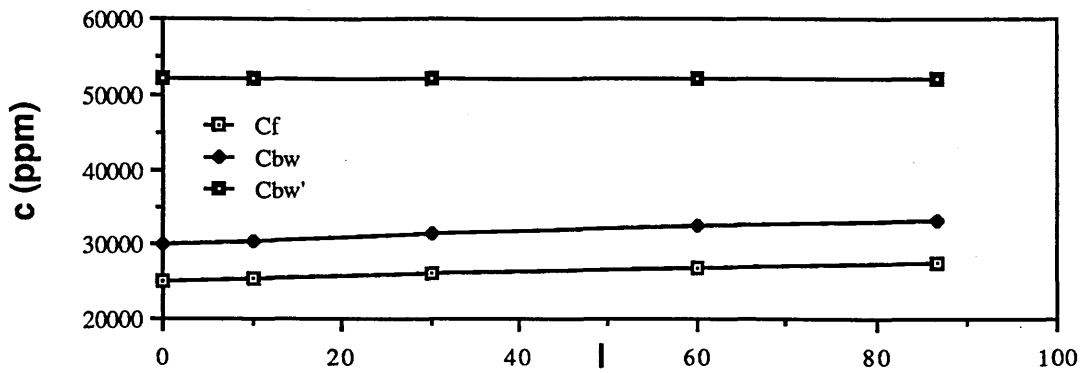


Fig.5.16 Variation of the brine concentration with the membrane length for 25,000 ppm at 25⁰ C , 60 bar and $u_f=23$ cm/sec.

It is obvious that very high wall concentrations will cause very high Osmotic Pressure (47 bar at 65,000 ppm) resulting in very small water flux, which is not consistent with the experimental facts.

Another point that should be mentioned is that in previous experimental work and analysis the feed concentration was considered as being constant along the membrane, either because of using a small cell for flat membranes or because low feed concentrations and recoveries for spiral wound modules were used. For sea-water as feed, though, and for moderate or high recoveries, the feed concentration varies, and in this work the brine concentration change was considered as being proportional to the axial distance, l , along the element, see Fig.5.15 and Fig.5.16.

It can be concluded that the equations used previously to calculate the mass transfer coefficient might be applicable for very low feed concentrations, but they fail to describe the real mass transfer conditions at high feed concentrations.

At this stage it will be useful to enter into a more detailed discussion about the mass transfer coefficient in Reverse Osmosis membrane systems. As was discussed earlier in this work the mass transfer coefficient can be considered to be proportional to the diffusion coefficient, $k \propto D^{1.0}$. This is questioned by Trettin and Doshi^[36], and a more realistic relationship, $k \propto D^n$ where $0.5 \leq n \leq 1.0$, was proposed. The extend of concentration polarization depends as well on the presence or absence of cross-flow over the membrane surface, so that it is questionable whether a constant value for the mass transfer coefficient along the membrane expresses the real situation, since the water withdrawal through the membrane decreases the driving pressure and the permeation rate falls with increasing distance down the channel. It is obvious that the velocity of cross-flow, suffers a fractional

decrease equal to the fraction of water removed from the channel. There is a lot of criticism as well by many authors^[37,38], as to whether, the use of mass transfer correlations from non-porous smooth duct flow, in the case of membrane operations is valid, since neither the porosity nor the roughness of the membrane nor the change of physical properties have been taken into account.

In this work the evaluation of the mass transfer coefficient has been done by solving eq.(3.86) numerically (see Appendix I, Programm PAR3) for different experimental data. The k values have been considered as being constant along the membrane. All these results and the experimental data are presented in Table 5.6, see page 111. The next step will be to find a correlation of the mass transfer coefficient using eq.(3.86) with simple experimental variables such as, feed concentration C_f , feed velocity u_f etc. The validity of this new equation giving the mass transfer coefficient and as well as that of eq.(3.86) will be tested by comparing experimental data for the flux and rejection of the membrane with theoretical values found by using the developed equations.

From the k values in Table 5.6 the following can be concluded:

- 1) The mass transfer coefficients found are much higher than the values reported in previous work.
- 2) The k values for the same pressure, concentration and temperature increase with increasing feed velocities.
- 3) The k values for the same concentration, feed velocity and pressure increase with increasing temperature.
- 4) When the feed concentration increases the k values decrease, with the other variables remaining constant.
- 5) For the same temperature and feed concentration the k values decrease with increasing pressure, although at the same time the feed velocity increases slightly.

If one goes back to the thin film theory and in eq.(3.4), then one can see that the idea is that an equilibrium has been established in the boundary layer between the salt moving by convection towards the membrane and the salt moving away from the membrane by diffusion. It is reasonable to assume that when the rate of solute salt transfer towards the membrane increases, either because of higher applied pressure or because of higher feed concentration, the boundary layer conditions must be readjusted so that a new equilibrium could be established. As a result of this, the definition of a convective mass transfer coefficient independent of the water flux, might be convenient for the analogy between the heat and the mass transfer coefficient, but its validity is questionable. Therefore the above conclusions seem realistic since an increase in temperature or cross-flow velocity will result

in lower concentration polarization effects and hence in higher mass transfer coefficient values. On the other hand, when the feed concentration or the pressure increase, higher concentration polarization effects are to be expected and therefore lower mass transfer coefficient values. In this work a mass transfer coefficient depending on the applied pressure and feed concentration as well as the flow conditions has been introduced.

It can be said that according to the analysis that has been presented together with the experimental data, the mass transfer coefficient, for the spiral wound modules and for sea-water as feed, is a function of the feed velocity, feed concentration, operating temperature geometry and applied pressure, see eq.(5.23).

$$k = f (u_f , c_f , T , \Delta P_b(0,w), \text{geometry}) \quad (5.23)$$

Let us now discuss these parameters in more details. In all these experiments, where in some cases extreme operating conditions were used, the Reynolds number for the feed solution was between 46-260. Although the existence of the brine spacer causes some turbulence, the hypothesis of a 'chopped' laminar flow, see section 3.2, is not unrealistic for these low Reynolds numbers. Eq.(5.23) could be written as,

$$Sh = k^o Sc^{n_1} Re_f^{n_2} \left[\frac{c_f}{\rho} \right]^{n_3} \left[\frac{P_b(0,w)}{P^o} \right]^{n_4} \quad (5.24)$$

where, Sh = Sherwood number = kh_b/D .

Sc = Schmidt Number = $\mu/\rho D$.

ρ = solution density.

c_f = feed concentration.

$P_b(0,w)$ = Pressure.

$P^o = 1$ bar.

n_1, n_2, n_3, n_4, k^o = constants.

D = Diffusivity coefficient.

Although the geometry of the module could play a significant role in determining the mass transfer coefficient, at this stage no assessment can be made about this since there are not experimental data available for membranes with different geometry. It can be said that eq.(5.24) is valid for spiral wound modules with structure similar to the FilmTec FT30 membranes.

The exponents can be determined if three of the variables are kept constant and only one

is varied. If only Re is varied, then eq.(5.24) can be transformed to,

$$\ln(\text{Sh}) = \ln\left\{ k^{\circ} \text{Sc}^{n_1} \left[\frac{c_f}{\rho}\right]^{n_3} \left[\frac{P_b(0,w)}{P^{\circ}}\right]^{n_4} \right\} + n_2 \ln(\text{Re}_f) \quad (5.25)$$

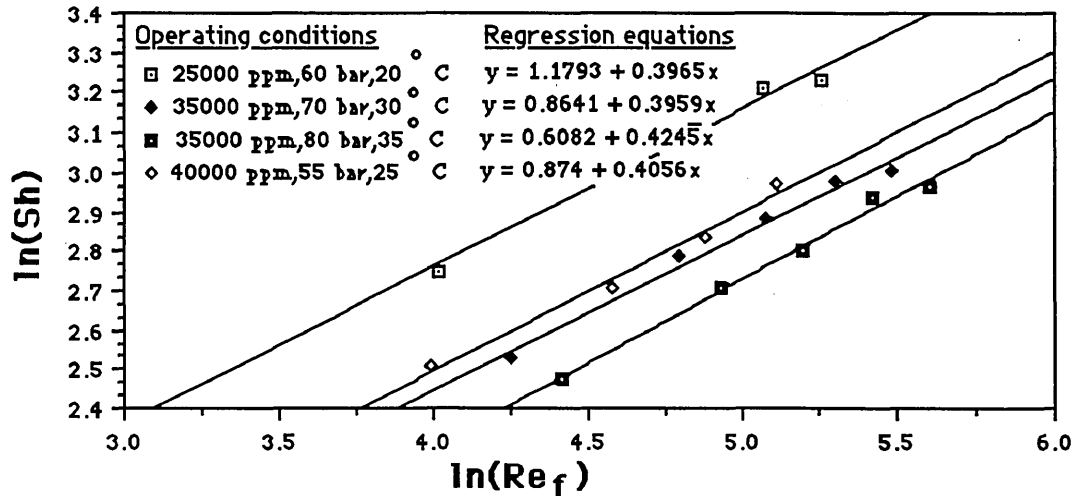


Fig.5.17 $\ln(\text{Sh})$ versus $\ln(\text{Re}_f)$ for different operating conditions.

A graph of $\ln(\text{Sh})$ versus $\ln(\text{Re}_f)$ is expected to be linear and the slope of the curve will give the value of n_2 , see Fig.5.17. If the conditions are changed (C_f , ΔP etc.) it would be expected that no changes will occur to the value of n_2 . The same procedure was applied for all the experimental data and the n_2 values were found to be fairly constant, so that a value at $n_2 = 0.4 \pm 0.06$ can be used.

The exponent n_3 could be determined if eq.(5.24) is written in the following form,

$$\ln(\text{Sh}) - n_2 \ln(\text{Re}_f) = \ln\left\{ k^{\circ} \text{Sc}^{n_1} \left[\frac{P_b(0,w)}{P^{\circ}}\right]^{n_4} \right\} + n_3 \ln\frac{c_f}{\rho} \quad (5.26)$$

so that even if the Reynolds number and the feed concentration varies, the graph of eq.(5.26) is expected to be linear and the slope of the curve will give the value of n_3 , as long as the pressure and the temperature are kept constant, see Fig.5.18 below. Plots for all the experimental data showed a greater variation for the n_3 values than for the n_2 values. However an average value at $n_3 = -0.77 \pm 0.3$ can be used with reasonable accuracy.

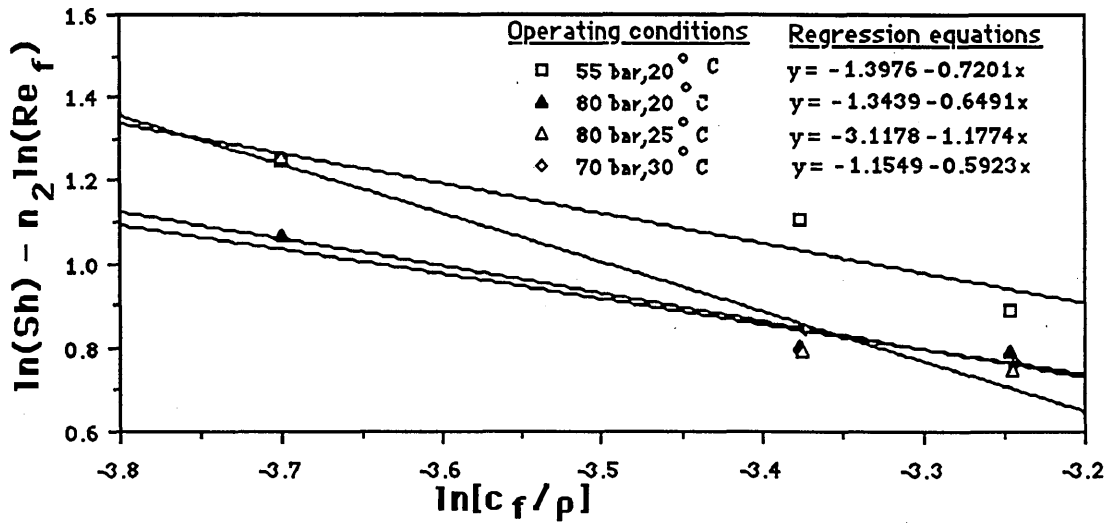


Fig.5.18 $\ln(\text{Sh}) - n_2 \ln(\text{Re}_f)$ versus $\ln(c_f/\rho)$.

The exponent n_4 can be found if the same procedure as before is applied. Eq.(5.24) can be written as eq.(5.27).

$$\ln(\text{Sh}) - n_2 \ln(\text{Re}_f) = \ln\left\{ k^0 \text{Sc}^{n_1} \left[\frac{c_f}{\rho}\right]^{n_3} \right\} + n_4 \ln\left[\frac{P_b(0,w)}{P^0}\right] \quad (5.27)$$

The graph of eq.(5.27) is expected to be linear and the slope of the curve is n_4 . By applying eq.(5.27) for all the experimental data the values of n_3 can be determined, see Fig.5.19. The value of n_4 was considered to be at $n_4 = -0.55 \pm 0.18$.

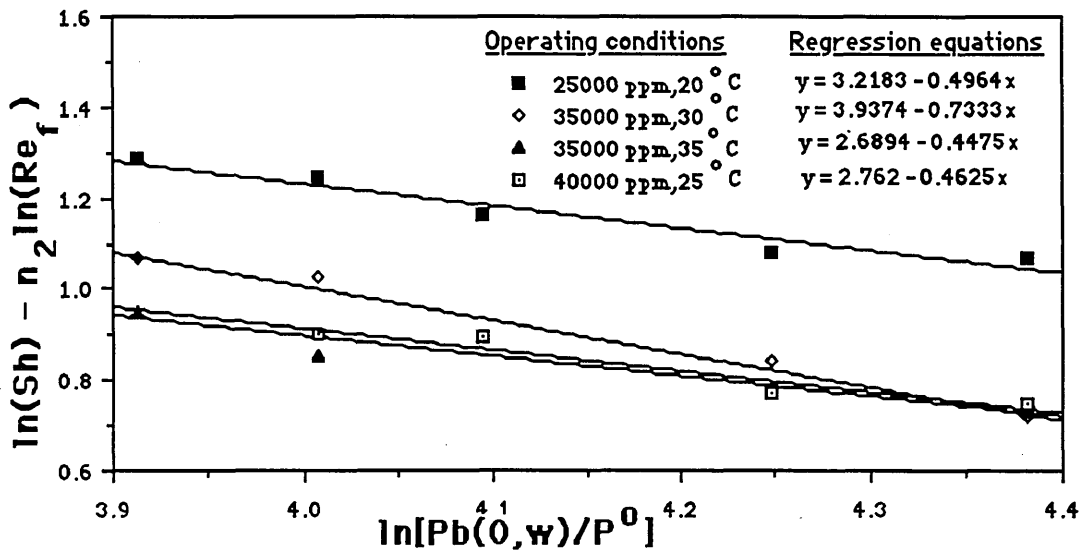


Fig.5.19 $\ln(\text{Sh}) - n_2 \ln(\text{Re}_f)$ versus $\ln[P_b(0,w)/P^0]$.

Finally the exponent n_1 can be found if eq.(5.24) is written in the form of eq.(5.28). The graph of eq.(5.28) can be seen in Fig.5.20.

$$\ln(\text{Sh}) - n_2 \ln(\text{Re}_f) = \ln\left\{ k^o \left[\frac{C_f}{\rho}\right]^{n_3} \left[\frac{P_b(0,w)}{P^o}\right]^{n_4} \right\} + n_1 \ln(\text{Sc}) \quad (5.28)$$

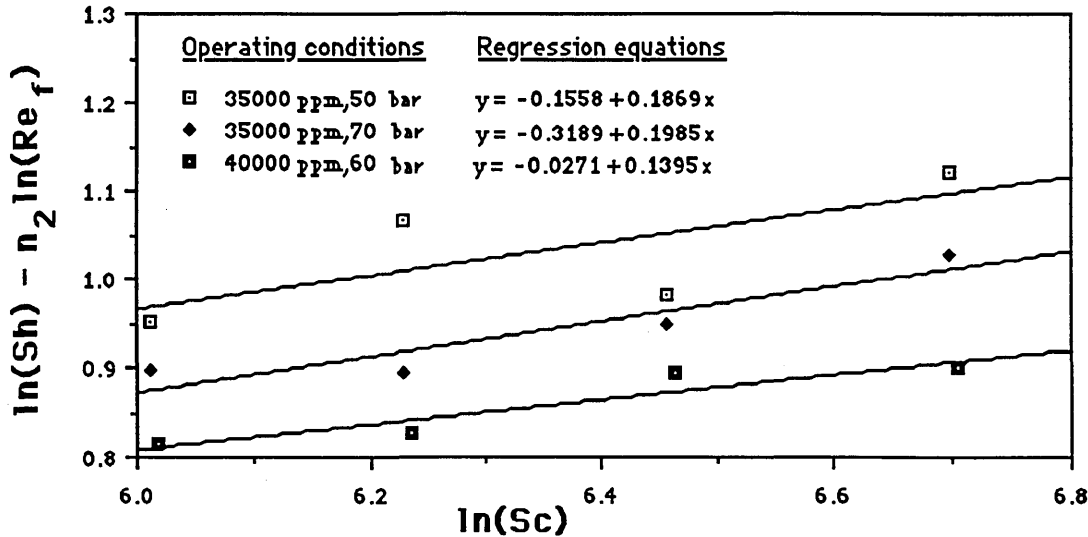


Fig.5.20 $\ln(\text{Sh}) - n_2 \ln(\text{Re}_f)$ versus $\ln(\text{Sc})$.

The value of n_1 has been found to be $n_1 = 0.17 \pm 0.06$.

Since the exponents are known the value of k^o can be found, which is $k^o = 0.63 \pm 0.03$, and therefore eq.(5.24) is transformed into eq.(5.29).

$$\text{Sh} = 0.63 \times \text{Sc}^{0.17} \text{Re}_f^{0.40} \left[\frac{C_f}{\rho}\right]^{-0.77} \left[\frac{P_b(0,w)}{P^o}\right]^{-0.55} \quad (5.29)$$

At this point it would be useful to be reminded the procedure which has been used so far. With the experimental data and by using eq.(3.86) the values of k were determined. These values show a tendency to follow a general pattern depending on the temperature, pressure, feed flow and feed concentration. If the simple and easy applicable eq.(5.24) is suggested, to describe the variation of k with the variables which have been mentioned, then it was found that most of the calculated k values follow eq.(5.29). Although eq.(5.29) has been found after experiments with the FilmTec membranes, it is believed that it could be also applied to other types of membranes as long as they have similar brine

spacers. It must be pointed out though that whenever eq.(5.29) is used, as h_b in the Sherwood number the value 0.077 cm should be used.

5.4 SOLUTE PERMEABILITY COEFFICIENT

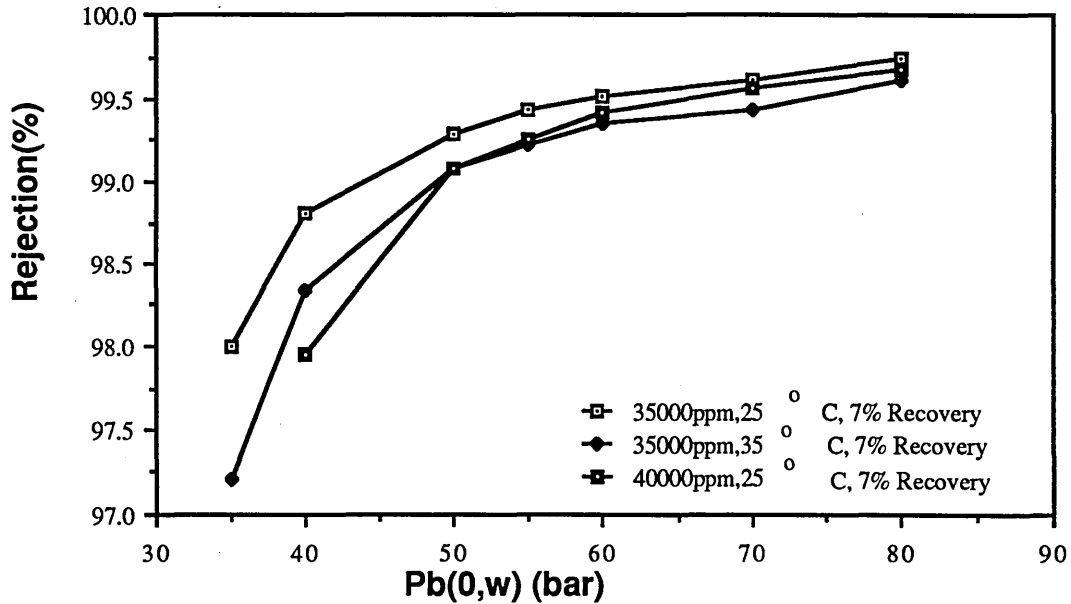


Fig.5.21 Rejection properties for different operating conditions.

The FT 30 SW 2.5" membranes have been proved to have excellent rejection properties. This can be seen in Fig.5.21 above, where the effect of the pressure on the rejection properties is presented.

These high rejection properties is expected to give very low solute permeability coefficient, k_2 , values. Indeed, if eq.(3.94) is applied, then the k_2 values can be found, see Table 5.6. Although they vary with the applied pressure and the concentration, these variations are random and an average value can be used without loss of accuracy. The k_2 varies with the temperature as well. If eq.(5.30) is suggested for the temperature dependence of the k_2 then a plot of this equation can give the values of β_T and k_2^0 , see Fig.5.22 below.

$$k_2^T = k_2^0 e^{\beta_T \frac{T-T_0}{T_0}} \quad (5.30)$$

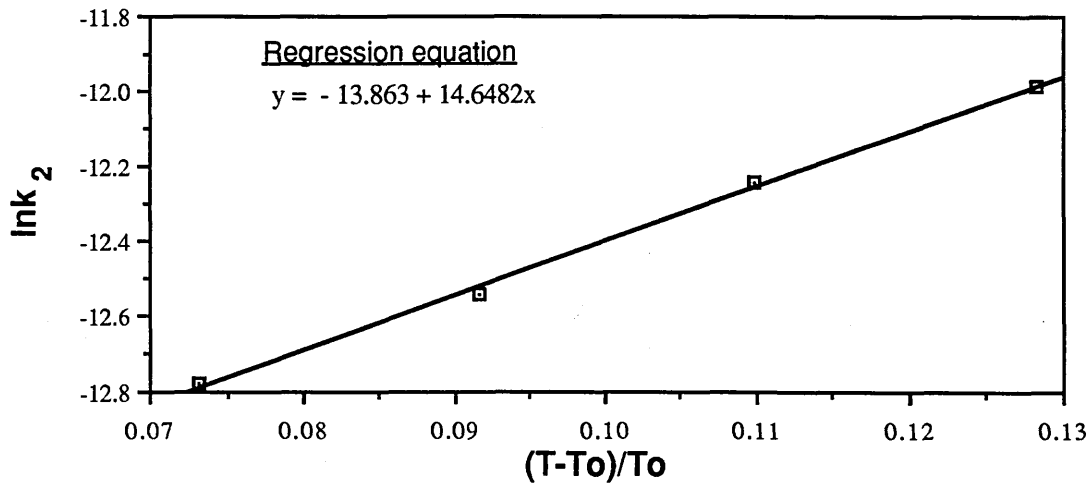


Fig.5.22 $\ln k_2$ versus the relative increase on temperature.

By using Fig.5.22, eq.(5.30) can be written as,

$$k_2 = 9.536 \times 10^{-7} e^{14.648 \frac{T - T_0}{T_0}} \quad (5.31)$$

5.5 EFFECTIVE PRESSURE, WATER FLUX, WALL CONCENTRATION AND VELOCITY PROFILES.

The analytical solution which has been developed could be useful to find the profile of different parameters in the (x,y) plane. Two different cases could be examined for each variable, one for pure water as feed and one for salt water. The distilled water profiles could be used when very dilute salt water solutions are used.

5.5.1 Pressure and flux profiles.

Eq.(3.43) gives the effective pressure for the case of distilled water for every point (x,y). If eq.(3.43) is multiplied by k_1 , then the water flux at every point could be found, so that the profile of the flux and the effective pressure are similar. The plot of eq.(3.43) can be seen in Fig.5.23 below. It can be seen that the effective pressure increases in the y direction and decreases in the x direction, as it was expected taking into account the pressure drops in the permeate and the brine channel respectively. A similar graph is expected for the water flux.

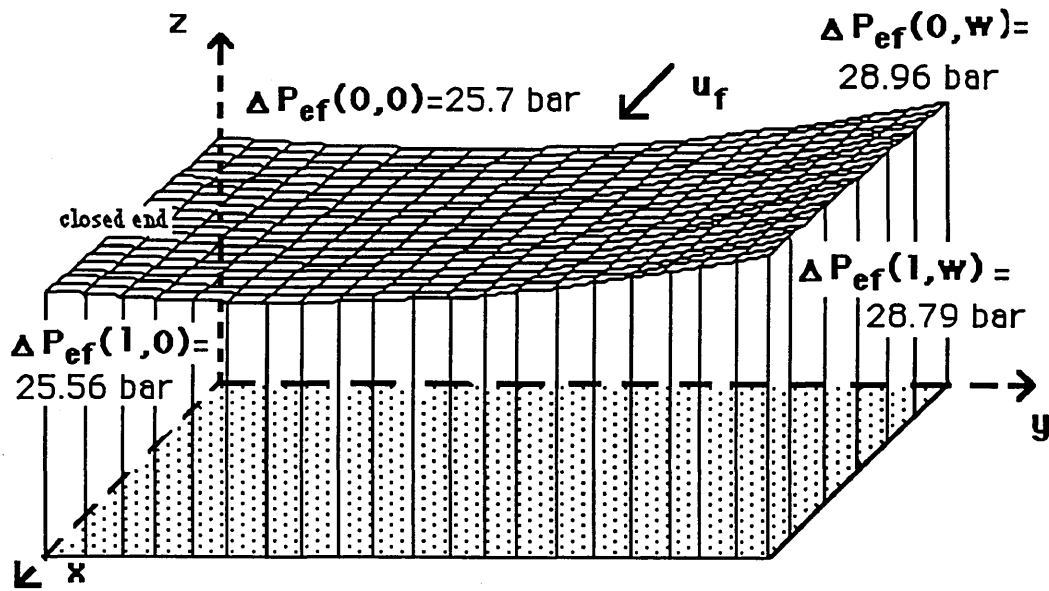


Fig.5.23 Effective pressure profile for distilled water solution at 20° C, $u_f = 30.15 \text{ cm/sec}$ and 30 bar.

For the plot of the effective pressure when salt water is used as feed, eq.(3.77) can be used, see Fig.5.24. As it was expected the decrease in the effective pressure in the x direction is higher than before because of the increasing salt concentration. A similar graph to Fig.5.24 can be obtained for the water flux.

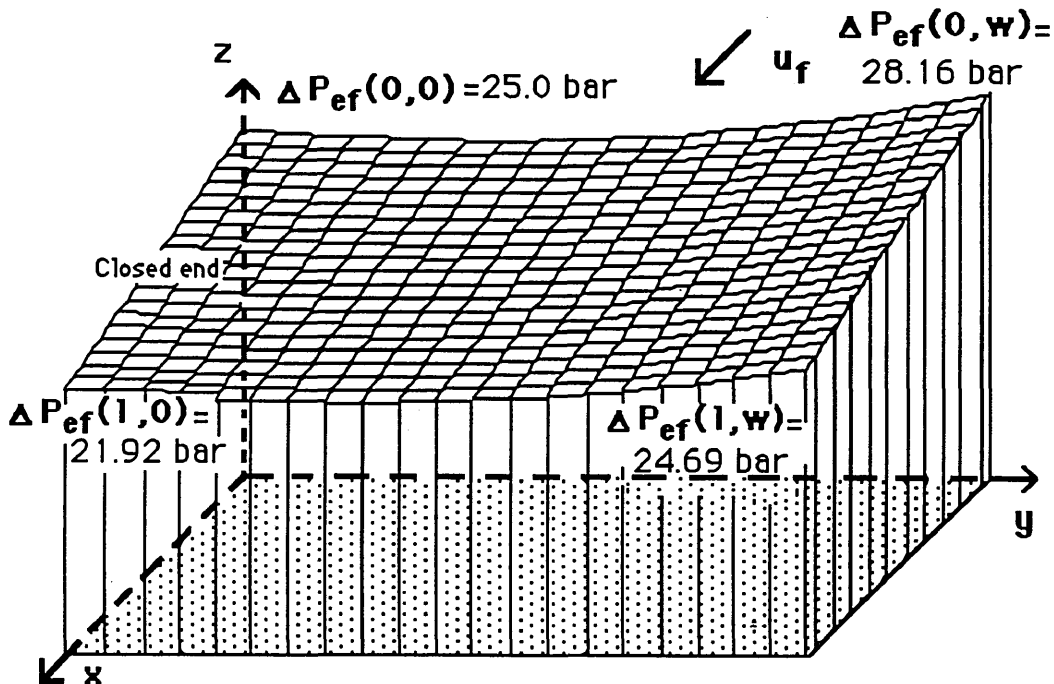


Fig.5.24 Effective pressure profile for 35,000 ppm sea-water solution at 20° C, $u_f = 12.25 \text{ cm/sec}$ and 55 bar.

5.5.2 Concentration profile.

The local water flux can be found by combining eq.(3.77) and eq.(3.16). Since the local flux is known as well as the mass transfer coefficient, eq.(5.27), the wall concentration could be found at every point (x,y),

$$c_{bw}(x,y) = c_b(x,y) e^{\frac{J(x,y)}{k}} \quad (5.32)$$

or,

$$c_{bw}(x,y) = [c_f + f x] e^{\frac{k_f \Delta P_f(x,y)}{k}} \quad (5.33)$$

The plot of eq.(5.33) can be seen in Fig.5.25. It must be noted that a constant k value has been assumed along the membrane, which is questionable, and it will be examined in a future work.

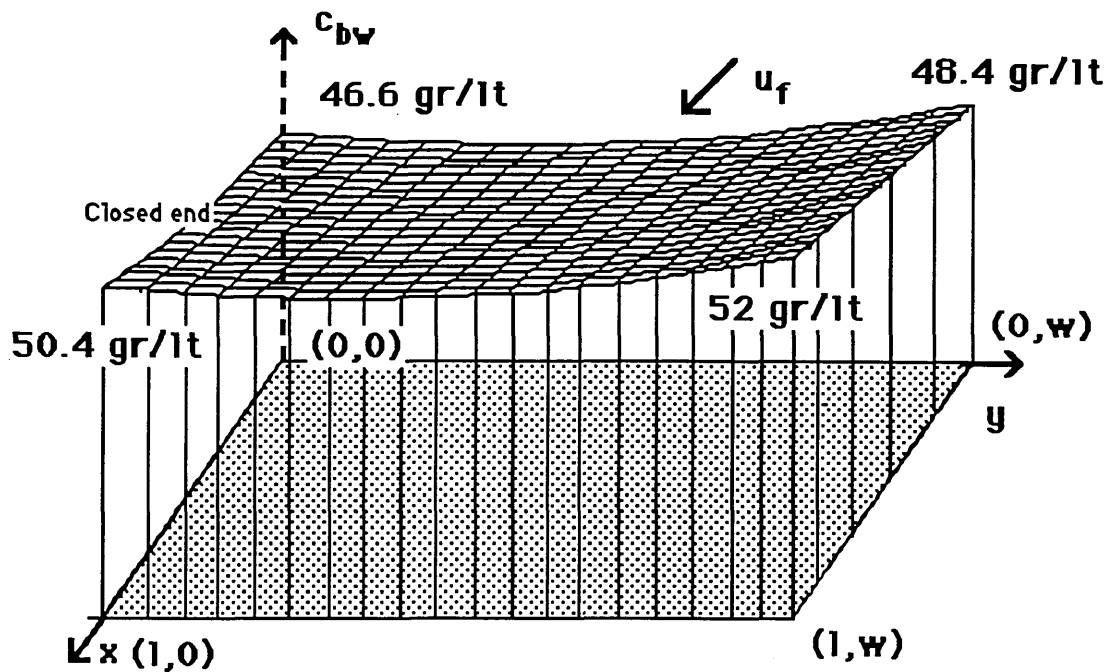


Fig.5.25 Salt wall concentration profile for 35,000 ppm sea-water solution at 20° C, $u_f = 12.25$ cm/sec and 55 bar.

5.5.3 Velocity profiles.

Brine velocity profile

Berman^[41] has developed velocity profile for laminar flow between parallel flat sheet membranes with constant permeate flux. Although this could be the case for very low feed concentrations pressure and brine flow, in reality and especially for sea water the flux varies quite significantly from point to point, so that it is questionable whether the equations developed by Berman can be applied for the spiral wound modules. In this work the brine velocity component in the y direction has been considered as zero so that the total brine velocity is equal with the brine velocity in the x direction. For distilled water as feed the brine velocity profile could be found if eq.(3.31) is integrated by using eq.(3.16) and (3.43), see eq.(5.34).

$$u_b(x,y) = u_f - \frac{2 k_1 \cosh \frac{y}{q}}{\cosh \frac{w}{q} h_b} [b \Delta P_{ef}^2(0,w) \sinh(ax) + \frac{u_f^2}{b} [1 - \cosh(ax)] + \Delta P_{ef}(0,w) u_f [1 - e^{-ax}]] / a [b \Delta P_{ef}(0,w) + u_f] \quad (5.34)$$

The plot of eq.(5.34) can be seen in Fig.5.26 .

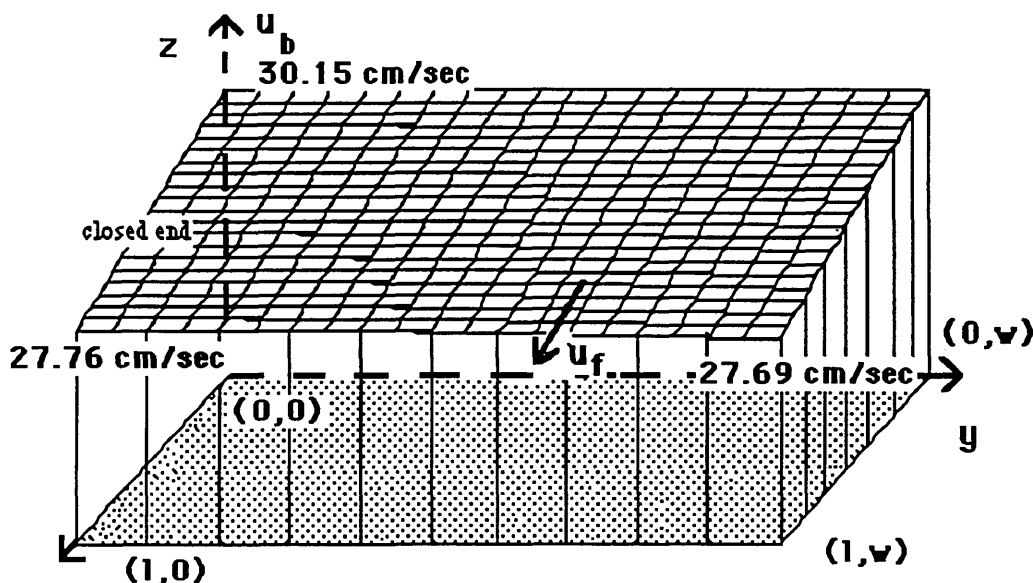


Fig.5.26 Brine velocity profile for distilled water at 20°C and 30bar.

The brine velocity profile for salt water as feed can be found if again eq.(3.31) is integrated by using eq.(3.16) and (3.77), see eq.(5.35).

$$u_b(x,y) = u_f - \frac{2 \cosh \frac{y}{q}}{h_b \cosh \frac{w}{q} \emptyset f} \left\{ [\Delta P - (c_f - c_p) \emptyset] \ln \gamma - \frac{k}{k_1} [\varphi - \ln \gamma] + \right. \\ \left. + \frac{(c_f - c_p) u_f k_{fb} \mu}{f} [\varphi - \ln \xi \ln \lambda - \frac{k_1^2 \emptyset^2}{4 k^2} (c_b^2(l) - c_f^2)] \right\} \quad (5.35)$$

The profile of eq.(5.35) is similar with that in Fig.(5.26) with the brine velocities at the limits as: $u_b(0,0) = u_b(0,w) = u_f = 12.25$ cm/sec, $u_b(l,0) = 10.65$ cm/sec and $u_b(l,w) = 10.2$ cm/sec, with 35,000 ppm sea-water solution at 20° C and 55 bar.

Permeate velocity profile

The permeate velocity profile could be found for distilled water if eq.(3.17) is integrated by using eq.(3.16) and (3.43).

$$u_p(x,y) = \frac{2 k_1 q \sinh \frac{y}{q}}{h_p \cosh \frac{w}{q}} \left[b \Delta P_{ef}^2(0,w) \cosh(ax) - \frac{u_f^2 \sinh(ax)}{b} + \right. \\ \left. + \Delta P_{ef}(0,w) u_f e^{-ax} \right] / (b \Delta P_{ef}(0,w) + u_f) \quad (5.36)$$

The plot of eq.(5.36) can be seen in Fig.5.27 below.

The permeate velocity variation for salt water is given by eq.(5.37).

$$u_p(x,y) = \frac{2 q k_1 \sinh \frac{y}{q} k}{h_p \cosh \frac{w}{q} [k + k_1 \emptyset (c_f + fx)]} \left\{ \Delta P_{ef}(0,w) \frac{(k + k_1 \emptyset c_f)}{k} + \right. \\ \left. + \frac{c_f u_f k_{fb} \mu}{f} \ln \frac{c_f}{c_f + fx} - \emptyset fx \right\} \quad (5.37)$$

The limits are $u_p(0,0) = u_b(1,0) = 0.0$ cm/sec, $u_p(0,w) = 2.764$ cm/sec and $u_p(1,w) = 2.1346$ cm/sec and a similar graph with that in Fig.5.27 could be found , with 35,000 ppm sea-water solution at 20° C and 55 bar.

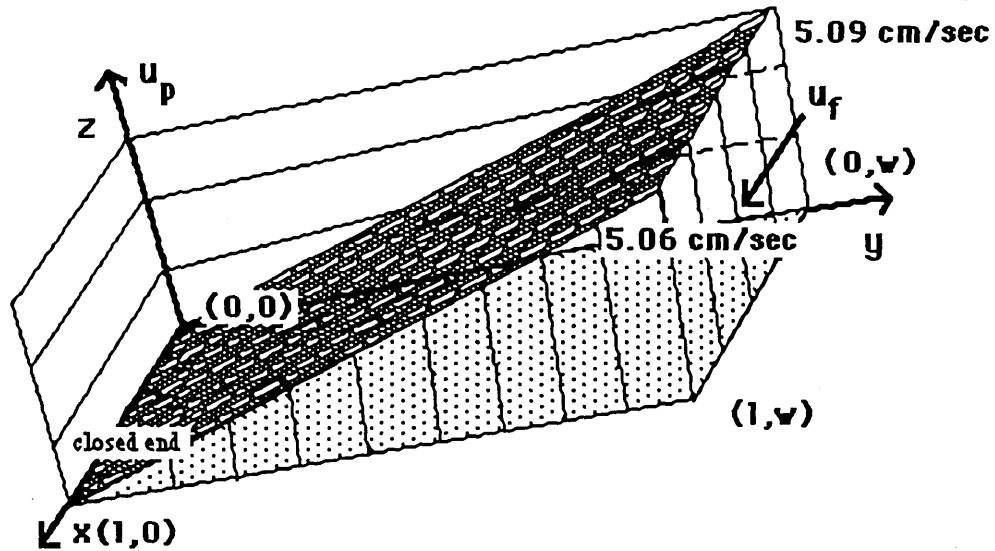


Fig.5.27 Permeate velocity profile for pure water at 20° C and 30 bar.

CHAPTER VI

SPIRAL WOUND MODULE PERFORMANCE PREDICTIONS

6.1 INTRODUCTION

In this chapter predictions are made for the spiral wound module performance. The basic working equations used are eq.(3.86) and eq.(3.94). In these equations the permeate concentration has been ignored as insignificant at the particular experimental conditions which have been used. Since the values of five parameters are needed for the performance predictions of the modules, the correlations which have been found in chapter V will be used. These are: eq.(5.5) for the brine friction parameter, eq.(5.16) for the water permeability coefficient, eq.(5.29) for the mass transfer coefficient, eq.(5.31) for the solute permeability coefficient, and the permeate friction parameter is considered as constant at $k_{fp} = 1,100,000 \text{ cm}^{-2}$. The validity of eq.(3.86) and eq.(3.94) is tested not only with experimental data at 25,000 ppm, 35,000 ppm and 40,000 ppm sea-water solutions but also at 25,200 ppm with a new membrane (No3). The effects of all the process variables (pressure, feed concentration etc.) on the water flux and the permeate concentration are examined and a comparison of theoretical and experimental results is made. The flux and the permeate concentration were found by using a computer programme, see Appendix I, PROGRAM PAR4. The brine concentration gradient, f , can be found by using mass balance equation (6.1).

$$f = \frac{2J w c_f}{Q_f - 2Jw} \quad (6.1)$$

Finally suggestions are made for optimum module design so that the maximum water flux could be achieved.

6.2 MODULE PERFORMANCE PREDICTIONS

In this section the effects of the applied pressure, feed velocity and feed concentration on the water flux and the permeate concentration is examined, by using eqs (3.86) and (3.94). At the same time comparisons are made between the calculated and the theoretical values.

6.2.1 Applied pressure effect on the module performance.

If all the conditions are kept constant and the pressure is allowed to vary, then the effect of the pressure on the membrane performance can be found, see Fig.6.1. Similar graphs can be found for different operating conditions.

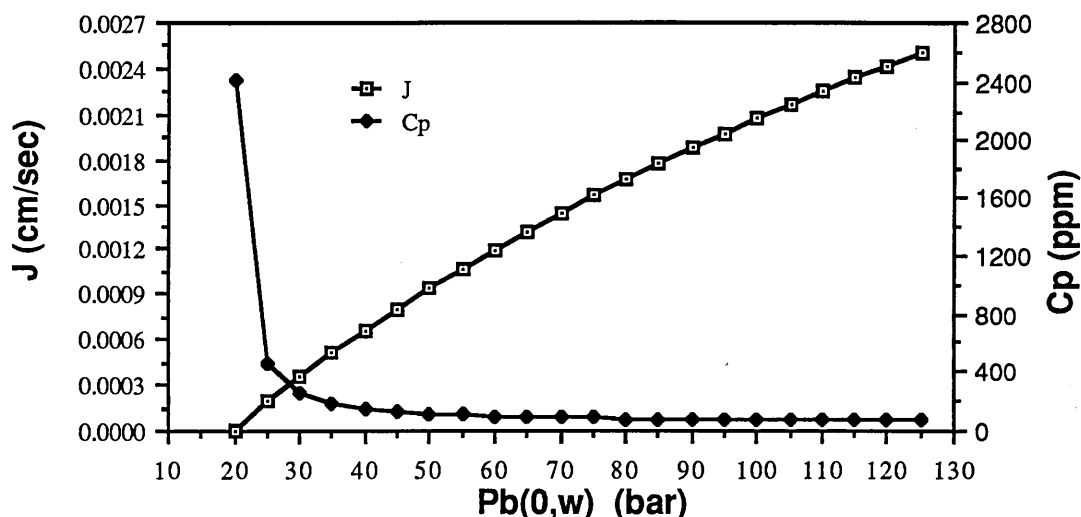


Fig.6.1 Average water flux and permeate concentration as a function of the applied pressure, for 25,000 ppm sea-water at 25° C and $Q_f=10.846$ lt/min.

It can be concluded that as the applied pressure increases the average water flux increases and the permeate concentration decreases. It has been suggested^[40] that the curve for high pressures is not linear but rather exponential reaching asymptotic a value. This behaviour though was not noticed under the experimental conditions which have been used here. As far as the permeate concentration is concerned, there is a great increase in permeate quality as the pressure increases, starting from 20 bar. The Osmotic pressure is 19 bar at 25,000 ppm. The permeate salt concentration decreases much slower for pressures higher than 40 bar.

The theoretical and the experimental values for the water flux and the permeate concentration for different conditions can be seen in Table 6.1 below. The differences between the theoretical and experimental values for the water flux are less than 6 % and for the permeate concentration less than 12 %. Some more data to compare experimental and theoretical values are presented in Fig.6.2 below, for membrane No1, where very good agreement between experimental and theoretical values can be seen.

Table 6.1

Comparison between experimental and calculated data for membrane No 1.

Cf (ppm)	Temp. (°C)	Pb(0,w) (bar)	Qf (lt/min)	Jx10 ⁴ (cm/sec)		Cp (ppm)	
				exp.	theor.	exp.	theor.
25000	25	50	7.935	9.589	9.096	115	129
25000	25	55	8.076	10.750	10.386	106	117
25000	25	60	10.849	12.270	11.986	89	101
25000	25	70	8.507	14.290	14.007	92	98
35000	20	50	7.453	5.240	5.548	235	216
35000	20	55	7.584	6.840	6.566	200	191
35000	20	60	7.692	7.750	7.543	182	174
35000	20	70	7.898	9.470	9.390	166	152
35000	20	80	8.101	11.180	11.110	161	139
40000	30	55	7.578	6.650	6.543	370	365
40000	30	60	7.722	7.840	6.731	317	324
40000	30	70	16.142	11.260	11.167	216	223
40000	30	80	13.674	13.520	13.209	189	209

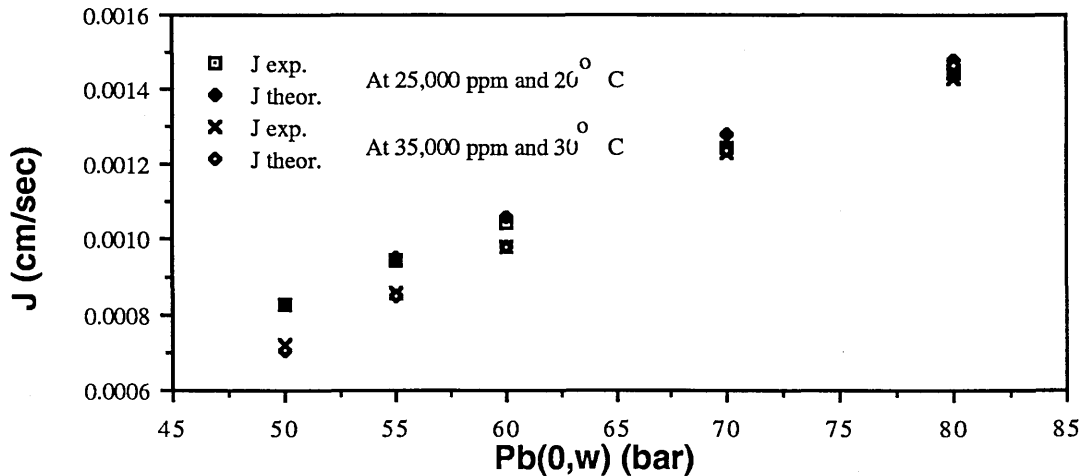


Fig.6.2.a Average water flux for different conditions for sea water solutions (membrane No1).

The validity of the model will be established when it can predict the module performance for data, which have never be used in order to find the correlation equations for the mass transfer coefficient and the solute permeability coefficient, such as that at 25,200 ppm. At this concentration a complete new membrane was used, (Membrane No3). The membrane was first tested in distilled water at Pressures from 20 bar to 50 bar and at temperatures 25° C and 30° C, see Table 6.2 below.

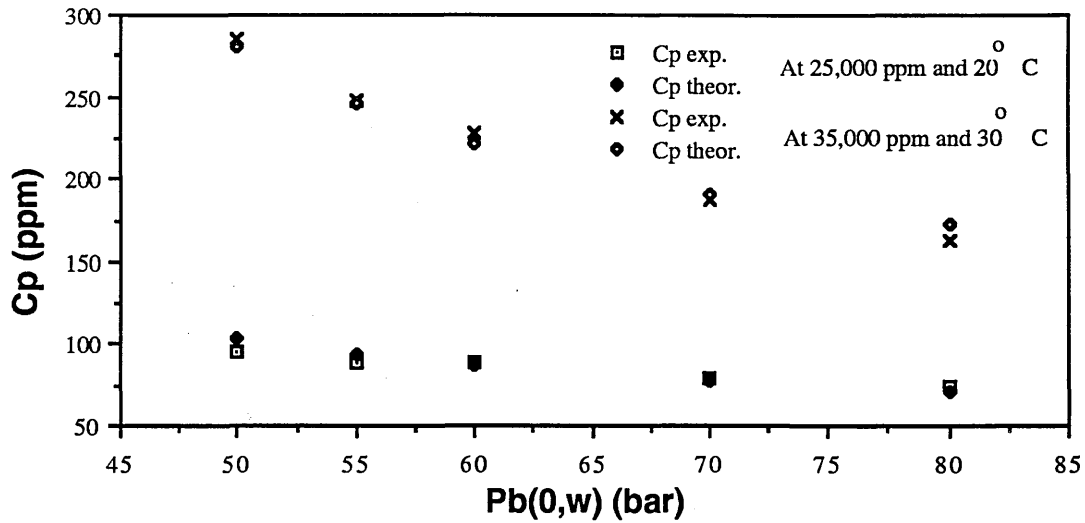


Fig.6.2.b Permeate concentration at different conditions for sea water (membrane No1).

Table 6.2

Experimental data with distilled water for membrane No3.

Temp.,(°C)	Pb(0,w), (bar)	Q _f ,(lt/min)	Q _p ,(lt/min)	k ₁ × 10 ⁵ , (cm/sec bar)
25	20	10.162	0.809	3.772
25	25	10.330	0.977	3.602
25	30	10.519	1.166	3.536
25	40	10.915	1.562	3.536
25	50	11.288	1.935	3.552
30	20	10.300	0.947	4.441
30	25	10.525	1.172	4.356
30	30	10.753	1.400	4.314
30	35	11.009	1.656	4.369
30	40	11.231	1.878	4.325
30	45	11.443	2.090	4.270

From these data and using Program PAR2, the water permeability values for this new membrane could be found. The equations giving k₁ as a function of the pressure can be seen in the following equations.

$$\text{at } 25^{\circ} \text{ C} \quad k_1 = 3.8225 \times 10^{-5} e^{-0.0018 P_b(0,w)} \quad (6.2)$$

$$\text{at } 30^{\circ} \text{ C} \quad k_1 = 4.515 \times 10^{-5} e^{-0.0012 P_b(0,w)} \quad (6.3)$$

Following this experiment the membrane was tested at 25° C and 30° C with 25,200 ppm seawater solution for different pressures and the data collected are presented in Table 6.3. The theoretical average water flux and permeate concentration can be found by using the PROGRAM PAR4. It must be mentioned that the friction parameters and the solute permeability coefficient were considered the same as for membrane No1. The water permeability coefficient were given by eqs.(6.2) and (6.3). The comparison of the experimental and the theoretical values can be seen in Table 6.3.

Table 6.3

Comparison between experimental and calculated data for membrane No 3.

Cf (ppm)	Temp. (°C)	Pb(0,w) (bar)	Qf (lt/min)	Jx10 ⁴ (cm/sec)		Cp (ppm)		
				exp.	theor.	exp.	theor.	theor.*
25200	25	50	10.403	8.64	8.47	96	132	100
25200	25	60	10.703	11.11	10.96	83	110	84
25000	25	70	11.003	13.58	13.32	78	97	74
25000	25	80	11.263	15.72	15.58	75	89	68
25200	25	90	11.443	17.20	17.73	74	83	64
25200	30	40	10.168	6.71	6.79	163	202	161
25200	30	50	10.476	9.25	9.91	112	150	120
25200	30	60	10.835	12.21	12.91	102	124	99
25200	30	70	11.155	14.84	15.78	97	110	88
25200	30	75	11.295	15.99	17.17	96	105	84
25200	30	80	11.449	17.26	18.54	95	101	82

The results in Table 6.3 show a very good agreement between the theoretical and experimental values for the average water flux. For the permeate concentration there are discrepancies when the solute permeability coefficient from membrane No1 was used, see column *theor.*. If the solute permeability coefficient was determined by using one set of data from Table 6.3, that is at 25° C $k_2=2.75 \times 10^{-6}$ cm/sec and at 30° C $k_2= 3.78 \times 10^{-6}$ cm/sec, then, there is a much better agreement between the theoretical and experimental values, see column *theor.**. It can be concluded that for sea-water solutions the analytical solution, which have been developed, can predict the spiral wound module performance with very good accuracy.

Since the analytical solution, which has been tried so far was for high feed concentrations, it is interesting to see what prediction can make at low feed concentrations. For this, data published for the ROGA spiral wound module[18] can be used. If the calculated values in Chapter III are used, which are: $k_1=2.085 \times 10^{-5} \text{ cm sec}^{-1} \text{ bar}^{-1}$, $k_{fb}=172000 \text{ cm}^{-2}$, $k_{fp}=567000 \text{ cm}^{-2}$, $k_2=1.79 \times 10^{-5} \text{ cm sec}^{-1}$, then the average water flux and the permeate concentration can be found, see Fig.6.3. The differences between all but one the calculated and the experimental values for the water flux is less than 3 %, and for the permeate concentration less than 7 %.

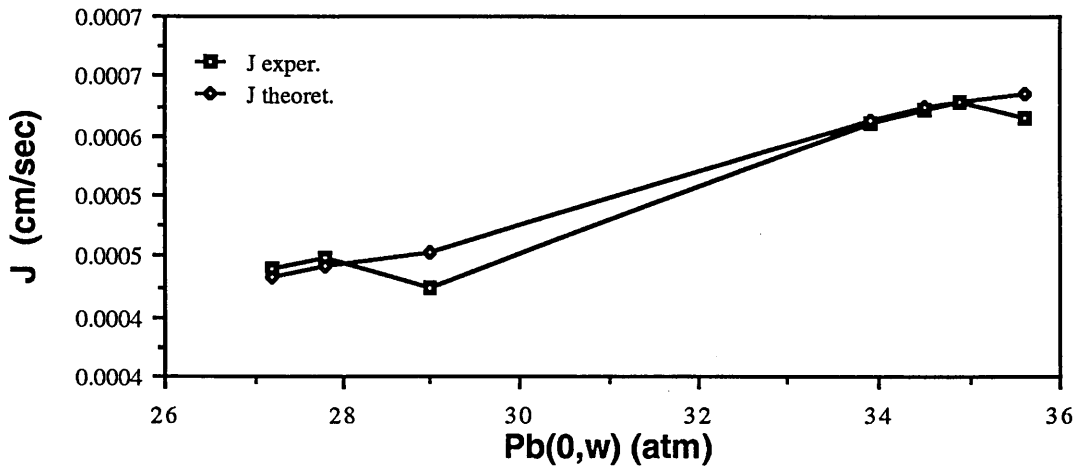


Fig.6.3.a Average water flux at different low feed concentrations and different feed flows for ROGA-4160 membrane.

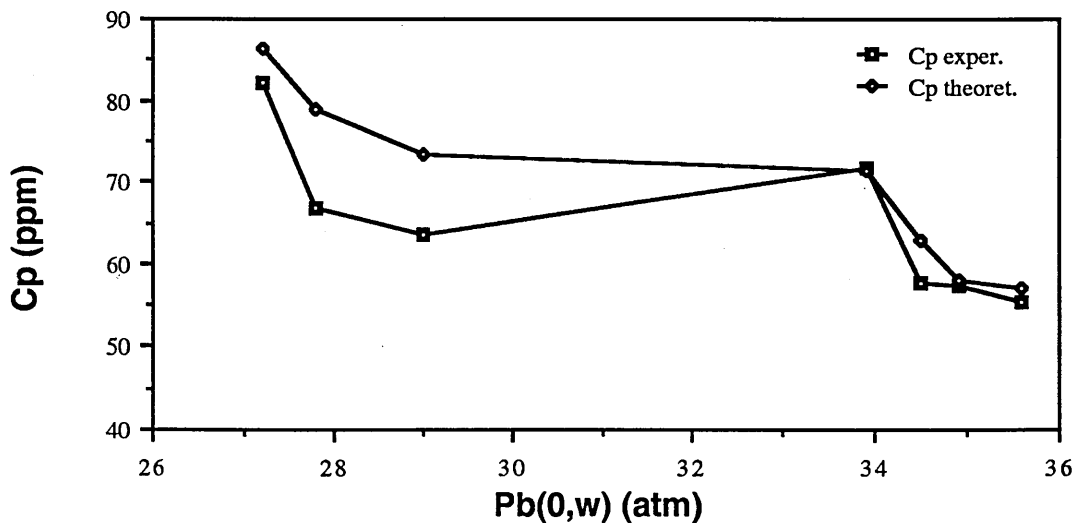


Fig.6.3.b Permeate concentration at different feed concentrations and different feed flows for ROGA-4160 membrane.

It can be concluded that the analytical solution, which has been developed for high feed concentration can also be applied for low feed concentrations.

6.2.2 Feed concentration and velocity effects on the module performance.

If the feed concentration varies, while all the other variables remain constant, it is expected that the water flux will decrease and the permeate concentration will increase. The exact effect of the feed concentration on the membrane performance can be predicted by using eqs (3.86) and (3.94), see Fig.6.4 below. It must be mentioned that increasing the feed concentration causes the flux and the recovery to decrease, since the feed velocity is kept constant.

It can be seen in Fig.6.4 that the predicted water flux and permeate concentration variations are not linear. The permeate concentration increases more rapidly at high feed concentrations than at low feed concentrations, that is closer to zero effective driving pressure. At 63.0 gr/lt feed concentration the flux is becoming zero, since the net driving pressure is zero. Although Osmotic pressure of 50 bar, in the feed side, is achieved for feed concentration at 68.6 gr/lt, one must bear in mind that because of the concentration gradient along the membrane this pressure will be achieved at lower feed concentration, which is at the given operating conditions 63.0 gr/lt. When the feed concentration exceeds 63.0 gr/lt the flux is becoming negative for obvious reasons.

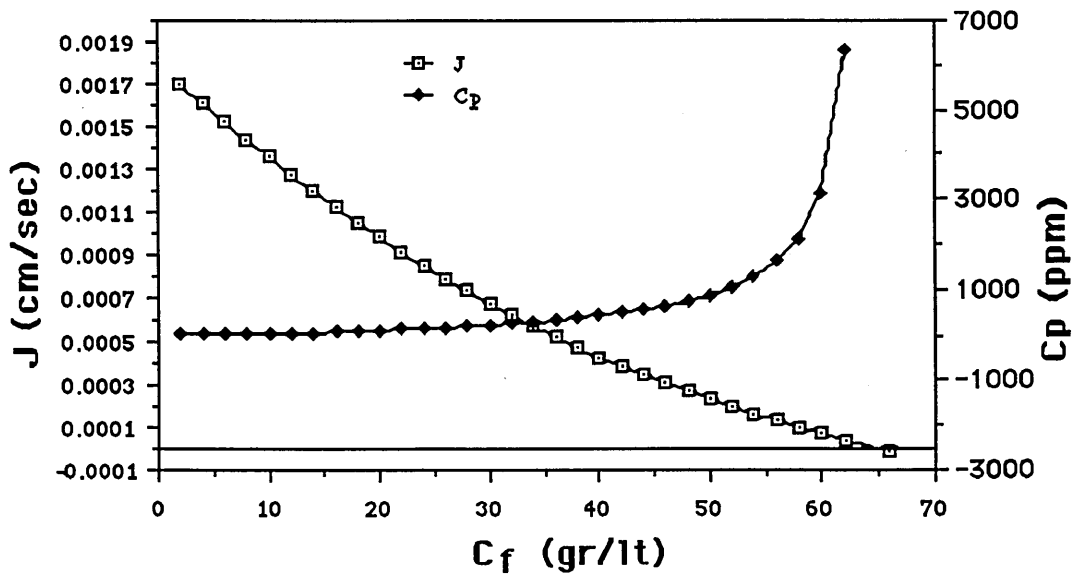


Fig.6.4 Average water flux and permeate concentration for different feed concentration at 50 bar, $u_f=6.7$ cm/sec and 25° C .

The effect of the feed velocity on the module performance can be seen in Fig.6.5.

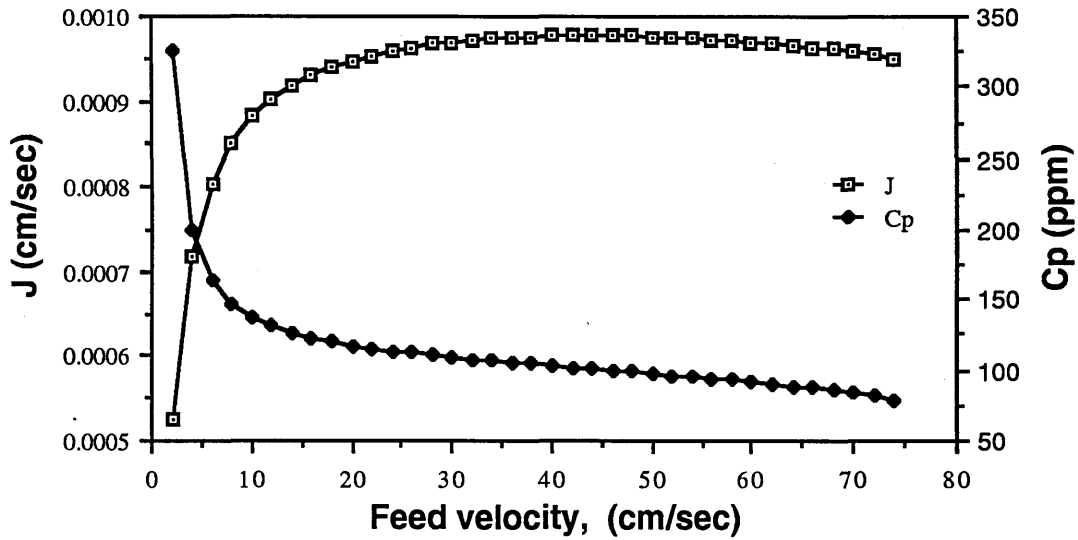


Fig.6.5 Average water flux and permeate concentration for different feed velocities at 50 bar, 25,000 ppm and 25° C .

The increase in feed velocity affects the membrane performance in many ways. The mass transfer coefficient increases, so that, the water flux increases and the permeate concentration decreases. The recovery decreases with increasing feed velocity so that the concentration gradient along the membrane decreases. As a result of that, one could expect an increase in the water flux and a decrease in the permeate concentration.

At very high feed velocity the pressure drop in the permeate channel is becoming significant with an obvious reduction in the effective driving pressure and the water flux. All these effects can be seen in Fig.6.5. As the velocity increases, starting from low values, the effects of the increasing mass transfer coefficient and the decreasing recovery are dominant result in a dramatic increase in the water flux and a decrease in the permeate concentration. Both of these effects are becoming less significant as the velocity increases and the slopes of both curves are getting smaller. At very high velocities though, it seems that the dominant factor is the increasing pressure drop in the brine channel and the obvious result is a water flux decline. The permeate concentration on the other hand continues to decrease. Although this appears to be an odd result, it can be explained if one considers eqs (3.16), (3.57), (3.87) and (3.93), which yield eq.(6.4) for the locally produced permeate concentration.

$$c_p(x,y) = \frac{k_2 c_{bw}(x,y)}{k_1 [P_b(x,y) - P_p(x,y) - \phi c_{bw}(x,y)] + k_2} \quad (6.4)$$

From eq.(6.4) it can be seen that although the denominator of the ratio, which expresses roughly the water flux may decrease at very high velocities, the numerator decreases faster so that the ratio decreases.

6.3 OPTIMUM MODULE DESIGN

In this section the effect of the module geometry on the spiral wound module performance will be examined by using the equations developed in section 3.8. The basic working equations are eq.(3.98) and eq.(3.102).

$$\frac{Q_p}{V} = \frac{2Bw l h_p^{1/2} \tanh \frac{w \sqrt{2k_1 k_{fp} \mu}}{h_p^{1/2}}}{l_2 w_2 \sqrt{2k_1 k_{fp} \mu} (h_p + h_b + 2h_m)} \quad (3.98)$$

where,

$$B = \frac{1}{wl\phi f} \left\{ (\Delta P - c_f \phi) \ln \gamma - \frac{k}{k_1} [\phi - \theta \ln \gamma] + \frac{c_f u k_{fb} \mu}{f} [\phi - \ln \xi \ln \lambda] \right\} \quad (3.95)$$

$$\frac{1}{h_p^2 + (h_b + 2h_m)h_p} \left[\frac{1}{h_p^2} \operatorname{sech}^2 \left(\epsilon h_p \right) \epsilon h_p + \tanh \left(\epsilon h_p \right) \left[\frac{1}{h_p^2} - \frac{1}{(h_b + 2h_m)h_p} \right] \right] = 0 \quad (3.102)$$

Eq.(3.102) can give us the optimum permeate channel height for a given membrane module. It is interesting to see that eq.(3.102) predicts that the optimum permeate channel height is independent of the operating conditions. It predicts that the factors which affect the optimum permeate channel height are: the water permeability coefficient, the permeate friction parameter, the brine channel height, the membrane thickness and the membrane width.

The optimum permeate channel height may be found by using eq.(3.98). With this equation the effects of other variables like width can be examined. In Fig.6.6.a, the effect

of the permeate channel height on the permeate flow per unit volume for different widths can be seen.

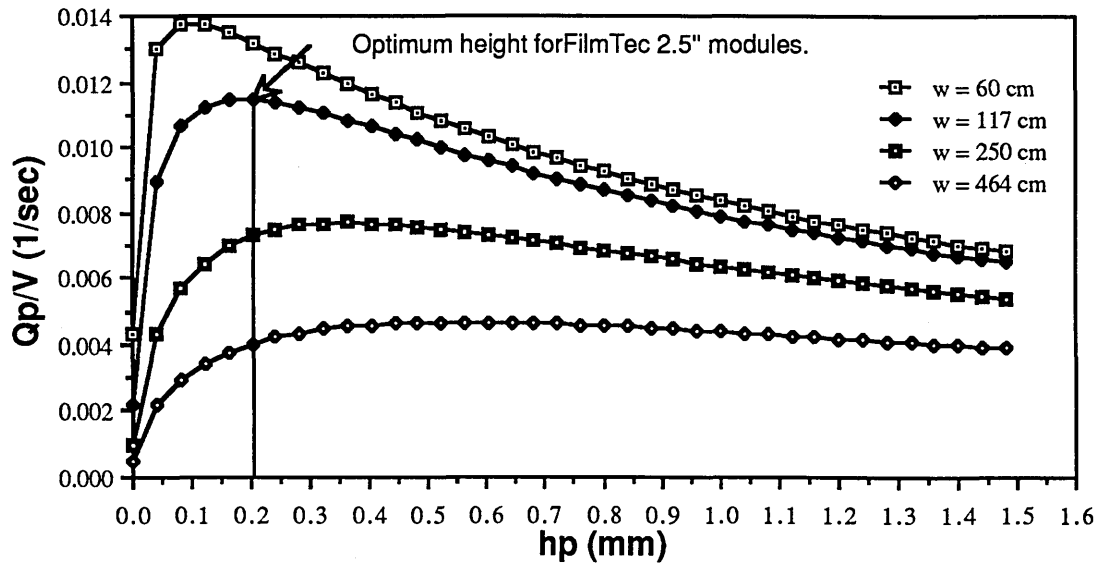


Fig.6.6.a Water flow per unit volume at 60 bar, 35,000 ppm, 25° C and $Q_f=10.421$ lt/min.

All the curves have a maximum and as the width increases the specific productivity of the module decreases and the maximum specific productivity is achieved at higher permeate channel height. For the normal width the maximum productivity is achieved for $h_p = 0.2$ mm approximately. At the same time for the high width values the curves are becoming broader at the maximum. This behaviour is due to the increasing pressure drop in the permeate channel with the increasing width. This affects the driving pressure and consequently the productivity of the module.

It could be concluded that for a given module diameter the number of leaves should be as many as possible in order to keep the membrane width (leaf spiral length) as small as possible, so that high productivity could be achieved. However the number of leaves is limited by manufacturing difficulties.

The effect on the permeate concentration can be seen in Fig.6.6.b below. There is a sharp decrease on the permeate concentration as the permeate height approaches the optimum value and after that point there is a much smaller decrease. The smaller the width is the better the permeate quality and smaller the effect of the permeate height on the permeate quality.

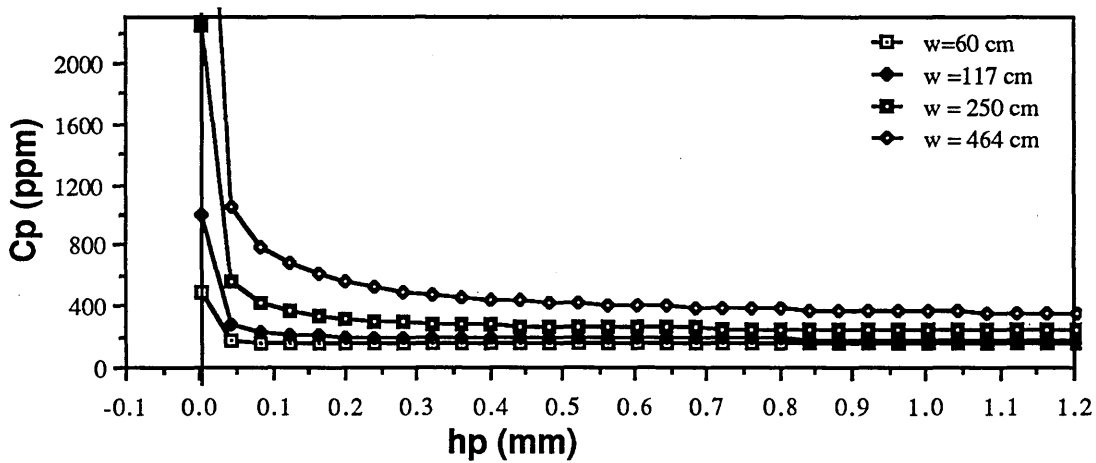


Fig.6.6.b Permeate concentration at 60 bar, 35,000 ppm, 25° C and $Q_f=10.421$ lt/min.

As it has been predicted by eq.(3.102) the feed concentration, see Fig.6.7, and the applied pressure, see Fig.6.8, have no effect on the optimum permeate channel height. There are however, differences on the membrane productivity depending on the feed concentration, or the applied pressure.

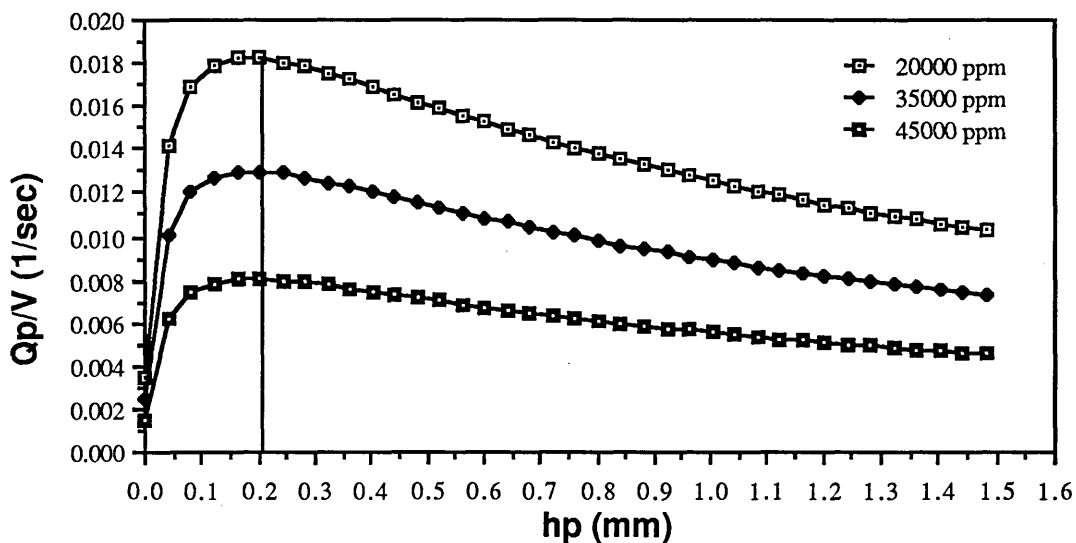


Fig.6.7 Water flow per unit volume at 60 bar, $Q_f=10.421$ lt/min and 25° C .

From Fig.6.7 and Fig.6.8 it can be seen that the lower is the specific productivity, because of high feed concentration or low applied pressure, the smaller the effects of the variation of the permeate height on the flow rate per unit volume.

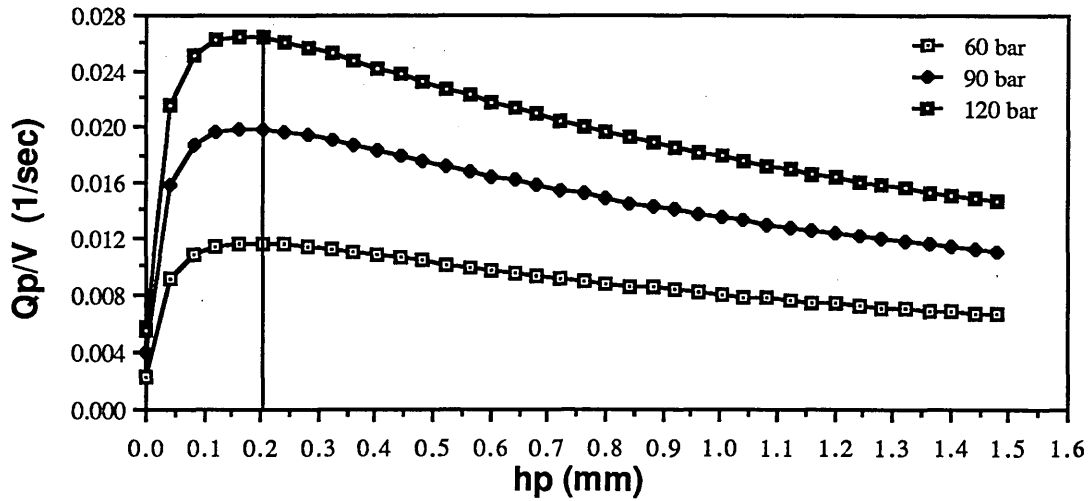


Fig.6.8 Water flow per unit volume at 35,000 ppm, $Q_f=10.421$ lt/min and 25° C .

The effect of the brine channel height to the membrane specific productivity and permeate quality can also be examined by using eq.(3.98). Since the brine channel height affects the brine velocity, two different conditions have been used. The first is when the feed velocity is kept constant and the second when the feed flow is kept constant. When the feed velocity is kept constant, there is an optimum brine channel height, where the specific productivity is maximum, see Fig.6.9.a.

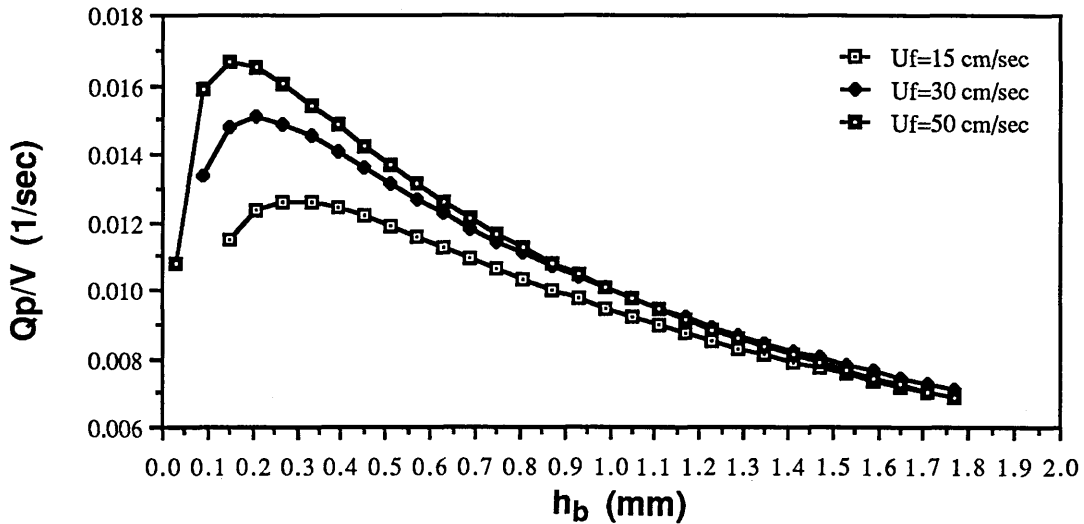


Fig.6.9.a Water flow per unit volume at 35,000 ppm, 60 bar and 25° C at constant feed velocity.

This is due to the fact that when the brine channel height increases the pressure drop in this channel decreases and the driving pressure increases. At the same time the volume

increases with increasing brine channel height, so that there is an optimum height where the ratio Q_p/V is maximum. The maximum shifts towards higher brine channel heights, as the velocity decreases. At the same time the specific productivity decreases and the maximum is becoming broader. These are results of higher concentration polarization effects at low velocities, so that the effects of the brine pressure drop and the module volume are less significant as compared to the concentration polarization effects. The higher the feed velocity the greater the effect of the brine channel height on the specific productivity.

The permeate concentration can be seen in Fig.6.9.b, for the same conditions. The permeate quality increases rapidly as the brine height approaches the optimum and the quality increases with the brine velocity due to smaller wall concentration.

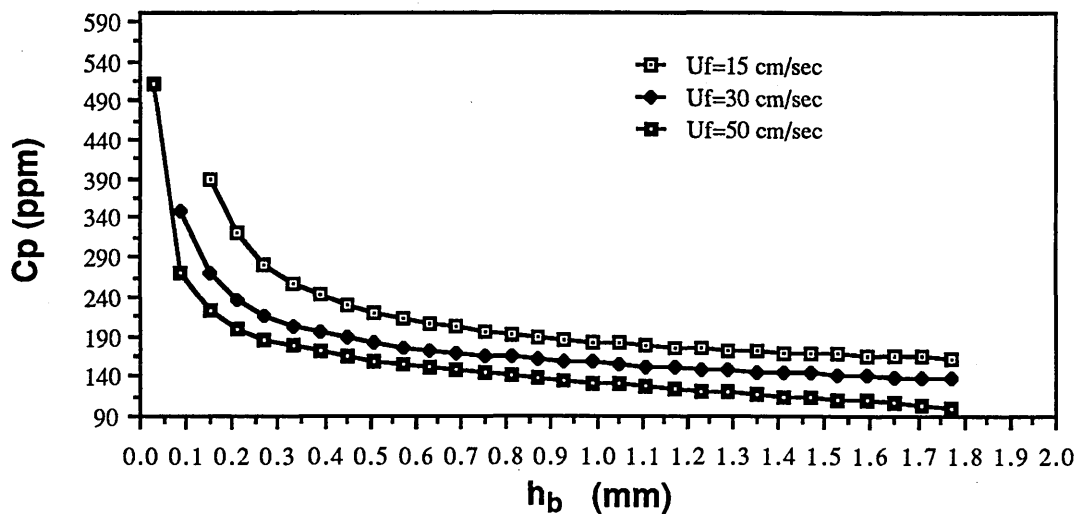


Fig.6.9.b Permeate concentration at 35,000 ppm, 60 bar and 25°C at constant feed velocity.

The effect of the brine channel height on the module specific productivity, when the feed flow is kept constant can be seen in Fig.6.10.a below. In this case the specific productivity for very small brine channel height increases initially with the brine channel height due to lower pressure drop in the brine channel. As the brine channel height continuous to increase the pressure drop in the brine channel becomes insignificant and the dominant factor is the concentration polarization effect. As a result of this the productivity decreases because the brine velocity decreases with increasing brine channel height.

The permeate quality for the same conditions can be seen in Fig.6.10.b. The permeate

concentration increases as the brine channel height increases for moderate and high feed flows, though for low feed flows it decreases. These occur as a result of a combination of the brine pressure drop and the wall concentration. Beyond a special brine channel height value, depending on the feed flow, the effect of the brine channel height is almost negligible, as far as the permeate concentration is concerned.

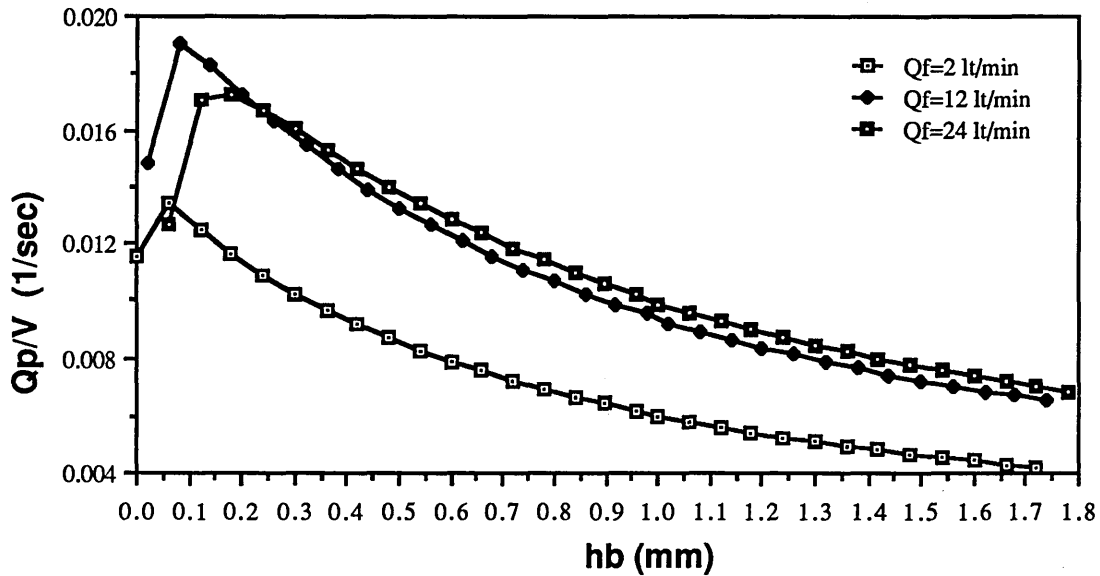


Fig.6.10.a Water flow per unit volume at 35,000 ppm, 60 bar and 25° C at constant feed flow.

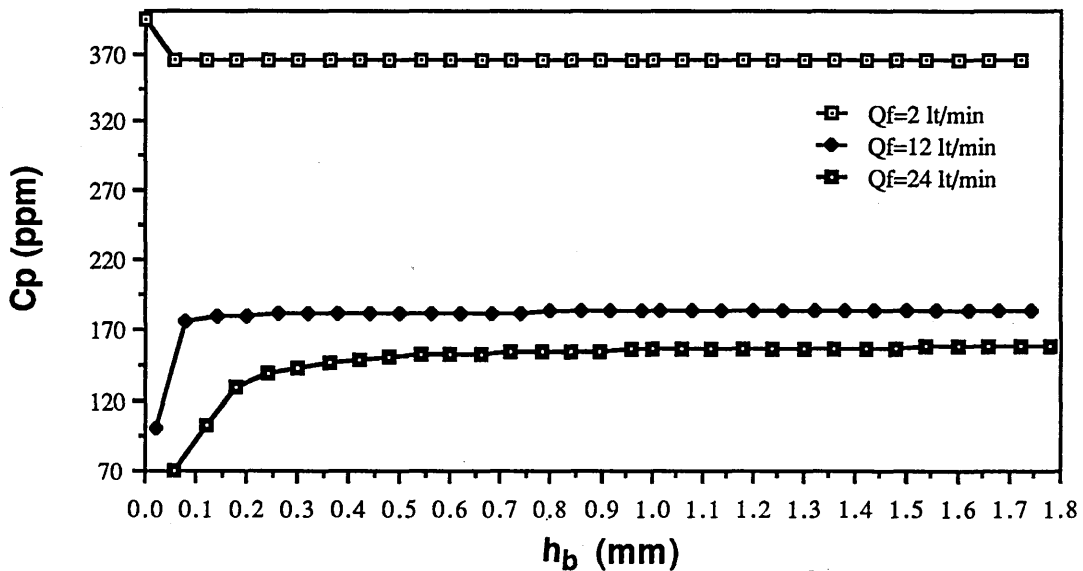


Fig.6.10.b Permeate concentration at 35,000 ppm, 60 bar and 25° C at constant feed flow.

6.4 THE EFFECTS OF THE VARIATION OF THE FIVE PARAMETERS ON THE PREDICTED VALUES OF FLUX AND PERMEATE CONCENTRATION

In this section the effects which the water permeability coefficient, solute permeability coefficient, mass transfer coefficient, brine friction parameter and permeate friction parameter, have on the predictions of the analytical model will be examined. All these 'five parameters' are essential for describing a particular module.

In Fig.6.11 the effects of the variation of water permeability coefficient, k_1 , on the flux and permeate concentration can be seen as well as the experimental and theoretical values for the actual operating conditions. It can be said that a 70 % decrease (from the measured value) of the k_1 value causes 61 % decrease in the water flux and 114 % increase in the permeate concentration. On the other hand 100 % increase in k_1 causes 51 % increase in water flux and 23 % decrease in permeate concentration. It can be conclude that the variation of k_1 affects the water flux and the permeate quality substantially. It is interesting to see that the relation between the flux and k_1 is not linear and the higher the k_1 is the smaller the effect on the water flux. This is due to the increasing pressure drop in the permeate channel because of higher permeate flow.

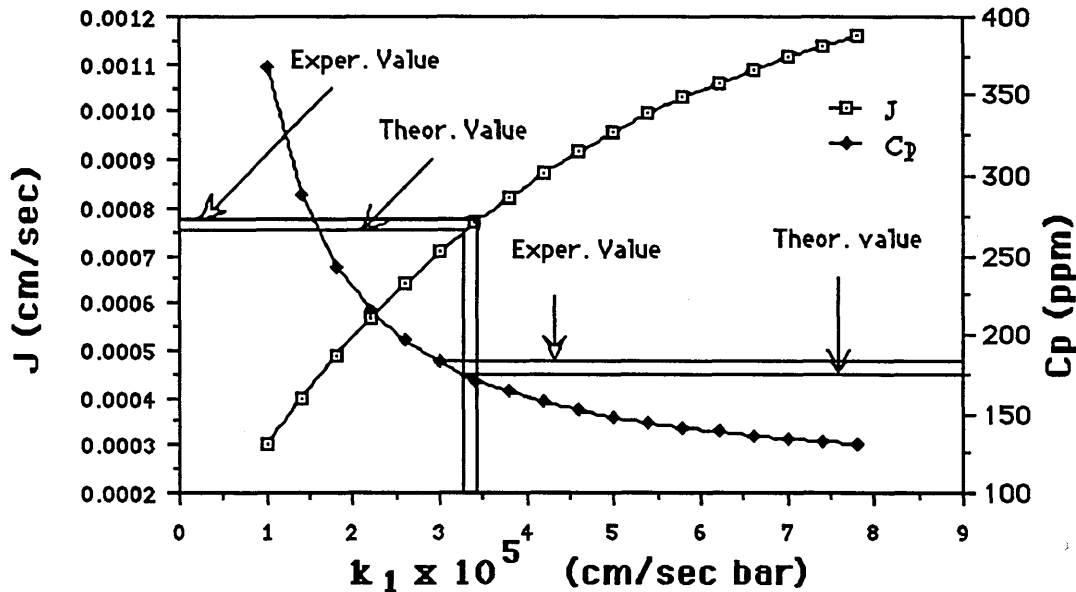


Fig.6.11 Average Water flux and Permeate concentration at 35,000 ppm, 60 bar, $Q_f=7.692$ lt/min and 20° C for Membrane No1 for different water permeability values.

The effects of the brine friction parameter values, k_{fb} , on the membrane performance

can be seen in Fig. 6.12. It apparent that the effect of the brine friction parameter can be ignored for this type of spacers and the dimensions of the module, since the effect on the module performance is less than 2 % even when the k_{fb} increases by a factor of 50.

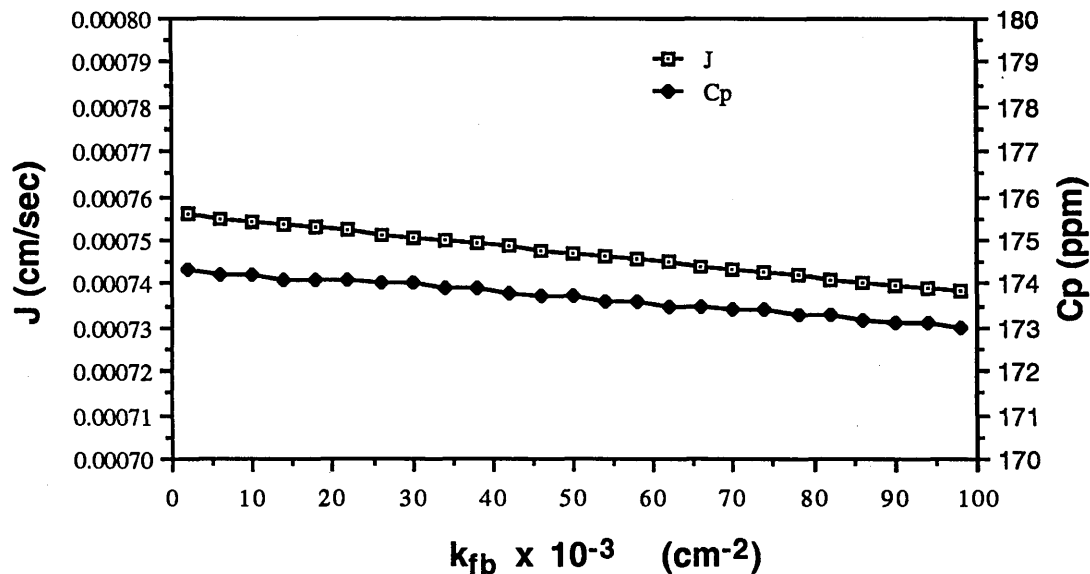


Fig.6.12 Average water flux and Permeate concentration at 35,000 ppm, 60 bar, $Q_f=7.692 \text{ lt/min}$ and 20° C for Membrane No1 for different brine friction parameter values.

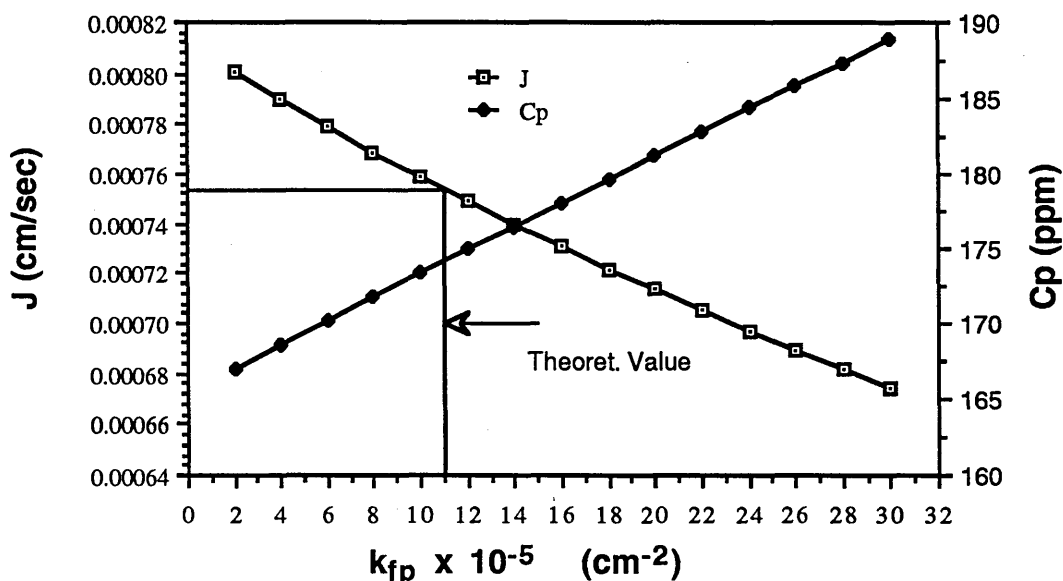


Fig.6.13 Average water flux and Permeate concentration at 35,000 ppm, 60 bar, $Q_f=7.692 \text{ lt/min}$ and 20° C for Membrane No1 for different permeate friction parameter values.

As one would expect, the effect of the permeate friction parameter variation on the module performance is greater than the brine friction parameter. An increase of the permeate friction parameter by a factor of 15, results in 15.7 % decrease in water flux and 13 % in permeate quality, see Fig.6.13 above.

The mass transfer coefficient values have a significant effect on the module performance, see Fig.6.14. It can be seen that as k increases the water flux increases and the permeate concentration decreases, because of smaller salt wall concentrations. The effect of k on the module performance becomes less significant at high k values.

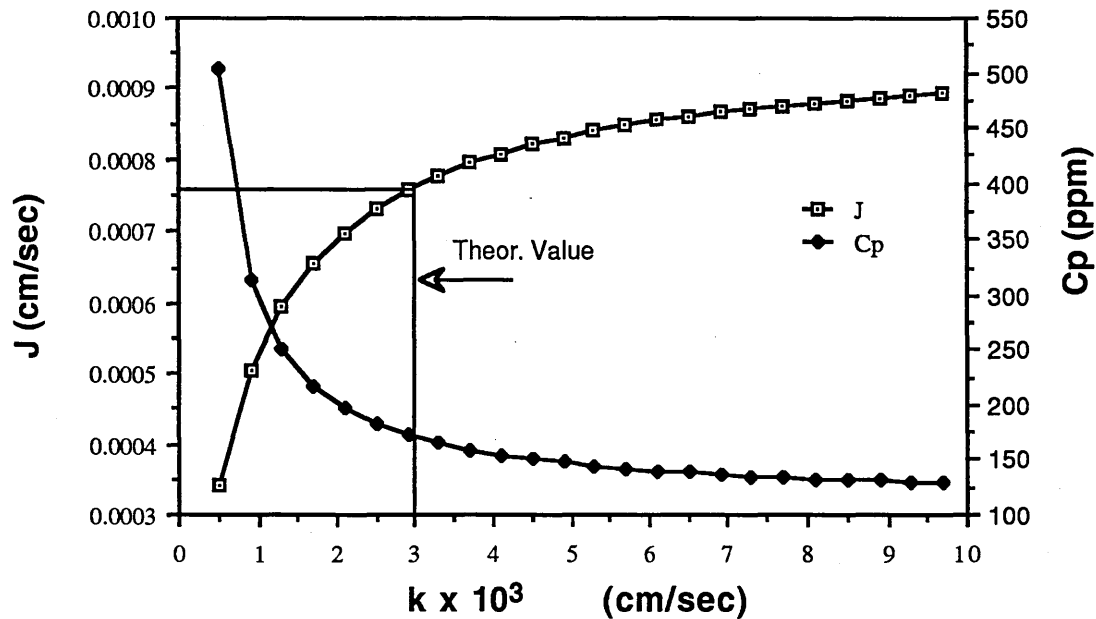


Fig.6.14 Average water flux and Permeate concentration at 35,000 ppm, 60 bar, $Q_f=7.692$ lt/min and 20° C for Membrane No1 for different mass transfer coefficient values.

According the analysis which has been presented in chapter III, the variation of k_2 has no effect on the permeate water flux. The permeate concentration is proportional to the k_2 , see Fig.6.15, below.

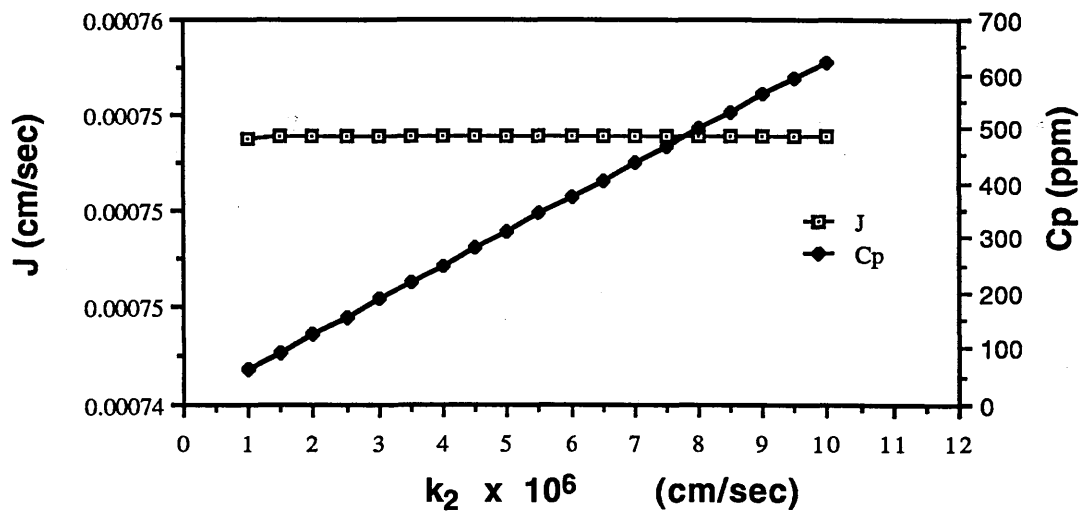


Fig.6.15 Average water flux and Permeate concentration at 35,000 ppm, 60 bar, $Q_f=7.692$ lt/min and 20° C for Membrane No1 for different solute permeability values.

CHAPTER VII

CONCLUSIONS AND RECOMMENDATION FOR FURTHER WORK

7.1 CONCLUSIONS

In this work an explicit analytical procedure to describe the performance of spiral wound R.O. modules has been presented. Based on the solution-diffusion model, explicit analytical equations have been proposed for the average water and salt fluxes in an element. In these equations, the pressure drop in both permeate and brine channels, the concentration polarization effect and the concentration gradient along the membrane have been taken into account, with some approximations, which have been detailed in sections 3.4 and 3.6.

The equations developed have been evaluated against experimental data for FilmTec FT30SW 2.5" modules operating on sea-water. The water and solute permeability coefficients (k_1 and k_2), the mass transfer coefficient, k , and the brine, k_{fb} , and permeate, k_{fp} , friction parameters have been found at a variety of different operating conditions. These 'five parameters' are needed to describe the performance of a spiral wound module.

The calculated values for the water and solute permeability coefficients follow the generally accepted trends for R.O. membranes and simple equations have been proposed to give these parameters at any pressure and temperature, see eqs (5.15) and (5.16).

The values found for the mass transfer coefficient, expressed in terms of Sherwood numbers, seem to depend on the Schmidt and Reynolds numbers, as all previous workers have suggested. More than this, it was found that the Sherwood number depends on the feed concentration and the applied pressure. As a result of this a mass transfer coefficient depending on the flow conditions as well as the feed concentration and the applied pressure has been introduced and a simple formula, see eq.(5.29), has been proposed to give the mass transfer coefficient at any operating conditions.

The friction parameters were found to be a function of the Reynolds number. The dependence on the Reynolds number is more obvious for the brine friction parameter than for the permeate friction parameter, see eqs (5.5) and (5.7).

For situations in which all of these 'five parameters' are known, further equations have been developed to give the local values for all the process variables (concentration, velocity, etc.) at any point within the element, so that the profiles for all these variables can be also derived.

The simple equations suggested for the 'five parameters', as well as the equations for the water and salt flux have been tested against experimental data and very good agreement between experimental and calculated values have been found for the water flux and the permeate concentration.

Finally the equations developed can be a useful tool in designing better modules, since they can give the geometrical characteristics like permeate height, membrane width etc. for an optimum module performance, for given situation.

Although numerical solutions have been suggested^[31] for the R.O. spiral wound modules, it is believed that an analytical solution is always more attractive than a numerical one, especially when all the physical effects have been taken into account, even if with some approximations.

7.2 FURTHER WORK

As far as the mathematical model is concerned improvements can be made if the variation of the brine concentration in the y (tangential) direction is taken into account. Although for small permeate velocities and small membrane widths this variation can be ignored, for high permeate velocities and long membrane widths it could be significant. Another possible improvement could be if the mathematical model was treated in polar coordinates so that the spiral form of the module could be considered rather the flat form which has been used in this analysis.

The effect of the brine spacer on the mass transfer coefficient could be also examined by using different spacers, and/or different length to height ratios.

Finally, the model could be validated as far as the optimum module design is concerned if modules from the same materials but different geometries were tried at the same experimental conditions and comparisons were made between the experimental and predicted values.

Table 5.1

Experimental data with distilled water for membranes No1 and No2.

T= 20 C								
Pb(0,w)	Pb(l,w) _i	Pb(l,w) _j	Pp(0,0) _j	(Qf) _i	(Qf) _j	(Qp) _i	(Qp) _j	Qb
(bar)	(bar)	(bar)	(bar)	(lt/min)	(lt/min)	(lt/min)	(lt/min)	(lt/min)
15	14.9	14.9	1.9	7.351	7.208	0.582	0.439	6.769
15	14.75	14.75	1.9	9.935	9.791	0.582	0.438	9.353
15	14.6	14.6	1.9	12.61	12.468	0.58	0.438	12.03
15	14.4	14.4	1.9	15.351	15.208	0.578	0.435	14.773
15	14.15	14.15	1.9	18.121	17.979	0.575	0.433	17.546
19	18.85	18.8	2.1	7.505	7.34	0.736	0.571	6.769
19	18.7	18.7	2.1	10.086	9.923	0.733	0.57	9.353
19	18.55	18.55	2.1	12.76	12.6	0.73	0.57	12.03
19	18.4	18.4	2.1	15.499	15.341	0.726	0.568	14.773
19	18.2	18.2	2.1	18.266	18.113	0.72	0.567	17.546
22	21.85	21.85	2.3	7.611	7.422	0.842	0.653	6.769
22	21.75	21.75	2.3	10.193	10.005	0.84	0.652	9.353
22	21.6	21.6	2.3	12.865	12.681	0.835	0.651	12.03
22	21.45	21.45	2.3	15.605	15.424	0.832	0.651	14.773
22	21.2	21.2	2.3	18.374	18.196	0.828	0.65	17.546
30	29.8	29.8	2.85	7.904	7.651	1.135	0.882	6.769
30	29.7	29.7	2.85	10.488	10.234	1.135	0.881	9.353
30	29.55	29.55	2.85	13.164	12.911	1.134	0.881	12.03
30	29.4	29.4	2.85	15.903	15.653	1.13	0.88	14.773
30	29.2	29.2	2.85	18.673	18.426	1.127	0.88	17.546
35	34.8	34.8	3.2	8.064	7.796	1.295	1.027	6.769
35	34.7	34.7	3.2	10.644	10.379	1.291	1.026	9.353
35	34.55	34.55	3.2	13.318	13.055	1.288	1.025	12.03
35	34.4	34.4	3.2	16.058	15.797	1.285	1.024	14.773
35	34.2	34.2	3.2	18.827	18.57	1.281	1.024	17.546
40	39.85	39.85	3.6	8.243	7.938	1.474	1.169	6.769
40	39.7	39.7	3.6	10.825	10.522	1.472	1.169	9.353
40	39.6	39.6	3.6	13.5	13.198	1.47	1.168	12.03
40	39.4	39.4	3.6	16.241	15.94	1.468	1.167	14.773
40	39.2	39.2	3.6	19.012	18.711	1.466	1.165	17.546
45	44.85	44.85	4.2	8.401	8.108	1.632	1.339	6.769
45	44.7	44.7	4.2	10.981	10.691	1.628	1.338	9.353
45	44.55	44.55	4.2	13.653	13.367	1.623	1.337	12.03
45	44.4	44.4	4.2	16.393	16.108	1.62	1.335	14.773
50	49.85	49.85	4.7	8.571	8.294	1.802	1.525	6.769
50	49.7	49.7	4.7	11.153	10.877	1.8	1.524	9.353
50	49.65	49.65	4.7	13.828	13.553	1.798	1.523	12.03

Table 5.3

Water permeability coefficients and friction parameters for membranes No1 and No2.

	T = 20 C					
	Pb(0,w)	Qb	(K1)j e5	(Kfb)j	(Kfp)j e-6	(K1)i e5
	bar	lt/min	cm/sec bar	cm-2	cm-2	cm/sec bar
	15	6.769	2.7529	9170	0.96994	3.7104
	15	9.353	2.7618	16739	0.9553	3.7286
	15	12.03	2.7771	20932	0.9606	3.7353
	15	14.773	2.7787	25659	0.97444	3.7475
	15	17.546	2.7919	30684	0.98816	3.7567
Average			2.77248	20636.8	0.96969	3.7357
	19	6.769	2.783	18119	0.91228	3.6581
	19	9.353	2.786	19849	0.89564	3.6706
	19	12.03	2.7979	23355	0.91038	3.6541
	19	14.773	2.8	25471	0.9065	3.6519
	19	17.546	2.8112	28682	0.91332	3.642
Average			2.79562	23095.2	0.90762	3.65534
	22	6.769	2.7243	13520	0.94111	3.505
	22	9.353	2.7268	16519	0.92337	3.5899
	22	12.03	2.7325	20706	0.93976	3.5802
	22	14.773	2.7426	23299	0.93158	3.5827
	22	17.546	2.7552	28635	0.93876	3.5834
Average			2.73628	20535.8	0.93492	3.56824
	30	6.769	2.6687	17769	0.96953	3.5129
	30	9.353	2.6703	19623	0.97235	3.5206
	30	12.03	2.6774	23117	0.98761	3.5271
	30	14.773	2.6815	25267	0.97864	3.5254
	30	17.546	2.6911	28498	0.98213	3.5292
Average			2.6778	22854.8	0.97805	3.52304
	35	6.769	2.6511	17606	0.98998	3.4188
	35	9.353	2.6525	19494	0.99244	3.4137
	35	12.03	2.656	23000	1.0088	3.4132
	35	14.773	2.6594	25168	0.9989	3.4145
	35	17.546	2.6675	28406	1.0019	3.4144
Average			2.6573	22734.8	0.9984	3.41492
	40	6.769	2.6325	13098	1.0275	3.3982
	40	9.353	2.6377	19386	1.0295	3.3988
	40	12.03	2.639	20364	1.0058	3.4009
	40	14.773	2.6437	25093	1.0354	3.4046
	40	17.546	2.6462	28344	1.0399	3.4097
Average			2.63982	21257	1.02762	3.40244
	45	6.769	2.6861	13017	1.1061	3.3359
	45	9.353	2.6889	19324	1.1089	3.3319
	45	12.03	2.6917	22879	1.1076	3.3269
	45	14.773	2.6925	25090	1.1154	3.3278
Average			2.6898	20077.5	1.1095	3.33063
	50	6.769	2.7532	12887	1.1238	3.3113
	50	9.353	2.7559	19193	1.1264	3.3118
	50	12.03	2.7556	17707	1.124	3.3134
	50	14.773	2.7612	24999	1.1315	3.3162
Average			2.75648	18696.5	1.12643	3.31318

Table 5.6

Experimental data for sea-water solutions and the values for mass transfer and solute permeability coefficients for membrane No1.

T = 20 C							
FEED CONC.	BRINE CONC.	Pb(0,W) bar	PERMEAT. FLOW lt/min	FEED FLOW lt/min	PERMEAT. CONC. gr/lt	Ke3 cm/sec	K2e6 cm/sec
25	31.311	50	0.893	4.417	0.121	2.743	2.502
25	28.589	50	0.971	7.74	0.103	3.586	2.527
25	27.708	50	1.007	10.36	0.095	4.347	2.532
25	27.138	50	1.026	13.063	0.092	4.885	2.578
25	26.752	50	1.032	15.805	0.089	5.082	2.562
							2.5402
25	32.336	55	1.032	4.556	0.115	2.932	2.653
25	29.128	55	1.111	7.88	0.095	3.602	2.573
25	28.089	55	1.147	10.5	0.089	4.19	2.604
25	27.428	55	1.16	13.19	0.089	4.389	2.698
							2.632
25	32.753	60	1.141	4.665	0.115	2.638	2.77
25	29.624	60	1.239	8.008	0.095	3.446	2.75
25	28.435	60	1.27	10.623	0.089	3.766	2.745
25	27.725	60	1.295	13.325	0.086	4.179	2.803
25	27.229	60	1.301	16.074	0.083	4.25	2.771
							2.7678
25	34.947	70	1.381	4.905	0.103	2.736	2.772
25	30.546	70	1.474	8.243	0.089	3.092	2.804
25	29.124	70	1.512	10.865	0.079	3.355	2.666
25	28.289	70	1.549	13.574	0.079	3.801	2.858
25	27.701	70	1.562	16.335	0.075	3.953	2.804
							2.7808
25	36.694	80	1.612	5.136	0.099	2.794	2.9
25	31.519	80	1.719	8.488	0.083	3.122	2.87
25	29.831	80	1.757	11.11	0.075	3.297	2.764
25	28.856	80	1.802	13.832	0.072	3.753	2.864
25	28.176	80	1.821	16.593	0.069	3.953	2.854
							2.8504
35	41.107	50	0.624	4.148	0.285	2.498	3.215
35	38.536	50	0.684	7.453	0.235	3.064	3.07
35	37.644	50	0.713	10.066	0.22	3.541	3.097
							3.1273
35	42.248	55	0.737	4.261	0.248	2.447	3.142
35	39.189	55	0.815	7.584	0.2	3.085	2.995
35	38.145	55	0.845	10.198	0.187	3.459	2.998
35	37.518	55	0.869	12.899	0.178	3.907	3.028
							3.0408

Table 5.6.b

T = 25 C							
FEED	BRINE	Pb(0,W)	PERMEAT.	FEED	PERMEAT.	Ke3	K2e6
CONC.	CONC.		FLOW	FLOW	CONC.		
gr/lt	gr/lt	bar	lt/min	lt/min	gr/lt	cm/sec	cm/sec
25	32.732	50	1.086	4.61	0.138	5.809	3.72
25	29.338	50	1.166	7.935	0.115	7.333	3.609
25	28.226	50	1.196	10.549	0.103	8.449	3.433
25	27.548	50	1.215	13.245	0.098	9.534	3.405
25	27.086	50	1.221	15.994	0.098	9.78	3.475
							3.5284
25	33.689	55	1.215	4.739	0.125	4.808	3.542
25	29.887	55	1.307	8.076	0.106	5.9	3.529
25	28.626	55	1.338	10.691	0.095	6.461	3.353
25	27.887	55	1.369	13.399	0.095	7.658	3.559
25	27.374	55	1.381	16.154	0.089	8.162	3.434
							3.4834
25	34.657	60	1.344	4.868	0.121	4.311	3.586
25	30.349	60	1.462	8.231	0.098	5.602	3.521
25	29.067	60	1.493	10.846	0.089	6.032	3.378
25	28.217	60	1.518	13.548	0.089	6.593	3.542
25	27.644	60	1.531	16.304	0.083	6.93	3.402
							3.4858
25	36.738	70	1.618	5.142	0.111	4.176	3.647
25	31.594	70	1.738	8.507	0.092	4.857	3.606
25	29.957	70	1.802	11.155	0.083	5.821	3.586
25	28.927	70	1.833	13.863	0.082	6.35	3.731
25	28.21	70	1.84	16.613	0.075	6.309	3.476
							3.6092
25	38.591	80	1.859	5.383	0.106	3.828	3.662
25	32.725	80	2.019	8.788	0.086	4.742	3.679
25	30.707	80	2.058	11.41	0.079	4.868	3.579
25	29.527	80	2.096	14.126	0.072	5.282	3.454
							3.5935
35	41.509	50	0.666	4.19	0.346	2.556	4.12
35	38.769	50	0.737	7.506	0.282	3.111	3.924
35	37.84	50	0.767	10.12	0.269	3.486	4.013
35	37.316	50	0.803	12.833	0.248	4.241	4.015
							4.018
35	42.839	55	0.797	4.32	0.293	2.609	3.977
35	39.596	55	0.893	7.662	0.235	3.326	3.825
35	38.536	55	0.947	10.3	0.216	4.091	3.891
35	37.701	55	0.971	13	0.207	4.329	3.948
35	37.33	55	0.983	15.756	0.196	4.872	3.94
							3.9162

Table 5.6.c

				T = 25 C			
FEED	BRINE	Pb(0,W)	PERMEAT.	FEED	PERMEAT.	Ke3	K2e6
CONC.	CONC.		FLOW	FLOW	CONC.		
gr/lt	gr/lt	bar	lt/min	lt/min	gr/lt	cm/sec	cm/sec
35	44.01	60	0.911	4.435	0.258	2.498	3.793
35	40.242	60	1.013	7.782	0.207	3.039	3.629
35	39	60	1.068	10.421	0.182	3.577	3.506
35	38.21	60	1.099	13.129	0.179	3.954	3.656
35	37.659	60	1.117	15.89	0.168	4.231	3.576
							3.632
35	46.267	70	1.129	4.653	0.2	2.351	3.297
35	41.636	70	1.27	8.039	0.176	2.943	3.564
35	40	70	1.319	10.672	0.146	3.21	3.182
35	39.042	70	1.369	13.399	0.141	3.651	3.317
35	38.37	70	1.4	16.173	0.135	3.989	3.347
							3.3414
35	48.512	80	1.344	4.868	0.192	2.307	3.459
35	42.969	80	1.512	8.281	0.15	2.863	3.354
35	40.945	80	1.556	10.909	0.136	2.981	3.228
35	39.779	80	1.606	13.636	0.129	3.275	3.28
35	39	80	1.65	16.423	0.122	3.623	3.303
							3.3248
40	47.24	55	0.648	4.172	0.379	2.351	3.811
40	44.238	55	0.725	7.494	0.314	2.868	3.722
40	43.221	55	0.761	10.114	0.296	3.264	3.798
40	42.608	55	0.791	12.821	0.277	3.746	3.809
							3.785
40	48.61	60	0.767	4.291	0.334	2.373	3.789
40	45	60	0.851	7.62	0.272	2.787	3.614
40	43.885	60	0.911	10.264	0.242	3.408	3.589
40	43.104	60	0.935	12.965	0.232	3.689	3.623
							3.6538
40	51.001	70	0.971	4.495	0.279	2.205	3.622
40	46.44	70	1.086	7.855	0.22	2.616	3.414
40	44.688	70	1.141	10.494	0.2	2.908	3.385
40	43.968	70	1.184	13.214	0.182	3.277	3.302
40	43.267	70	1.196	15.969	0.169	3.369	3.161
							3.3768
40	53.38	80	1.172	4.696	0.243	2.149	3.488
40	47.892	80	1.319	8.088	0.189	2.579	3.304
40	46.082	80	1.4	10.753	0.162	2.993	3.153
40	44.839	80	1.432	13.462	0.15	3.142	3.063
40	44.03	80	1.462	16.235	0.141	3.348	3.019
							3.2054

Table 5.6.d

				T = 30 C			
FEED	BRINE	Pb(0,W)	PERMEAT.	FEED	PERMEAT.	Ke3	K2e6
CONC.	CONC.		FLOW	FLOW	CONC.		
gr/lt	gr/lt	bar	lt/min	lt/min	gr/lt	cm/sec	cm/sec
25	33.726	50	1.221	4.745	0.161	7.352	4.873
25	29.956	50	1.325	8.094	0.129	9.819	4.63
25	28.726	50	1.375	10.728	0.121	13.225	4.727
25	27.98	50	1.412	13.442	0.118	18.806	4.907
25	27.427	50	1.421	16.194	0.111	19.655	4.715
							4.7704
25	34.971	55	1.387	4.911	0.15	6.778	4.912
25	30.616	55	1.493	8.262	0.118	8.029	4.542
25	29.225	55	1.549	10.902	0.111	10.155	4.661
25	28.341	55	1.574	13.604	0.108	11.186	4.734
25	27.767	55	1.6	16.373	0.104	13.407	4.769
							4.7236
25	36.06	60	1.531	5.055	0.141	5.826	4.809
25	31.334	60	1.675	8.444	0.115	7.833	4.806
25	29.77	60	1.738	11.091	0.103	9.849	4.719
25	28.794	60	1.776	13.806	0.1	11.693	4.859
25	28.102	60	1.783	16.556	0.093	11.502	4.596
							4.7578
25	38.477	70	1.846	5.37	0.133	5.628	5.04
25	32.694	70	2.012	8.781	0.103	7.14	4.817
25	30.778	70	2.083	11.436	0.095	8.525	4.882
							4.913
35	42.459	50	0.761	4.285	0.368	3.47	5.09
35	39.237	50	0.827	7.596	0.314	3.788	4.934
35	38.273	50	0.881	10.234	0.285	4.677	4.954
35	37.6	50	0.899	12.929	0.279	4.996	5.056
35	37.19	50	0.929	15.702	0.271	5.888	5.226
							5.052
35	43.748	55	0.887	4.411	0.322	3.133	4.884
35	40.073	55	0.983	7.752	0.275	3.669	4.9
35	38.886	55	1.038	10.391	0.248	4.316	4.843
35	38.149	55	1.111	13.141	0.238	5.849	5.225
							4.963
35	44.732	60	0.983	4.507	0.322	2.641	5.046
35	40.892	60	1.135	7.904	0.255	3.584	5.02
35	39.479	60	1.19	10.543	0.228	4.051	4.878
35	38.616	60	1.233	13.263	0.22	4.572	5.034
35	37.976	60	1.245	16.018	0.207	4.689	4.871
							4.9698

APPENDIX I

```
PROGRAM PAR1
=====
*
C THIS PROGRAM CALCULATES THE MEMBRANE PARAMETERS K1,Kfb,Kfp
*
IMPLICIT DOUBLE PRECISION (A-H,O-Z)
CHARACTER*5 WORDS(11)
COMMON/PAR1/DPEFOW,DPEFLW,DW,DW2,DHB,DM,QF,QB
COMMON/PAR2/DPEFOO,DHP,QP
COMMON/PAR3/DKFB,DKFP
COMMON/PAR4/DJ,DL,DL2,UF
*
OPEN(10,FILE='INPUT.DAT',STATUS='OLD')
OPEN(20,FILE='OUTPUT.DAT',STATUS='OLD')
*
READ(10,100)WORDS(1),DW,WORDS(1),DW2,WORDS(2),DL,WORDS(2),DL2,
&WORDS(3),DHP,WORDS(4),DHB,WORDS(5),PIN,
&WORDS(6),POUT,WORDS(7),PNEW,WORDS(8),DM,WORDS(9),QF,
&WORDS(10),QP,WORDS(11),QB
100 FORMAT(15(2X,A5,2X,F10.5/:))
*
WRITE(*,100)WORDS(1),DW,WORDS(1),DW2,WORDS(2),DL,WORDS(2),DL2,
&WORDS(3),DHP,WORDS(4),DHB,WORDS(5),PIN,WORDS(6),POUT,
&WORDS(7),PNEW,WORDS(8),DM,WORDS(9),QF,WORDS(10),QP,
&WORDS(11),QB
*
DJ=3.0E4*QP/(DW*DL)
DPEFOW=PIN-1.
UF=(6.0E4/DW2)*(QF/DHB)
DPEFLW=POUT-1.
DPEFOO=PIN-PNEW
*
DKOLD=DJ/DPEFOW
DKNEW=DKOLD/1000.+DKOLD
FOLD=FBJ(DKOLD)
10 CONTINUE
FNEW=FBJ(DKNEW)
C CHECK FOR SOLUTION
IF(DABS(FNEW).LT.1.D-8)GO TO 50
DIFF=FNEW*(DKNEW-DKOLD)/(FNEW-FOLD)
IF(DABS(DIFF).LT.1.D-5)GO TO 50
DKOLD=DKNEW
FOLD=FNEW
DKNEW=DKNEW-DIFF
GO TO 10
*
50 CONTINUE
DKNEW=DNEW/3600.
WRITE(*,*)DKNEW,DKFB,DKFP
WRITE(20,*)DKNEW,DKFB,DKFP
*
60 STOP
END
```

FUNCTION FBJ(DK)

*

=====

IMPLICIT DOUBLE PRECISION (A-H,O-Z)
COMMON/PAR1/DPEFOW,DPEFLW,DW,DW2,DHB,DM,QF,QB
COMMON/PAR2/DPEFOO,DHP,QP
COMMON/PAR3/DKFB,DKFP
COMMON/PAR4/DJ,DL,DL2,UF

*

DKFB1=DPEFOW**2-DPEFLW**2
DKFB2=1.962*DK*DW*DW*DHB
DKFB3=DM*(QF*QF-QB*QB)
DKFB=DKFB1*DKFB2/DKFB3
DKFP=(DPEFOW**2-DPEFOO**2)*1.962*DK*DL2*DL2*DHP/
&(DM*QP*QP)
Q=DSQRT((176.58*DHP/(DK*DM))*1.E7/DKFP)
B=DSQRT((DK/(DM*DHB))*7.060E9/DKFB)
A=DSQRT((DKFB*1.E-7)*(DK*DM/(DHB*176.5)))

*

FOBJ1=DK*Q*DTANH(DW/Q)
FOBJ2=B*DPEFOW**2*DSINH(A*DL)
FOBJ3=(UF*UF/B)*(1.-DCOSH(A*DL))
FOBJ4=DPEFOW*UF*(1.-DEXP(-A*DL))
FOBJ5=A*DW*DL*(B*DPEFOW+UF)
FOBJ=FOBJ1*(FOBJ2+FOBJ3+FOBJ4)/FOBJ5-DJ

*

RETURN
END

```

PROGRAM PAR 2
*
=====
C THIS PROGRAM CALCULATES THE MEMBRANE PARAMETERS K1
*
IMPLICIT DOUBLE PRECISION (A-H,O-Z)
CHARACTER*5 WORDS(8)
COMMON/PAR1/DPEFOW,DW,DW2,DHB,DM,QF
COMMON/PAR2/DHP,QP
COMMON/PAR3/DKFB,DKFP
COMMON/PAR4/DJ,DL,DL2,UF
*
OPEN(10,FILE='DATA.IN', STATUS='OLD')
OPEN(20,FILE='OUTPUT.DAT', STATUS='OLD')
*
READ(10,100)WORDS(1),DW,WORDS(1),DW2,WORDS(2),DL,WORDS(2),DL2,
&WORDS(3),DHP,WORDS(4),DHB,WORDS(5),PIN,
&WORDS(6),DM,WORDS(7),QF,WORDS(8),QP
100 FORMAT(15(2X,A5,2X,F10.5/:))
*
WRITE(*,100)WORDS(1),DW,WORDS(1),DW2,WORDS(2),DL,WORDS(2),DL2,
&WORDS(3),DHP,WORDS(4),DHB,WORDS(5),PIN,
&WORDS(6),DM,WORDS(7),QF,WORDS(8),QP
*
DJ=3.0E4*QP/(DW*DL)
DPEFOW=PIN-1.
UF=(6.0E4/DW2)*(QF/DHB)
*
DKOLD=DJ/DPEFOW
DKFB=3.*(UF**0.8)
DKFP=1038152.*(QP**0.25)
DKNEW=DKOLD/1000.+DKOLD
FOLD=FBJ(DKOLD)
10 CONTINUE
FNEW=FBJ(DKNEW)
C CHECK FOR SOLUTION
IF(DABS(FNEW).LT.1.D-8)GO TO 50
DIFF=FNEW*(DKNEW-DKOLD)/(FNEW-FOLD)
IF(DABS(DIFF).LT.1.D-8)GO TO 50
DKOLD=DKNEW
FOLD=FNEW
DKNEW=DKNEW-DIFF
GO TO 10
*
50 CONTINUE
DKNEW=DKNEW/3600.
WRITE(*,*)DKNEW,DKFB,DKFP
WRITE(20,*)DKNEW,DKFB,DKFP
*
60 STOP
END
FUNCTION FBJ(DK)
*
=====
IMPLICIT DOUBLE PRECISION (A-H,O-Z)

```

```
COMMON/PAR1/DPEFOW, DW, DW2, DHB, DM, QF
COMMON/PAR2/DHP, QP
COMMON/PAR3/DKFB, DKFP
COMMON/PAR4/DJ, DL, DL2, UF
```

*

```
Q=DSQRT((176.58*DHP/(DK*DM) )*1.E7/DKFP)
B=DSQRT((DK/(DM*DHB) )*7.060E9/DKFB)
A=DSQRT( (DKFB*1.E-7) * (DK*DM/(DHB*176.5)) )
```

*

```
FOBJ1=DK*Q*DTANH(DW/Q)
FOBJ2=B*DPEFOW**2*DSINH(A*DL)
FOBJ3=(UF*UF/B) * ( 1.-DCOSH(A*DL) )
FOBJ4=DPEFOW*UF * ( 1.-DEXP(-A*DL) )
FOBJ5=A*DW*DL * (B*DPEFOW+UF)
FOBJ=FOBJ1*(FOBJ2+FOBJ3+FOBJ4)/FOBJ5-DJ
```

*

```
RETURN
END
```

PROGRAM PAR3

```

*
=====
C THIS PROGRAM CALCULATES THE MASS TRANSFER COEFFICIENT K
C AND THE SOLUTE PERMEABILITY COEFFICIENT K2
*

IMPLICIT DOUBLE PRECISION (A-H,O-Z)
CHARACTER*5 WORDS(15)
COMMON/PAR1/DPEFOW,DW,DW2,DHB,DM,QF,QB,CF,CB,DK1
COMMON/PAR2/T,DHP,QP,CON,F,Q
COMMON/PAR3/DKFB,DKFP,PIN
COMMON/PAR4/DJ,DL,DL2,UF,CP,D

*

OPEN(10,FILE='SALT.DAT',STATUS='OLD')
OPEN(20,FILE='SALT.OUT',STATUS='OLD')

*

READ(10,100)WORDS(1),DW,WORDS(2),DW2,WORDS(3),DL,WORDS(4),DL2,
&WORDS(5),DHP,WORDS(6),DHB,WORDS(7),DM,WORDS(8),T,WORDS(9),CON,
&WORDS(10),CF,WORDS(11),CB,WORDS(12),PIN,WORDS(13),QP,WORDS(14),
&QP,WORDS(15),CP
100 FORMAT(15(2X,A5,2X,F10.5/:))

*

WRITE(*,100)WORDS(1),DW,WORDS(2),DW2,WORDS(3),DL,WORDS(4),DL2,
&WORDS(5),DHP,WORDS(6),DHB,WORDS(7),DM,WORDS(8),T,WORDS(9),CON,
&WORDS(10),CF,WORDS(11),CB,WORDS(12),PIN,WORDS(13),QP,WORDS(14),
&QP,WORDS(15),CP

*

DJ=3.0E4*QP/(DW*DL)
UF=(6.0E4/DW2)*(QF/DHB)
F=(CB-CF)/DL
D=(0.72598+2.308D-2*T+2.7657D-4*T*T)*1.D-5

*

DK1=0.14061*DEXP(8.6464*(T-20)/293.-0.0028*PIN)
DKFB=3.*(UF**0.8)
DKFP=1038152.*(QP**0.25)
Q=DSQRT((176.58*DHP/(DK1*DM))*1.E7/DKFP)
DKUP=500.
DKLOW=0.1
FUP=FBJ(DKUP)
FLOW=FBJ(DKLOW)
C CHECK THE LIMITS
IF(FUP*FLOW.LT.0.0)GO TO 10
WRITE(*,*) 'NEW LIMITS'
GO TO 50
10 DKM=(DKUP+DKLOW)/2.
FKM=FBJ(DKM)
IF(DABS(FKM).LT.1.D-8)THEN
GO TO 40
ELSE IF(DABS(DKUP-DKLOW).LT.1.D-8)THEN
GO TO 40
ELSE IF((FUP*FKM).GT.0.0)THEN
GO TO 30
ELSE
DKLOW=DKM
GO TO 10
30 DKUP=DKM
GO TO 10

```

```

END IF
40 CONTINUE
FINAL=FBJ (DKM)

FUN1=Q*DTANH (DW/Q) / (DK1*F*CON*CON*DKM)
FUN2=DK1*CON* (CB-CF)
DPEF0W= ( (PIN-1. -CON* (CF-CP)) / (DKM+CON*CF*DK1)) *DKM
FUN3=DKM+DK1*CON* (CF-CP)
FUN4=DKM+DK1*CON* (CB-CP)
FUN5=DLOG (FUN3)
FUN6=DLOG (FUN4)
FUN7=DPEF0W*FUN3
FUN8=DKM*DKM/DK1
FUN9=DKM*CON* (CB-CF)
FUN10=DKM* (CF-CP) *UF*1.D-6
FUN11=DKFB*2.831D-4
FUN12=DM/F
FUN13=DLOG (CB-CP)
FUN14=DLOG (CF-CP)
FUN15=FUN11*FUN12*FUN10* (FUN13-FUN14)
FUN16=DLOG (DKM)
FUN17=FUN2* (FUN7+FUN8-FUN9/2.)
FUN18=DPEF0W+DKM/DK1
FUN19=DKM*FUN18*FUN3* (FUN6-FUN5)
FUN20=FUN15* (DKM* (FUN6-FUN16) -DK1*CON*CB+
&DK1*DK1*CON*CON*CB* (CB-CF) /DKM)
FUN21=FUN1* (FUN17-FUN19+FUN20)
FUN22= (CB-CF) *DL*DW/2.
FUN23= (CF-CP) *DL*DW
FUN24=FUN21+FUN22+FUN23
DK2=DJ*DW*DL*CP/FUN24
DK2=DK2/3600.

DKM=DKM/3600.
DK1=DK1/3600.
UF=UF/3600.
RE=DLOG (UF*DHB*1.0252/DM)
SH=DLOG (DKM*DHB/D)
WRITE (*, *) DKM, DK2, RE, SH
WRITE (20, *) DKM, DK2, UF, RE
*
50 STOP
END

FUNCTION FBJ (DK)
=====
IMPLICIT DOUBLE PRECISION (A-H, O-Z)
COMMON/ PAR1/ DPEF0W, DW, DW2, DHB, DM, QF, QB, CF, CB, DK1
COMMON/ PAR2/ T, DHP, QP, CON, F, Q
COMMON/ PAR3/ DKFB, DKFP, PIN
COMMON/ PAR4/ DJ, DL, DL2, UF, CP
*
FB1=Q*DTANH (DW/Q) / (CON* (CB-CF) *DW)
FB2=DK+DK1*CON* (CF-CP)
FB3=DK+DK1*CON* (CB-CP)
FB4=DLOG (FB2)

```

```

FB5=DLOG (FB3)
FB6=FB5-FB4
FB7=FB2*FB6
DPEF0W= (PIN-1.-CON* (CF-CP) ) *DK/ (DK+CON*CF*DK1)
FB8=DK/DK1
FB9=FB8+DPEF0W
FB10=FB7*FB9
FB11=DK*CON* (CB-CF)
FB12=UF* (CF-CP) *1.D-6
FB13=DKFB*2.831D-4
FB14=DM/F
FB15=FB12*FB13*FB14
FB16=DK1*CON* (CB-CF)
FB17=DLOG (CB-CP)
FB18=DLOG (CF-CP)
FB19=DK* (FB17-FB18)
FB20=DLOG (DK)
FB21=FB5-FB20
FB22=FB19*FB21
FB221= (DK1*DK1*CON*CON/ (4.*DK) ) * (CB*CB-CF*CF)
FB23=FB15* (FB16-FB22-FB221)
FB24=FB10-FB11+FB23
FB25=FB24*FB1
FBJ=FB25-DJ

```

*

```

RETURN
END

```

PROGRAM PAR4

```

*
=====
C THIS PROGRAM PREDICTS THE MEMBRANE PERFORMANCE
*
IMPLICIT DOUBLE PRECISION (A-H,O-Z)
CHARACTER*5 WORDS(15)
COMMON/PAR1/DW,DW2,DHB,DM,QF
COMMON/PAR2/T,DHP,CON,Q,DK,DK2
COMMON/PAR3/DKFB,DKFP,PIN,DEN
COMMON/PAR4/DL,DL2,UF,CF,DK1,D
*
OPEN(10,FILE='IN',STATUS='OLD')
OPEN(20,FILE='OUT',STATUS='OLD')
*
READ(10,100)WORDS(1),DW,WORDS(2),DW2,WORDS(3),DL,WORDS(4),DL2,
&WORDS(5),DHP,WORDS(6),DHB,WORDS(7),DM,WORDS(8),T,WORDS(9),CON,
&WORDS(10),CF,WORDS(11),PIN,WORDS(12),QF,WORDS(13),DEN
100 FORMAT(15(2X,A5,2X,F10.5/:))
*
WRITE(*,100)WORDS(1),DW,WORDS(2),DW2,WORDS(3),DL,WORDS(4),DL2,
&WORDS(5),DHP,WORDS(6),DHB,WORDS(7),DM,WORDS(8),T,WORDS(9),CON,
&WORDS(10),CF,WORDS(11),PIN,WORDS(12),QF,WORDS(13),DEN
*
UF=(QF*16.666)/(DW2*DHB)
*
DK1=3.906D-5*DEXP(8.6464*(T-20)/293.-0.0028*PIN)
DK1=3.8225D-5*DEXP(-0.0018*PIN)
DKFB=309.*(DHB*UF*DEN/DM)**0.83
DKFP=1.1D6
Q=DSQRT(9.81D5*DHP/(2.*DK1*DM*DKFP))
D=(0.7259+2.308D-2*T+2.7657D-4*T*T)*1.D-5
DK=(D*0.63/DHB)*((DM/(DEN*D))**0.17)*((UF*DHB*DEN/DM)**0.4)*
&((CF/(1000.*DEN))**-0.77)*(PIN**-0.55)
DK2=9.536D-7*DEXP(14.648*T/273)
DJIN=(PIN-1.-CF*CON)*DK*DK1/(DK+CON*CF*DK1)
DJOLD=(PIN-1.-CF*CON)*DK*DK1/(DK+CON*CF*DK1)
FJOLD=FBJ(DJOLD)
DJNEW=DJOLD/1000.+DJOLD
*
10 CONTINUE
FJNEW=FBJ(DJNEW)
C CHECK FOR SOLUTION
IF(DABS(FJNEW).LT.1.D-8)GO TO 50
DIFF=FJNEW*(DJNEW-DJOLD)/(FJNEW-FJOLD)
WRITE(*,*)DJNEW
IF(DABS(DIFF).LT.1.D-7)GO TO 50
DJOLD=DJNEW
FJOLD=FJNEW
DJNEW=DJNEW-DIFF
GO TO 10
50 CONTINUE
DJ=DJNEW
F=2*DJ*DW*CF/(UF*DHB*DW2-2*DJ*DW*DL)
CB=CF+F*DL

```

```

FUN1=Q*DTANH(DW/Q)/(DK1*F*CON*CON*DK)
FUN2=DK1*CON*(CB-CF)
DPEF0W=( (PIN-1.-CON*CF)/(DK+CON*CF*DK1) ) *DK
FUN3=DK+DK1*CON*CF
FUN4=DK+DK1*CON*CB
FUN5=DLOG(FUN3)
FUN6=DLOG(FUN4)
FUN7=DPEF0W*FUN3
FUN8=DK*DK/DK1
FUN9=DK*CON*(CB-CF)
FUN10=DK*CF*UF*1.019D-6
FUN11=DKFB
FUN12=DM/F
FUN13=DLOG(CB)
FUN14=DLOG(CF)
FUN15=FUN11*FUN12*FUN10*(FUN13-FUN14)
FUN16=DLOG(DK)
FUN17=FUN2*(FUN7+FUN8-FUN9/2.)
FUN18=DPEF0W+DK/DK1
FUN19=DK*FUN18*FUN3*(FUN6-FUN5)
FUN20=FUN15*(DK*(FUN6-FUN16)-DK1*CON*CB+
&DK1*DK1*CON*CON*(CB*CB-CF*CF)/(4.*DK))
FUN21=FUN1*(FUN17-FUN19+FUN20)
FUN22=(CB-CF)*DL*DW/2.
FUN23=CF*DL*DW
FUN24=FUN21+FUN22+FUN23
CP=(DK2*FUN24)/(DJ*DW*DL)
CP=CP*1000.

```

```

WRITE(*,*)PIN,DJNEW,CP,DK1
WRITE(20,*)PIN,DJNEW,CP,DK

```

*

```

60 STOP
END

```

```

FUNCTION FBJ(DJ)

```

*

```

=====
IMPLICIT DOUBLE PRECISION (A-H,O-Z)
COMMON/PAR1/DW,DW2,DHB,DM,QF
COMMON/PAR2/T,DHP,CON,Q,DK,DK2
COMMON/PAR3/DKFB,DKFP,PIN,DEN
COMMON/PAR4/DL,DL2,UF,CF,DK1,D

```

*

```

F=2*DJ*DW*CF/(UF*DHB*DW2-2*DJ*DW*DL)
CB=CF+F*DL

```

```

FB1=Q*DTANH(DW/Q)/(CON*F*DW*DL)
FB2=DK+DK1*CON*CF
FB3=DK+DK1*CON*CB
FB4=DLOG(FB2)
FB5=DLOG(FB3)
FB6=FB5-FB4
FB7=FB2*FB6
DPEF0W=(PIN-1.-CON*CF)*DK/(DK+CON*CF*DK1)
FB8=DK/DK1

```

FB9=FB8+DPEF0W
FB10=FB7*FB9
FB11=DK*CON*(CB-CF)
FB12=UF*CF*1.019D-6
FB13=DKFB
FB14=DM/F
FB15=FB12*FB13*FB14
FB16=DK1*CON*(CB-CF)
FB17=DLOG(CB)
FB18=DLOG(CF)
FB19=DK*(FB17-FB18)
FB20=DLOG(DK)
FB21=FB5-FB20
FB22=FB19*FB21
FB221=(DK1*DK1*CON*CON/(4.*DK))* (CB*CB-CF*CF)
FB23=FB15*(FB16-FB22-FB221)
FB24=FB10-FB11+FB23
FBJ=FB24*FB1-DJ

*

RETURN
END

APPENDIX II

PROPERTIES OF DISTILLED WATER AND SEA-WATER (Ref.30,42)

Viscosity values of distilled water, (gr/cm sec)

20° C	25° C	30° C	35° C
1.005x10 ⁻²	8.92x10 ⁻³	7.98x10 ⁻³	7.202x10 ⁻³

Viscosity values of sea-water, (gr/cm sec)

Conc. (ppm)	20° C	25° C	30° C	35° C
25,000	1.054x10 ⁻²	9.391x10 ⁻³	8.43x10 ⁻³	7.612x10 ⁻³
35,000	1.077x10 ⁻²	9.6x10 ⁻³	8.621x10 ⁻³	7.792x10 ⁻³
40,000	1.089x10 ⁻²	9.712x10 ⁻³	8.717x10 ⁻³	7.879x10 ⁻³

Density values of sea-water, (gr/cm³)

Conc. (ppm)	20° C	25° C	30° C	35° C
25,000	1.0132	1.0119	1.0104	1.0085
35,000	1.0239	1.0224	1.021	1.0191
40,000	1.0281	1.0266	1.0252	1.0233

Diffusivity values of sea-water, (cm²/sec)

20° C	25° C	30° C	35° C
1.298x10 ⁻⁵	1.475x10 ⁻⁵	1.667x10 ⁻⁵	1.872x10 ⁻⁵

Osmotic pressure coefficient, ϕ , (Atm lt/gr)

20° C	25° C	30° C	35° C
0.711	0.728	0.744	0.758

APPENDIX III

CALIBRATION OF THE INSTRUMENTS

1. Pressure transducers.

Although the pressure transducers were calibrated by the supplier, they were tested with a dead-weight pressure gauge tester and they were found to perform perfectly.

2. Conductivity cells and transmitters.

The conductivity cells were calibrated by using sea-water solutions at known concentrations and for each solution the output from the transmitters was measured in mA. A standard graph was found, see Fig.A.1 and Fig.A.2, to give the concentration as a function of the output current of the transmitter in mA, for the permeate and the feed side respectively. Similar graphs were found at different temperatures.

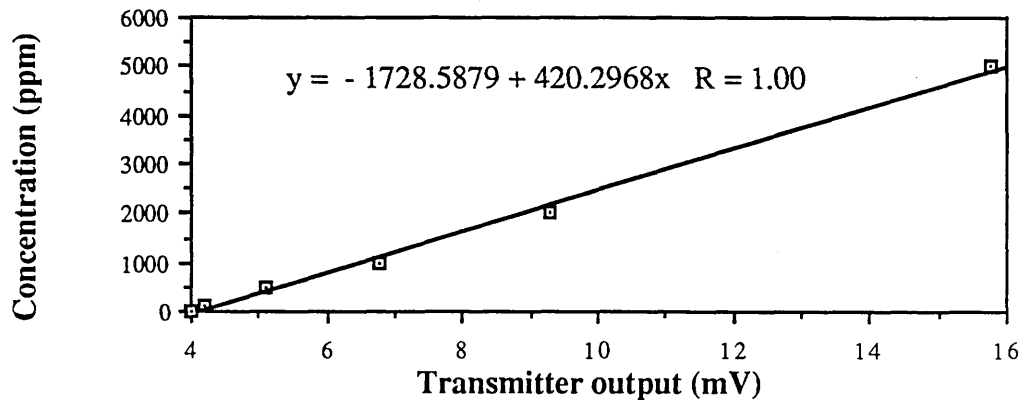


Fig.A.1 Calibration curve for the permeate side conductivity-meter at 25°C.

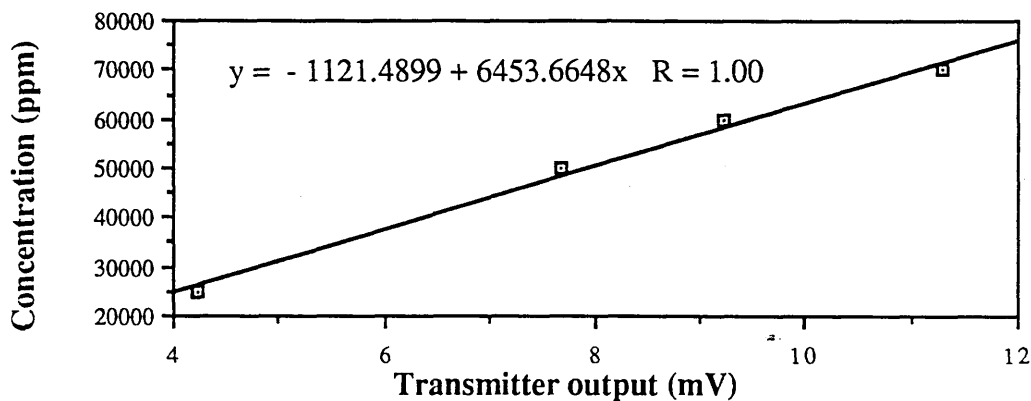


Fig.A.2 Calibration curve for the feed side conductivity-meter at 25°C.

3. Paddle wheel Flow-meters

The flow-meters were calibrated by measuring the volume of the liquid passing at a given time from the flow-meter and the output value from the transmitter in Volts. Two correlation equations were found for the permeate side flow-meter and the feed side flow-meter to give the flow rate as a function of the output of the transmitter in Volts, see Fig.A.3.

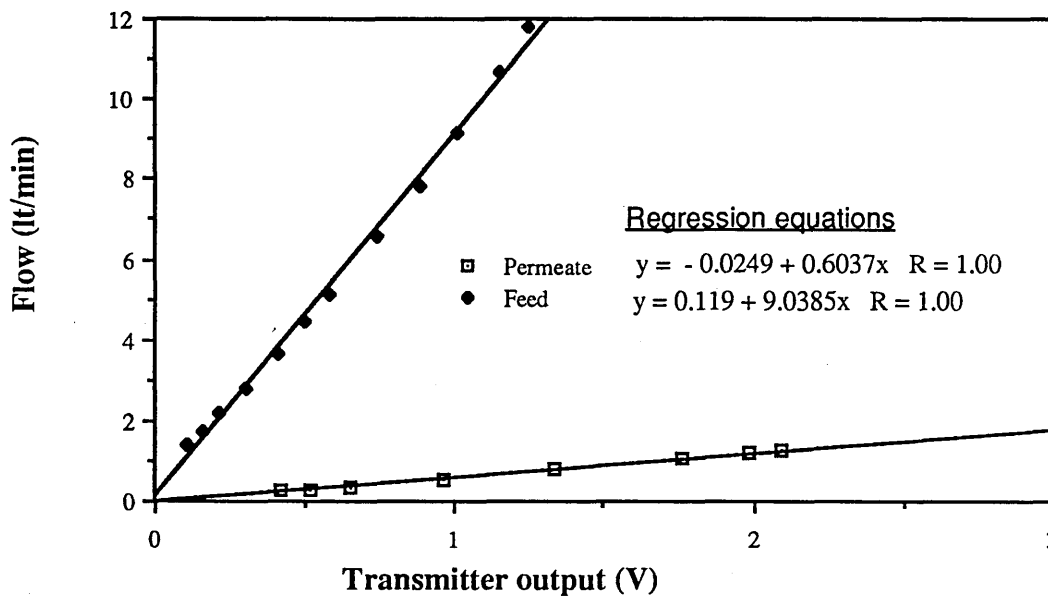


Fig.A.3 Calibration curve for the feed and permeate side flow-meters.

REFERENCES

- 1) J.W. McCutchan, Univ. California (Los Angeles), Dept. Eng. Report 60-19, (1960).
- 2) G.L. Hassler and McCutchan, Advan. Chem. Ser. 27,192 (1960).
- 3) J.D. Ferry, Chem. Rev., 18, 373 (1936).
- 4) L.C. Craig, Science 144, 1093 (1964).
- 5) T.R. Yuster, S. Sourirajan and K. Bernstein, University of California (Los Angeles) Dept. Eng. Report 7, 26-58, (1958).
- 6) S. Sourirajan, Ind. Eng. Chem. Fundam. 2,51 (1963).
- 7) S. Sourirajan, Ind. Eng. Chem. Fundam. 3, 206 (1964).
- 8) E.J. Breton, J. Appl. Polymer Science, 5, 147 (1962).
- 9) C.E. Reid and E.J. Breton, J. Appl. Polymer Science, 1, 133 (1959).
- 10) U. Merten, Desalination by Reverse Osmosis , MIT Press, Mass., (1966).
- 11) H.K. Lonsdale, U Merten, and R.L. Riley, J. Appl. Polym. Science, 9, 1341 (1965).
- 12) S. Sourirajan, Ind. Eng. Chem. Fundam. 2, 51-55 (1965).
- 13) S. Sourirajan Reverse Osmosis and Synthetic Membranes, National Research Council Canada, Canada, (1977).
- 14) S. Sourirajan, Ind. Eng. Chem. Fundam. 15, 87-56 (1978).
- 15) R. Routenbach, Membrane Separation , John Wiley and Sons, London, (1988).
- 16) R. Routenbach and W. Dahm, Design and Optimization of Spiral-wound and Hollow fibers R.O. modules , Desalination 65, 259-275, (1987).
- 17) G.Gefford, G.A. Guter, An experimental study of electro dialysis hydrodynamics,

- Desalination, 10, 221-262, (1972).
18. Y. Taniguchi, An Analysis of R.O. characteristics of ROGA spiral-wound modules , Desalination, 15, 71-88, (1978).
 - 19) S.K. Gupra, Analytical design equations for R.O. systems, Ind. Eng. Chem. Process Des. Dev. , 24, 1240-1244,(1985).
 - 20) G. Schock and A. Miquel, Mass transfer and pressure loss in spiral wound modules, Desalination, 64, 339-352, (1987).
 - 21) R.L.C. Flemmer, C.A. Buckley, G.R.Groves, An analysis of the performance of a spiral wound ultrafiltration membrane with a turbulence promoting net, Desalination, 41, 25-32, (1982).
 - 22) K.K. Sirkar, D.T. Dang, G.H. Rao, Approximate design equations for R.O. desalination by spiral wound modules , Ind. Eng. Chem. Process Des. Dev. 21, 517-527, (1982).
 - 23) F. Evagelista and G. Jonsson, Optimal Design and performance of spiral wound modules , Chem. Eng. Comm., 72, 83-94, (1988).
 - 24) K.S. Spiengler, O. Kedem, Desalination, 1, 311, (1966).
 - 25) A. Solan, Y. Winograd, U. Katz, Desalination, 9, 89, (1971).
 - 26) R. Rautenbach and W. Dahm, Proc. Europe-Japan Congress on Membrane and Membrane Process, June 1984, Stresa, Italy.
 - 27) F. Evagelista and G. Jonsson, Optimal design and Performance of spiral wound modules, Chem. Eng. Com., 72, 69-81, (1988).
 - 28) S. Loeb, " Desalination by Reverse Osmosis" U.Merten edit. , Chaptr 3, M.I.T. Press, Cambridge, Mass, (1977).
 - 29) H.K. Lonsdale, U. Marten, M. Tagami, J. Applied Polymer Science, 11, 1807, (1967).

- 30) S. Sourirajan, Reverse Osmosis, Publ. Logos Press Ltd., N.Y.,1970.
- 31) A. Chiolle, G. Gianotti, M. Gramondo, G. Parini, Mathematical Model of Reverse Osmosis in Parallel-wall channels with Turbulence Promoting Nets, Desalination 26, 3-16, (1978).
- 32) W. Yinograd, A Solan, M. Toren, Mass transfer in narrow channels with turbulence promoters , Desalination 13, 47-64, (1973).
- 33) R.G.Gutman,The Chemical Eng. No 322, 510, (1977).
- 34) H.Ohya, Y. Taniguchi, An analysis of Reverse Osmotic characteristics of ROGA-4000 spiral wound module , Desalination, 16, 359-373, (1975).
- 35) F. Evagelista, Improved Analytical method for the design of spiral wound modules, The Chemical Eng. Journal, 38, 33-40, (1988).
- 36) V.Gekas and B.Hallostrom, Mass transfer in the membrane concentration polarization layer under turbulent cross-flow. Part I.,Journal of membrane Science,30, 153-170, (1987).
- 37) D.R. Trettin and M.R.Doshi, Ind.Eng. Chem. Fund., 19(2), 189, (1980).
- 38) G.Jonsson, Boundary layer phenomena during ultrafiltration of dextran and whey protein solutions, Desalination, 51, 61-67, (1984) .
- 39) G.Belford and N.Nagata, Fluid mechanics and cross-flow filtration, Desalination 53, 57-59, (1985).
- 40) G.B.Van den Berg, I.G. Ratz and C.A.Smolders, Mass transfer coefficient in Cross-flow ultrafiltration, J.Membrane Science, 47, 25-51, (1989).
- 41) A.S.Berman, Laminar flow in channels with porous walls, J. of Applied Physics, 24, No9, (1953).
- 42) K.S. Spiegler, A.D.K. Laird, Principles of Desalination, Academic Press, N.Y.,1980.

